Earth Observing System

TROPOSPHERIC EMISSION SPECTROMETER

(TES)

Scientific Objectives & Approach, Goals & Requirements

Revision 6.0

April 14, 1999

Jet Propulsion Laboratory
California Institute of Technology
Pasadena, CA 91109

Earth Observing System

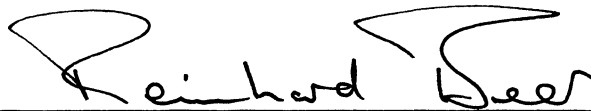# TROPOSPHERIC EMISSION SPECTROMETER

(TES)

Scientific Objectives & Approach, Goals & Requirements

Revision 6.0

Approved: _____

Reinhard Beer
Principal Investigator

April 14, 1999

Jet Propulsion Laboratory
California Institute of Technology
Pasadena, CA 91109

THIS PAGE INTENTIONALLY LEFT BLANK

TABLE OF CONTENTS

LIST OF FIGURES

viii

LIST OF TABLES

THIS PAGE INTENTIONALLY LEFT BLANK

1: INTRODUCTION

1.1: Purpose

This document presents the current revision of the scientific objectives, approaches, goals and requirements for the Tropospheric Emission Spectrometer (TES), selected for flight on the Earth Observing System (EOS) CHEM I polar orbiting platform.

1.2: Definitions

OBJECTIVES are the deliverable science products specified in **TES SCIENCE OBJECTIVES** (April 10, 1990; revised October 18, 1993 & January 17, 1994) and expanded upon herein. The Goals and Requirements (see below) flow down from these objectives. The TES-specific objectives, in turn, are traceable to the EOS Mission Objectives.

APPROACHES are the suggested methods by which the goals and requirements may be achieved.

GOALS are those measurement and performance parameters whose attainment is highly desirable but not mandatory.

REQUIREMENTS are those measurement and performance parameters whose attainment is mandatory to meet the objectives.

1.3: Scope

The document begins with an overview of the TES experiment and how it relates to the objectives of the Earth Science Enterprise, followed by a summary of the Instrument Goals & Requirements (cross-referenced to later sections where they are developed in detail). Note that, in general, these are *science* requirements, not engineering requirements (i.e., more "what" & "why", less "how"). For specific engineering requirements, refer to the TES Functional Requirements Document (JPL D-13376).

The first main chapter provides an outline of the scientific basis of the experiment and is followed by chapters which explain in detail the origin of the Goals & Requirements.

A following chapter then discusses a provisional mission plan in order to estimate the data rates and volumes that, in turn, impact data processing (the last chapter).

All tutorial material is relegated to appendices (including the derivation of the equations on which many of the requirements depend). However, no actual requirements are developed in the appendices.

1.4: Revisions

While it is expected that subsequent revisions will be issued as required, it should be noted that the contents form a contractual obligation on the investigators. Following approval, therefore, this document will be subject to formal Project Change Control procedures.

However, paper copies of this document may not be current and should not be relied on for official purposes. The current version is in the TES Library at http://knowledge.jpl.nasa.gov/teslib/.

2: EXPERIMENT OVERVIEW

2.1: EOS Program Requirements

The goals of the Earth Science Enterprise (ESE) and, specifically, EOS (the Earth Observing System) are encapsulated in the *Earth Science Strategic Enterprise Plan 1998-2002* issued by NASA HQ in October 1998 (http://www.earth.nasa.gov/visions/stratplan/index.html). In that document, 5 "research questions" were identified as the focus of the program:

1) What are the nature and extent of land-cover and land-use change and the consequences for sustained productivity?

2) How can we enable regionally useful forecasts of precipitation and temperature on seasonal-to-interannual time frames?

3) Can we learn to predict natural hazards and mitigate natural disasters?

4) What are the causes and impacts of long-term climate variability and can we distinguish natural from human-induced drivers?

5) How and why are concentrations and distributions of atmospheric ozone changing?

TES is specifically designed to address item 5, with particular emphasis on *tropospheric* ozone (although with some contribution to items 2 & 3). The TES Level 1 Requirement is therefore:

TES shall determine, through a combination of measurement and modeling, the global distribution of tropospheric ozone and the factors that control its concentration.

Specifically:
TES shall, to the extent possible given cloud interference and other fundamental physical limitations, generate vertical concentration profiles of ozone, carbon monoxide, methane, water vapor, nitric oxide, nitrogen dioxide and nitric acid from the surface to the lower stratosphere.

TES shall provide these measurements on a latitude grid of 5° or better on a continuous basis for 4 days out of every 8.

2.2: TES Scientific Objectives

Consistent with the ESE Program Objectives and the TES Level 1 Requirement, the general objectives of TES are to generate a database of the 3-dimensional distribution of gases important to tropospheric chemistry, troposphere-biosphere interactions, and troposphere-stratosphere exchange, on global, regional and local scales and to employ the database to calibrate models of the present and future state of the Earth's lower atmosphere. TES may also study volcanic emissions for: hazard mitigation; indications of the chemical state of the magma; eruption prediction; and quantification of the role of volcanos as sources of atmospheric aerosols.

The resultant models will investigate topics such as:

- The distribution of tropospheric ozone as modified by natural and anthropogenic sources of its precursors (particularly carbon monoxide, nitrogen oxides, methane and other hydrocarbons) and the consequent changes in the oxidizing power of the troposphere;

- Global climate modification caused by the increase in radiatively-active gases;

- The exchange of gases between the troposphere and the stratosphere;

- Sources and sinks of species important to the generation of tropospheric and stratospheric aerosols;

- Natural sources of trace gases such as methane from organic decay, nitrogen oxides from lightning and sulphur compounds from volcanos.

- Biogeochemical cycles of the interaction of the lower atmosphere and the biosphere;

Secondary objectives for TES include:

- Determination of local atmospheric temperature and humidity profiles;

- Determination of local surface temperatures, emissivities and reflectances;

- Detection of species that may be indicative of new atmospheric chemical mechanisms;

- Measurement of effluents from biomass burning and major industrial accidents.

Fig. 1: Cartoon of the TES Data Acquisition Modes

Limb Views

Downlooking Views

TES
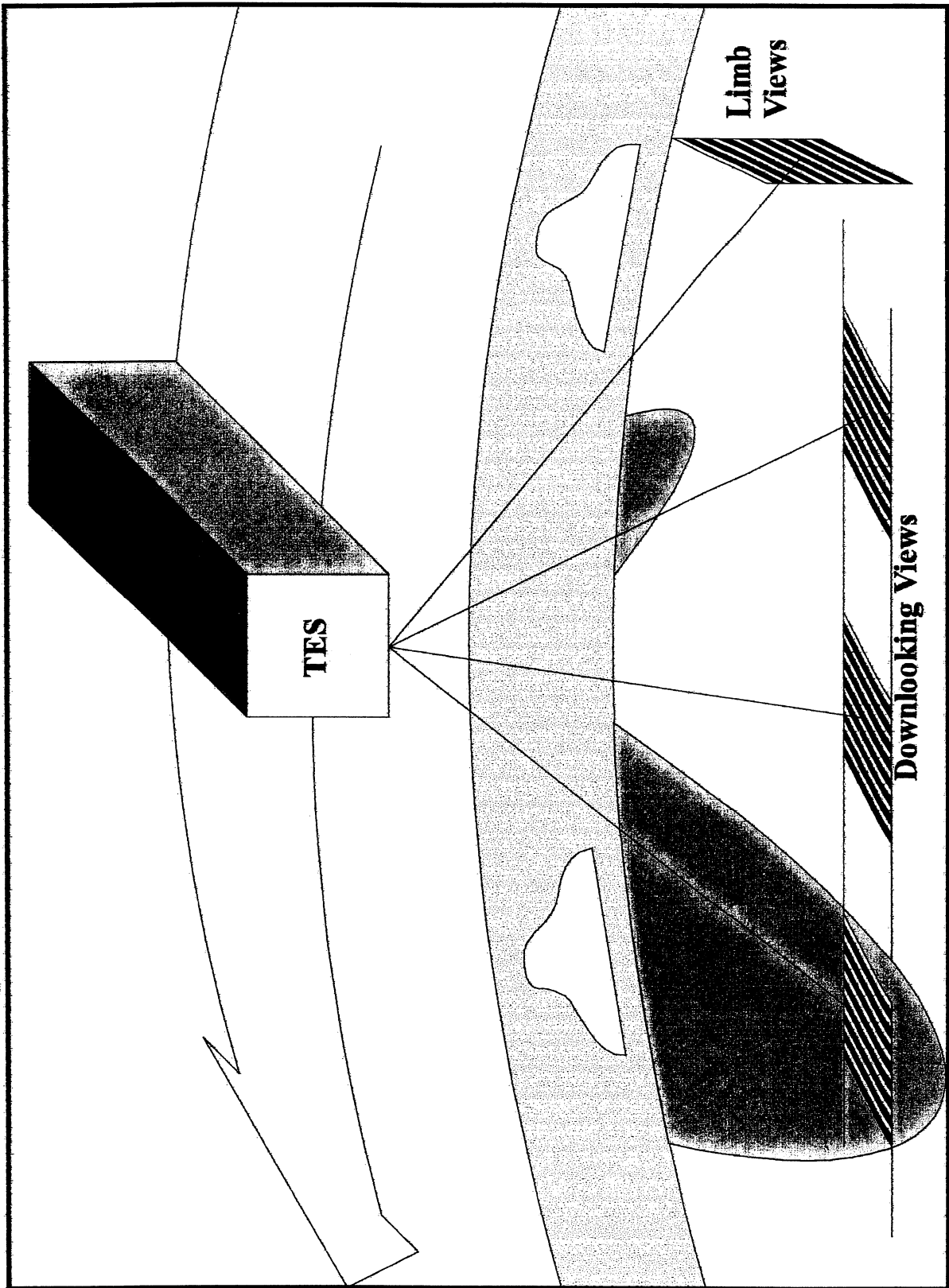
2.3: Instrument and Experiment Introduction

TES is an infrared (650 - 4250 cm^{-1}; 2.4 - 15.4 μm), high resolution (0.025 cm^{-1}), imaging (1 x 16 pixels) Fourier Transform Spectrometer intended for the measurement and profiling of essentially all infrared-active molecules present in the Earth's lower atmosphere (0 - 30+ km).

TES operates by natural thermal emission (650 - 2450 cm^{-1}; 4.1 - 15.4 μm) and by solar reflection (2000 - 3050 cm^{-1}; 3.3 - 5.0 μm) when appropriate. TES will obtain its data in single scans of 4 seconds each in downlooking (nadir $\pm$ 45°) operations and in 16 seconds while staring at the trailing limb (0 - 30+ km). Longer integrations (up to 221 seconds) by scan-averaging are possible for improved sensitivity or multiple scans over the same interval can be used to investigate time variability. Spatial variability can be studied by "stacking" footprints contiguously to generate along-track transects up to 830 km long. Spatial resolution from the EOS 705 km orbit is interchangeably 0.5 km cross-track x 5 km in-track or 2.5 x 25 km in the nadir and 2.3 km high x 23 km (parallel to the Earth's surface) at the limb (Fig. 1).

The primary (Standard Product) TES objective is to measure the global 3-dimensional distribution of concentration of a large suite of molecules (Table I) important to tropospheric physics and chemistry, especially those of intermediate lifetime (hours - months). On regional and local scales, TES will (as Special Products) also measure additional species that are sporadic or of specialized interest Table II). If, during the course of the mission, it becomes clear that some of theses added species can be routinely extracted from the Global Survey data, they will be added to the Standard Products list.

Table I: TES Standard Data Products

Product No.	Product Name	Product Source	
		Nadir	Limb
1	Level 1A Interferograms	✔	✔
2	Level 1B Spectral Radiances	✔	✔
3	Atmospheric Temperature Profile, T	✔	✔
4	Surface Temperature, T_s	✔	
5	Land Surface Emissivity[†], ϵ_s	✔	
6	Ozone (O_3) VMR Profile	✔	✔
7	Water Vapor (H_2O) VMR Profile	✔	✔
8	Carbon Monoxide (CO) VMR Profile	✔	✔
9	Methane (CH_4) VMR Profile	✔	✔
10	Nitric Oxide (NO) VMR Profile		✔
11	Nitrogen Dioxide (NO_2) VMR Profile		✔
12	Nitric Acid (HNO_3) VMR Profile		✔

[†] Water (and, probably, snow & ice) emissivities are known and are therefore *input*, not output, parameters

Table II: TES Special Data Products (Partial List)

H_xO_y	C-compounds	N-compounds	Halogen-compounds	S-compounds
H_2O_2	C_2H_6	HO_2NO_2	HCl*	SO_2
HDO	C_2H_2	NH_3	$ClONO_2$	COS
	HCOOH	HCN	CCl_4	H_2S*
	CH_3OH	N_2O**	CCl_3F	SF_6
	PAN	N_2O_5	CCl_2F_2	
	$CH_3C(O)CH_3$		$CHCl_2F$	
	C_2H_4		$CHClF_2$	

* Volcanic plume column densities only   ** Tropospheric Control (VMR known)

2.4: Summary of Instrument Goals & Requirements

REQUIREMENTS are those measurement and performance parameters whose attainment is mandatory to meet the TES Science Objectives. Within this summary, requirements are suffixed with (R) and referenced to the sections where they are discussed in detail.

GOALS are those measurement and performance parameters whose attainment is highly desirable but not mandatory. Within this summary, goals are suffixed with (G) and referenced as above.

2.4.1: Spectral coverage

1) TES shall be capable of acquiring spectra over the range 650 - 3050 cm^{-1} (3.28 - 15.4 μm) (R; §5.3) and has the goal of acquiring spectra over the range 600 - 3050 cm^{-1} (3.28 - 16.7 μm) (G; §5.3)

2) An appropriate portion of the TES system shall have significant response at 1.06 μm to permit passage and detection of Nd:YAG laser light (R; §5.3) and achieve, at this wavelength, a modulation index > 50% (G; §5.3).

3) TES shall be provided with 4 1x16 linear detector arrays (R; §5.7) covering the ranges (R; §5.3)

1900 - 4250 cm^{-1}	[Array 1A]
820 - 1150 cm^{-1}	[Array 1B]
1100 - 1950 cm^{-1}	[Array 2A]
650 - 900 cm^{-1}	[Array 2B]

4) TES shall be based on a Connes-type interferometer having two input and two output ports (R; §5.2) and the detector arrays shall be arranged in pairs such that Arrays 1A and 1B are illuminated by one output port and 2A and 2B by the other (R; §5.3).

5) The array pairs 1A & 1B at output port 1 shall be optically separated by a dichroic beamsplitter having its reflection-transmission crossover at 1525 ±25 cm^{-1} (R; §5.3)

6) The array pairs 2A & 2B at output port 2 shall be optically separated by a dichroic beamsplitter having its reflection-transmission crossover at 1000 ±25 cm^{-1} (R; §5.3)

7) Array 1A shall be preceded with a filter wheel in which the following filters are installed (50% of peak transmittance points indicated) in the order shown (R; §5.3):

Position 0	2600 (+0, -50) - 2850 (-0, +50) cm^{-1}	[Filter 1A4]
Position 1	2800 (+0, -50) - 3050 (-0, +50) cm^{-1}	[Filter 1A5]
Position 2	1900 (+0, -50) - 2250 (-0, +50) cm^{-1}	[Filter 1A1]
Position 3	2200 (+0, -50) - 2450 (-0, +50) cm^{-1}	[Filter 1A2]
Position 4	2425 (+0, -50) - 2650 (-0, +50) cm^{-1}	[Filter 1A3]
Position 5	Fully-closed	
Position 6	Fully-open	
Position 7	Fully-closed	

8) Array 1B shall be preceded with a filter wheel in which the following filters are installed (50% of peak transmittance points indicated) in the order shown (R; §5.3):

Position 0	950 (+0, -50) - 1150 (-0, +50) cm^{-1}	[Filter 1B2]
Position 1	820 (+0, -50) - 1050 (-0, +50) cm^{-1}	[Filter 1B1]
Position 2	Fully-closed	
Position 3	Fully-closed	
Position 4	Fully-closed	
Position 5	Fully-closed	
Position 6	Fully-open	
Position 7	Fully-closed	

9) Array 2A shall be preceded with a filter wheel in which the following filters are installed (50% of peak transmittance points indicated) in the order shown (R; §5.3):

Position 0	1700 (+0, -50) - 1950 (-0, +50) cm^{-1}	[Filter 2A4]
Position 1	1100 (+0, -50) - 1325 (-0, +50) cm^{-1}	[Filter 2A1]
Position 2	1500 (+0, -50) - 1750 (-0, +50) cm^{-1}	[Filter 2A3]
Position 3	1300 (+0, -50) - 1550 (-0, +50) cm^{-1}	[Filter 2A2]
Position 4	Fully-closed	
Position 5	Fully-closed	
Position 6	Fully-open	
Position 7	Fully-closed	

10) Array 2B shall be preceded with a filter wheel in which the following filters are installed (50% of peak transmittance points indicated) in the order shown (R; §5.3):

Position 0   650 (+0, -50) - 900 (-0, +50) cm^{-1} [Filter 2B1]
Position 1   Fully-closed
Position 2   Fully-closed
Position 3   Fully-closed
Position 4   Fully-closed
Position 5   Fully-closed
Position 6   Fully-open
Position 7   Fully-closed

11) The peak transmittance of all filters shall exceed 80% (R;§5.3)

12) The integrated out-of-band effective transmittances of each filter shall be less than 1% below and above the following frequencies (R; §5.16):

Filter 1A1: below 1762 cm^{-1} and above 2349 cm^{-1}
Filter 1A2: below 2088 cm^{-1} and above 2610 cm^{-1}
Filter 1A3: below 2349 cm^{-1} and above 2741 cm^{-1}
Filter 1A4: below 2349 cm^{-1} and above 2937 cm^{-1}
Filter 1A5: below 2610 cm^{-1} and above 3133 cm^{-1}

Filter 1B1: below 587 cm^{-1} and above 1175 cm^{-1}
Filter 1B2: below 854 cm^{-1} and above 1281 cm^{-1}

Filter 2A1: below 940 cm^{-1} and above 1410 cm^{-1}
Filter 2A2: below 1175 cm^{-1} and above 1762 cm^{-1}
Filter 2A3: below 1410 cm^{-1} and above 1880 cm^{-1}
Filter 2A4: below 1566 cm^{-1} and above 2088 cm^{-1}

Filter 2B1: below 522 cm^{-1} and above 1044 cm^{-1}

13) All filters shall be operable, and meet the preceding specifications in near-normal-incidence light, at 65 kelvin (R;§5.3)

2.4.2: Spectral resolution

1) TES shall be capable of providing a maximum path difference, in either direction, of at least 34 cm about Zero Path Difference (ZPD) (R; §5.4)

2)   TES shall be capable of starting, stopping and reversing the scan at any point in its travel under software control (R; §5.4) to within ±1 mm (G; §5.16)

3)   Zero Path Difference (ZPD) shall be physically centered in the total travel of both interferometer arms to ±1 mm (G; §5.16)

2.4.3: Spectral accuracy

1)   Following correction for Doppler shifts, off-axis and aberration effects and control laser drifts, TES shall provide spectra with a frequency accuracy of ±0.00025 cm^{-1} (G; §5.5).

2)   The fringe-to-fringe amplitude stability of the control laser output shall be better than 0.5% (R; §5.5)

3)   Random interferogram sampling interval errors shall not exceed 2 nm RMS (R; §5.16)

4)   Periodic interferogram sampling interval errors shall not exceed 1 nm peak-to-peak (R; §5.16)

2.4.4: Spectral purity

1)   All transmissive elements (windows, filters, beamsplitters, etc) shall be wedged so that no parasitic reflections reach the detector elements (R; §5.16)

2)   Wedged elements shall be installed with a rotational azimuth such that the the beam deviations due to wedging are compensating, not cumulative (G; §5.16)

3)   No detectable light from the control laser shall impinge on the infrared detector arrays (R; §5.16)

2.4.5: Spatial coverage

1)   TES shall be equipped with a 2-axis pointing mirror to permit the line-of-sight to project to 72° at the trailing limb defined by the spacecraft velocity vector and to at least 45° at all azimuths in a cone centered on the nadir direction (R; §5.8)

2)   The 2-axis pointing mirror shall be commandable in both axes to permit observation of targets at specific latitudes and longitudes for up to 221 seconds. To permit this, the spacecraft/instrument attitude shall be known to 0.375 mrad in pitch and roll and 0.75 mrad in yaw (R; §5.16).

3) The 2-axis pointing mirror shall be capable of viewing all internal calibration sources and cold space (R; §5.16).

4) The four 1x16 element detector arrays shall be optically conjugated so that their geometric images at the Earth's surface or limb are superimposed and their position known to 1% of a pixel (R; §6.2)

2.4.6: Spatial & Angular resolution

1) The external angular field-of-view of each pixel shall be 0.75 x 7.5 mrad (R; §5.6)

2) The detector arrays shall be constructed such that the narrow fields-of-view are adjacent (R; §5.6)

3) Any "dead" space between adjacent pixels shall be less than 10% of a pixel (G; §5.7).

4) The detector sizes shall be identical to better than 10% (G; §5.7)

2.4.7: Spatial purity

1) End-to-end crosstalk between adjacent pixels from whatever cause (optical, electrical or electronic) shall be less than 10% (G; §5.13)

2) TES shall be capable of staring at a point on the ground to within 10% of a pixel for 4 seconds (R; §5.16) and to within 1 pixel for 221 seconds (G; §5.9)

3) Pointing jitter shall not exceed 75 μrad peak-to-peak in pitch, 1.1 mrad in roll and 750 μrad in yaw over any 16 second period as referenced to the spacecraft coordinates (R; §5.16).

2.4.8: Temporal coverage & lifetime

1) TES shall be operable for 5 years on orbit plus 2 years pre-flight (R; §5.9)

2) TES shall be capable of being turned on and off on command (R; §5.9)

3) TES shall be capable of performing not less than 10,000,000 strokes (scans) (R; §5.9)

2.4.9: Temporal resolution

1) The nominal rate-of-change of optical path difference shall be 4.2235 ± 0.2 cm/sec and shall be constant within a single scan to 3% peak-to-peak or better (R; §5.10; §5.17)

2) The cycle time to perform a Global Survey sequence of 2 calibration scans plus 2 nadir scans (each ±8.447 cm OPD) plus 3 limb scans (each ±32.788 cm OPD) plus set-up for the next cycle shall be 81.2 seconds (R; §5.10; §5.15)

2.4.10: Radiometric coverage (dynamic range)

1) TES shall, with appropriate commandable gain changes, be capable of observing sources as cold as deep space and as hot as 340 Kelvins without overload (R; §7.5)

2) The dynamic range within any one observation shall not exceed 16 bits (R; §5.11)

2.4.11: Radiometric accuracy

1) Following calibration, the measured output spectral radiances shall be identical to the input source spectral radiances to

   1% or better: below 2500 cm^{-1}
   2% or better: 2500 - 3050 cm^{-1} (R; §5.12)

2) The spectral radiances shall be traceable to NIST standards (R; §5.12)

3) TES shall be outgassed (decontaminated) when the calibration signal in Filter 1B2 falls by 5% (R; §5.15)

2.4.12: Signal-to-Noise ratio

1) All spectra shall have a signal-to-noise ratio of at least 30:1 (R; §5.12), to be accomplished if necessary by pixel averaging and/or staring, and preferably greater than 100:1 (G; §5.12). The overall goal shall be for TES to be source photon shot noise limited (G; §5.14).

2.4.13: Interferometric properties

1) The modulation index of the TES interferometer shall be 0.7 or better at all infrared wavelengths of interest (G; §5.16)

2) Residual channel spectra (following decalibration) shall be less than 1% peak-to-peak (G; §5.16)

3) The engineering data shall permit the direction of travel to be determined (R; §5.16)

2.4.14: Signal Chains

1) The signal chains shall be designed so that the various types of signals to be observed shall use the available A-D converter dynamic range through the use of fixed and programmable gain stages (G; §5.17)

2) The signal chains shall incorporate tunable or switchable electrical filters to reduce electrical noise. The filters shall not, as a consequence of OPD scan rate variations, impose amplitude fluctuations on the signal in excess of 3% peak-to-peak (G; §5.17)

2.4.15: Data stream

1) No more than 1% of TES interferograms shall be irretrievably corrupted by data transmission errors (G; §5.17)

2) The TES data stream shall be tagged to permit determination of the time, date, latitude and longitude of observation, and calibration source temperature. Time tags shall be accurate to 70 msec or better (R; §8.2)

2.4.16: Data processing

1) Level 1A processing shall provide reconstructed interferograms in 16-bit integer format and be fully reversible to Level 0 data packets (R; §8.2)

2) Level 1B processing shall accept Level 1A output and provide mathematically-real spectra, decalibrated to units of $watts/cm^2/sr/cm^{-1}$ (radiance) (R; §8.2)

3) Level 2 processing shall accept Level 1B output and extract volume mixing ratio and temperature profiles (R; §8.2)

4)   Standard Product generation (from Global Surveys) at the DAAC shall be accomplished within 8 days from receipt of all necessary inputs (R; §8.3)

5)   For Special Product generation (if implemented) and Quality Control purposes, certain user-selectable input/output operations shall be provided (R; §8.3)

THIS PAGE INTENTIONALLY LEFT BLANK

3: DETAILED SCIENTIFIC OBJECTIVES

3.1: Introduction

Because tropospheric chemistry is such a complex topic, the discussion of scientific objectives is necessarily lengthy. In addition, the objectives are dependent on the region of the lower atmosphere being considered: the *mixing layer* (the region of turbulent mixing within a few meters of the surface, probably not measurable from space); the *planetary boundary layer* (the lowest 2 to 3 km of the atmosphere); the *free troposphere* (the region between the boundary layer and the tropopause); the *tropopause* itself (typically 10 to 15 km above the surface but strongly latitudinally and seasonally variable) and the *lower stratosphere* (a region of increasing temperature strongly influenced by ozone absorption of sunlight).

3.2: Tropospheric Ozone (O_3) and its Precursors

3.2.1: Introduction. While only about 10% of the Earth's ozone resides in the troposphere, it is nevertheless exceedingly important because of the multiple roles it plays: O_3 is the principal source of OH, the "detergent" molecule that removes atmospheric pollutants and species such as the halocarbon substitutes that are being employed in an effort to reduce stratospheric ozone depletion; it is the source of photochemical smog that is becoming a world-wide problem; it is a significant greenhouse gas in the upper troposphere; and is known phytotoxicant, causing serious damage to trees and plants. The main problem is that the global distribution of tropospheric ozone is largely unknown and the processes of ozone formation and destruction are exceedingly complex (see Fig. 3), making modelling of its distribution virtually impossible. Thus a multi-year series of global surveys of tropospheric ozone itself and as many of its precursors as possible is crucial and, furthermore, vertical profiles are essential because the chemical reactions involved are strongly height-dependent. The current consensus within the community is that at least 3 levels in the troposphere must be resolved - total column densities are not useful.

3.2.2: OH The OH radical provides the main sink for a number of environmentally-important atmospheric gases (see Fig. 3) including CH_4, other hydrocarbons (see Table III), CO, NO_x (= NO + NO_2) and HCFC's (i.e., CFC substitutes). OH is produced in the atmosphere by photolysis of ozone, yielding atomic oxygen in the $O(^1D)$ state, which then reacts with water vapor. Model calculations suggest that OH concentrations may have decreased globally by 20% since preindustrial times, largely due to increased emissions of CH_4 and CO. There is concern that a catastrophic depletion of OH could occur if anthropogenic emissions of CH_4 and CO continue to increase. However, anthropogenic increases of ozone and NO_x stimulate OH production, complicating the assessment of human influence. Although tropospheric OH concentrations are too low to be measurable by TES (or, indeed, any other known space-borne remote sensor), it will be possible to infer its distribution by profiling the concentrations of the regulating species and combining these with knowledge of the solar UV flux.

17

Fig 2: Tropospheric Ozone and its Principal Precursors

Note: "R" denotes any radical

● = Requires Limb Viewing

○ = Observable Nadir or Limb

3.2.3: O_3. As previously mentioned, ozone is the principal precursor of OH. Trial retrievals with simulated TES nadir data suggest that 3 levels in the troposphere can be measured with 20% (or better) accuracy. Mapping of the lower atmosphere is critical because OH production peaks at 1-3 km altitude. Furthermore, some tropospheric ozone (possibly as much as 50%) originates in the stratosphere (being transported down at mid and high latitudes in so-called "tropopause fold events"). Limb viewing of ozone is necessary to quantify this phenomenon, as is its activity as an upper-troposphere greenhouse gas.

3.2.4: H_2O. Water vapor is required to convert $O(^1D)$ produced by ozone photolysis to OH. The major determinant of the OH production rate is the covariance of ozone and water vapor concentrations. Simultaneous retrieval of these two species will provide a precious input to photochemical models. Our current best estimate is that TES water vapor profiles should be accurate to a few percent.

3.2.5: CH_4. Methane is an important OH sink and, in turn, OH is the main sink for methane. Increases in CH_4 emissions can therefore provide a positive feedback mechanism for OH depletion. Unfortunately, owing to its long lifetime in the troposphere (about 7 years), there is a large permanent background of methane so changes will be difficult (but not impossible) to measure.

3.2.6: CO. CO is a major OH sink and, in turn, OH is the major sink for CO. The lifetime of CO is relatively short ($\approx$ 2 months). Tropospheric concentrations are therefore quite variable (from 50 to 1000 ppbV). Profile accuracies of 10% or better are expected except in the boundary layer, where lack of thermal contrast renders measurement difficult.

3.2.7: NO_x. NO_x helps to maintain a high oxidizing power in the atmosphere by recycling the OH consumed in the oxidation of trace gases. The source of NO_x is both anthropogenic (combustion) and biogenic (biota, lightning). The atmospheric concentration is regulated in part by chemical cycling with HNO_3 and organic nitrates (in particular PAN - peroxyacetylnitrate). TES will measure NO by limb-viewing to 20-30% in the mid and upper troposphere (it is too heavily blanketed by water vapor to be measured in the lower troposphere). HNO_3 (also measured by limb-viewing) can be measured to a few percent throughout the troposphere (at least down to the cloud deck). The detectabilities of NO_2 and PAN are uncertain at this time, but will certainly require limb-viewing.

3.2.8: Other Hydrocarbons. The most abundant non-methane-hydrocarbon, ethane (C_2H_6) will be determinable to about 10% in the free troposphere by limb sounding and TES should be capable of at least a detection of C_2H_2. The detectability/measurability of other hydrocarbons is conjectural due to the inadequacy of the spectral databases for such species. This important topic is further discussed in §4.

3.3: Global Climate Change

3.3.1: Introduction. It is widely accepted that the observed increases in certain radiatively-active gases in the troposphere will lead to a general increase in the temperature of the lower atmosphere, with the increase disproportionately evident at high latitudes. Indeed, some evidence exists for an increase in the mean global temperature of about $0.5°C$ over the past 100 years. Whether the observed increase is evidence for global climate change is a topic of current research and considerable public debate. A critical missing element is a long-term global inventory of the important species. TES will contribute to this isssue.

3.3.2: H_2O. Water vapor is the most important greenhouse gas. Not only are its infrared absorption features widespread and strong, but it also displays a significant continuum absorption. Thus, while not one of the "gases of concern" in the sense of anthropogenic modification, the feedbacks engendered by the higher water content of a warmer atmosphere (and, potentially, greater cloud cover) are an important element of these studies. Furthermore, water vapor, through continua centered at 100 and 1600 cm^{-1}, is a crucial element in the radiative balance of the upper troposphere. TES routinely monitors the humidity profile as a necessary adjunct to temperature retrieval and, on the basis of retrievals performed on HIS aircraft data, profiles to better than 5% should be available from TES.

3.3.3: CO_2. As discussed elsewhere (§3.7.2), carbon dioxide is *used* by TES to determine temperature/pressure profiles. In any case, CO_2 is continuously monitored by *in situ* sensors to a precision well beyond that available from remote sensors.

3.3.4: CH_4. Monitoring of this species, which is a significant greenhouse gas, is a secondary goal for TES. Profile accuracies of better than 10% seem feasible.

3.3.5: O_3. Ozone is an important contributor to the Earth's radiative balance. It is both a major absorber of incoming UV in the stratosphere (leading to stratospheric heating) and a strong emitter in the thermal infrared. TES can contribute measurements of ozone in the lower atmosphere but a significant fraction of the total column will be above the region where TES performance becomes marginal (> 30 km). Thus this part of the problem will require input from other instruments (e.g., HiRDLS). Retrievals should be good from the surface to the lower stratosphere (see §3.2.3).

3.4: Troposphere-Stratosphere Exchange

3.4.1: Introduction. The topic of stratospheric ozone depletion has received major attention over the past few years, both in terms of specific phenomena like the polar ozone holes, and the threat of a gradual thinning of the Earth's protective ozone shield at all latitudes. The problem arises because odd-nitrogen and halogen-containing molecules are able to reach the stratosphere, where they participate in photochemical reactions which enhance the rates at which ozone is destroyed and alter the natural balance between production and removal. TES, in common with a number of other instruments, has the ability to measure many of the species which participate in these reactions, as discussed earlier. However, TES can also observe the region of the polar vortices (to $\pm 82°$ latitude) during the polar night when they are inaccessible to instruments relying on backscattered sunlight (e.g., TOMS) or solar occultation (e.g., SAGE).

3.4.2: Troposphere-Stratosphere Exchange Mechanisms. Key questions in understanding and limiting stratospheric ozone depletion are the processes whereby the depletor molecules (mainly N_2O and halocarbons) reach the stratosphere and the reservoir species for reactive nitrogen and halogen (such as HNO_3 and HCl) make the return journey into the troposphere where they can be removed by rainout. To first order, the tropopause is a quite efficient barrier against vertical motion, which means that sporadic events (in cumulus towers, for instance) and diffusive processes combine in unknown proportions to inject tropospheric gases into the stratosphere. Equally obscure processes, probably involving tropopause folding events, bring stratospheric gases (including ozone) down to the surface. The global budgets of these transfers, which are crucial to any long-term understanding of the evolution of the ozone layer, are very difficult to quantify, because so little is known about the processes involved.

The key to understanding the vertical transfer processes in the region of the tropopause is obtaining, on a global and seasonal basis, vertical profiles of species which originate in either the troposphere or the stratosphere and therefore normally have large gradients across the tropopause. H_2O, N_2O and CH_4 are the best candidates in the former category and O_3 itself in the latter. Changes in these gradients will allow the transfer process to be modeled and their statistics of occurrence established. The problem with obtaining such measurements is that instruments flown before TES will either have lower spectral resolution (and therefore very limited penetration into the troposphere), or are solar occultation instruments with very limited coverage. Preliminary calculations suggest that TES resolution is sufficient to resolve "microwindows" at wavelengths where the opacity is controlled by absorptions of all the important species named above, thus permitting limb observations well down into the troposphere (to 4 km when the absence of high clouds permits).

3.5: Tropospheric and Stratospheric Clouds & Aerosols

3.5.1: Introduction. Aerosols (which, for the present discussion, include both liquid droplets and solid particulates) form an extremely heterogeneous group. They include more or less pure water droplets, acid droplets, dust particles and crystalline condensates (e.g., water ice). While considerable further work is required on the scattering radiative transfer inevitably involved in discussions of remote measurements of aerosols, it seems likely that TES will be able to make crude compositional measurements (through the broad vibrational and electronic features associated with liquids and solids). Circumstantial evidence in support of this conjecture was provided by the ATMOS experiment on the ATLAS 1 mission in the Spring of 1992. This was several months after the eruption of Mt. Pinatubo but, nevertheless, very strong features of sulphuric acid are plainly evident in the spectra acquired in the lower stratosphere. Indeed, the opacity was so great that the sun-tracker usually lost control in transiting this region.

3.5.2: Polar stratospheric clouds. The Stratospheric Aerosol Measurement (SAM) II sensor was launched in 1978 as part of the instrument complement of the Nimbus 7 spacecraft. The data obtained by this sensor as well as those obtained by the Stratospheric Aerosol and Gas Experiments (SAGE) I & II revealed the presence of persistent "clouds" in the Arctic and Antarctic stratospheres during the local winter. The presence of these clouds (PSC's) is very well correlated with regions of very low temperatures. However, their presence was very puzzling since the temperatures were not low enough to give rise to stratospheric "clouds" under the then-current stratospheric aerosol models. When the depletion of ozone in the the spring Antarctic stratosphere was reported, interest in PSC's increased since the explanation of the ozone "hole" depended on heterogeneous chemistry; the PSC's provided surfaces for such reactions to occur. Subsequent studies showed that these clouds are of two types, one of which appears to be composed of nitric acid trihydrate which condenses at higher temperatures than normal water or sulphuric acid clouds. The proposed role of heterogeneous chemistry in the photochemistry of the ozone layer has lead to increased interest in the stratospheric aerosol layer at low latitudes as well as in PSC's.

Stratospheric aerosols will produce significant signatures in the spectra obtained by TES when limb-viewing. TES will be able to provide information not only on the presence of PSC's, but also on their composition. Similar data will be available on the stratospheric aerosols at lower latitudes.

3.5.3: Cirrus Clouds. Cirrus clouds are believed to have an important role in the radiative balance of the atmosphere even when they are "sub-visible". When TES is limb-viewing, the effective path length through the atmosphere is increased by a factor ~ 20 over nadir viewing, which permits otherwise weak absorption/scattering to be strongly enhanced. Cirrus clouds are composed of ice crystals which can be quite large (crystals as big as 1 mm have been recovered by specially-equipped aircraft) and therefore can display the well-quantified infrared ice bands. Retrieval of microphysical parameters from such spectra is non-trivial because the

crystals are asymmetric and far from spherical, so Mie scattering theory can be applied only for the crudest measures. However, significant work on the properties of non-spherical scatterers is in process, so there is every likelihood that a useful algorithm will be available by the time TES flies.

3.6: Biogeochemical Cycles

3.6.1: Introduction. The interdisciplinary arena of biogeochemical cycles encompasses the fields of terrestrial and aquatic ecology, aquatic chemistry, hydrology, glaciology, plant physiology and tropospheric chemistry. TES will provide crucial inputs to the last topic. For most species of interest, TES capabilities are as discussed in §3.2. Here we add only CO_2 and NH_3.

3.6.2: CO_2. In the mixing layer, the most important biogeochemical molecule requiring inventory is CO_2. Although CO_2 is usually regarded as being uniformly mixed, in areas such as Amazonia 10 - 20% diurnal variations in mixing layer concentration have been observed. Normally, the CO_2 concentration is taken as a "given" in atmospheric remote sensing and the value used in the determination of the atmospheric pressure/temperature profile, a crucial element in the extraction of the concentration profile of all other species. Obviously, in regions where variability is known or suspected, a different approach must be used.

While the specific approach to the determination of mixing layer temperatures is a subject for detailed research prior to, and during, the EOS mission, some possibilities are:

- Employ temperatures derived from other instruments *not* assuming a CO_2 concentration (e.g., radiosondes);

- Use climatology to extrapolate downwards from the free troposphere. Note that the surface brightness temperature is independently determinable by TES, providing a rough boundary condition for the extrapolation.

- Use N_2O. While N_2O itself is somewhat variable, it is less so than CO_2 and the two are generally uncorrelated. The spectral features of N_2O are well resolved by TES and fall in relatively favorable regions throughout the infrared and is therefore a candidate as an alternative means of temperature profiling.

Assuming that the temperature problem is soluble, analysis would probably proceed through the use of relatively temperature-insensitive lines of isotopically-substituted CO_2 (the main isotope lines will certainly be saturated). The accuracy goal for mixing layer concentration is <5%.

CO_2 will also be emitted in unusual concentrations and at high temperatures by forest fires and "slash-and-burn" agriculture. While the expected high gas temperatures in the region immediately above the fire would simplify detection and measurement (i.e., distinction from background CO_2), the likely presence of dense smoke will make accuracies unpredictable.

3.6.3: NH$_3$. Ammonia is a substantial product of biomass burning (as are H_2O, CO, CO_2 and CH_4). While its lifetime is very short (it readily dissolves in the water clouds generated by fires), it provides a significant source of nitrogen nutrient (as ammonium compounds) to the downwind regions. NH_3 is readily measured in downlooking data provided that the source is a significant fraction of the size of the TES footprint (i.e., a very large fire). This has been demonstrated with our Airborne Emission Spectrometer (AES), a TES precursor.

3.7: Atmospheric Temperature and Humidity Profiles

TES is an emission sensor that, especially when downlooking (§5), operates in a very complex radiative transfer environment (see Appendix B); much more so than for the pure limb sounders commonly used for stratospheric studies. It follows that an essential precursor to the determination of concentration profiles is good knowledge of the atmospheric temperature profile (to 2 K or better, 0 - 30+ km). Investigation also shows that it is impossible to decouple the temperature profile from the humidity (H_2O) profile. Most retrieval algorithms, therefore, solve for both temperature and humidity in a double iteration. An added requirement on TES, therefore, is that the spectral regions necessary to determine temperature and humidity profiles be encompassed by the system. TES *must* make these measurements itself so that they are co-located and coeval with the species retrievals. Climatology or "transferred" profiles from other instruments are worthless.

Although TES requires these data for its own internal use, the results will certainly be of benefit and interest to other investigators.

3.8: Surface Temperatures

By the same token, solution of the full equation of radiative transfer generates values of the surface *brightness* temperature in the downlooking footprint (i.e., a pixel average T_b). If the surface emissivity can be independently extracted (§3.9), then the surface sensible temperature T_s is immediately available.

3.9: Surface Emissivity

Surface brightness temperature is a frequency-dependent parameter (even for a perfectly "grey" surface). If, from the frequency dependence of T_b, the surface material(s) can be identified, then the absolute emissivity can be obtained from laboratory measurements. Thus a dual purpose of surface material identification and surface sensible temperature can, in principle, be accomplished. However, most TES data will be acquired over the oceans, whose

emissivities are well-known. That is, the parameter will be introduced as an *input* to the retrieval process. The same may be true for snow and ice.

3.10: Surface Reflectance

Surface reflectance for TES downlooking data would be a non-standard product. However, it will almost certainly be necessary to parameterize the value as either Lambertian or specular because no useful data are available.

3.11: Unexpected Species

Because TES has complete spectral coverage, it follows that it will be able to detect and monitor unexpected species such as new chemicals not currently found in the atmosphere but which may occur in the future, or transient events such as major industrial accidents (e.g., methyl isocyanate from a Bhopal-type of accident) and volcanic eruptions. It should also be noted that, in general, the Level 2 retrieval algorithm must be able to incorporate these species because of the likelihood that their omission would corrupt the retrieval process.

3.12: Summary

Table I shows the list of Standard Product molecules which TES will provide during Global Surveys. In addition, unusual or unexpected species will be "flagged" in the data stream. Their retrieval and analysis would be undertaken as Special Products, as would all local and regional observations.

3.13: Synergism

3.13.1: Introduction. While TES is a "stand-alone" instrument in that data from other instruments are not *required* (beyond spacecraft ephemeris and timing information), significant benefits will accrue both to TES and the EOS mission in general from the synergistic application of data products from other instruments.

3.13.2: EOS Facility Instruments

- **Atmospheric Infrared Sounder (AIRS; EOS PM1) (TL: M. Chahine, JPL).** A strong synergism should develop with AIRS because, while TES has better spectral, spatial and height resolution, its spatial coverage is limited. AIRS has global coverage capability and can be used to extrapolate TES coverage over wider regions. Conversely, TES can offer AIRS help in resolving spectral overlap problems, especially if new and unexpected chemicals appear in the atmosphere.

- **Measurements of Pollution in the Troposphere (MOPITT; EOS AM1) (PI: J. Drummond, U. Toronto).** MOPITT maps tropospheric CO and CH$_4$ by gas correlation techniques. These gases also form part of the TES inventory, so there is a clear-cut benefit to both systems by collaboration. Unfortunately, the period when both MOPITT and TES are in orbit is likely to be limited.

- **Microwave Limb Sounder (MLS; EOS CHEM) (PI: J. Waters, JPL).** MLS and TES are complementary systems in that they observe many of the same species and the retrieval approaches are quite similar. Furthermore, their height coverages overlap from the upper troposphere through the lower stratosphere, so concentration intercomparisons will obviously be beneficial to both experiments.

- **High-Resolution Dynamics Limb Sounder (HIRDLS; EOS CHEM) (Co-PI's: J. Barnett, Oxford U.; J. Gille, NCAR).** Although primarily aimed at the dynamical processes of the lower stratosphere, HIRDLS observes many of the same species as TES with very good vertical resolution (1 km). Thus TES - HIRDLS intercomparisons would be mutually beneficial.

- **Ozone Measuring Instrument (OMI; EOS CHEM) (Netherlands/Finland).** OMI is a recent addition to the CHEM platform. It is a TOMS-like total ozone measuring instrument (i.e., works only in daylight). Nevertheless, OMI-TES intercomparisons will be beneficial to both instruments. Furthermore, OMI being an imager, its cloud-cover product could be very useful to TES.

3.13.4: Other investigations. A number of other non-EOS investigations are pertinent to TES, in particular our own airborne system AES which was specifically designed to generate TES-like products using very similar technology. In addition, a number of other ground, aircraft and balloon-based systems are likely candidates for field verification studies. These are discussed later in the Calibration Plan (§6.3). There are, in addition, a number of spaceflight programs that are pertinent to the TES investigation. Among these are the European ENVISAT & METOP Polar Platforms. Two infrared spectrometers (MIPAS and IASI) are being proposed for these spacecraft and it is possible that, in the future, Japan will replace the IMG instrument that was lost due to the ADEOS spacecraft failure. Through workshops and personal contacts, the TES team will keep abreast of these developments and pool results when appropriate. Certainly, multiple sensors flying simultaneously will be of great benefit in overcoming the spatial sampling problems of single spectrometers in polar orbits.

4: SPECTRAL DATABASE REQUIREMENTS

4.1: Introduction

Reliable inversion of spectral remote sensing data (TES or otherwise) requires accurate spectroscopic parameters. By operating in the infrared, TES takes advantage of a long history of efforts to catalogue and refine atmospheric line parameter data (e.g., the HITRAN compilations since 1973) in a region where most telluric molecules have strong vibration-rotation bands. For many years NASA and other agencies have also funded IR laboratory spectroscopic research to support spectral database improvements for other remote sensing programs (e.g., ATMOS, UARS). As proven by the success of the ATMOS/ATLAS science analysis, such work is crucial for the successful identification and quantitative inversion of weak features of key trace gases (e.g., NO, NO_2) superimposed on stronger lines of more abundant species (e.g., H_2O, CO_2, O_3).

4.2: Types of Database

There are two categories of spectral databases: the "line-by-line" listings maintained and periodically updated by HITRAN (Table III shows the species currently available in HITRAN) as well as special versions for projects such as ATMOS; and "absorption coefficient" or "cross section" tabulations, generally used for complex molecules exhibiting little or no rotational fine structure at atmospheric temperatures and pressures (Tables IV and V), or molecules of such limited interest to the atmospheric community that line-by-line analysis is a low priority. Although mostly of poorer quality than the "line-by-line" data, the "absorption coefficient" data are gradually improving. Temperature-dependent cross-section measurements have been reported recently for a number of heavy molecules, and these coefficients are now included as a separate file on updates of the HITRAN line parameters compilation. Laboratory studies are also in progress to measure temperature-dependent cross-sections at improved spectral resolution and also to define the pressure-dependence of the absorption coefficients. In addition, formulations have been generated to describe the various types of continuum absorption that are observed in the infrared - notably H_2O, N_2 and O_2. These are also updated from time-to-time.

It should also be noted that HITRAN "bundles" isotopomers into the same grouping (i.e., the abundance ratios are pre-assigned). However, it is well-known that certain isotopomers (notably HDO) show significant height variability relative to the parent molecule, so they will be extracted and maintained as separate suitably-scaled files to permit retrieval. Table III reflects this decision.

Table III: Current HITRAN Line List Species

HITRAN [TES] Index No.	Molecule	Comments
1	H_2O	HDO & $H_2^{17}O$ Separated
[1a]	HDO	
[1b]	$H_2^{17}O$	
2	CO_2	
3	O_3	$^{16}O^{17}O^{16}O$ & $^{17}O^{16}O^{16}O$ Separated
[3a]	$^{16}O^{17}O^{16}O$	
[3b]	$^{17}O^{16}O^{16}O$	
4	N_2O	
5	CO	
6	CH_4	CH_3D Separated
[6a]	CH_3D	
7	O_2	
8	NO	
9	SO_2	
10	NO_2	
11	NH_3	
12	HNO_3	
13	OH	
14 **	(HF)	** Not Used by TES **
15	HCl	
16 **	(HBr)	** Not Used by TES **
17 **	(HI)	** Not Used by TES **
18	ClO	

19	OCS	
20	HCOH	
21	HOCl	
22	N_2	
23	HCN	
24	CH_3Cl	
25	H_2O_2	
26	C_2H_2	
27	C_2H_6	
28 **	(PH_3)	** Not Used by TES **
29	COF_2	
30	SF_6	Also need X-sections
31	H_2S	
32	HCOOH	
33 **	(HO_2)	** Not Used by TES **
34 **	(O)	** Not Used by TES **
35	$ClONO_2$	Also need X-sections
36 **	(NO+)	** Not Used by TES **
37 **	(HOBr)	** Not Used by TES **

4.3: Tropospheric Requirements

For TES, there is a need for IR spectroscopic research to be directed more toward key tropospheric molecules. For example, there is a clear need for temperature-dependent absorption coefficient measurements of peroxynitric acid (HO_2NO_2) and PAN and common organic solvents such alcohols, ketones, benzene, etc.). The requirements for the laboratory measurements depend on the molecule. Table IV shows the heavy-molecule species that are currently available and Table V those for which data are urgently needed to support TES retrievals.

Table IV: HITRAN Cross-Section Species Used by TES

Molecule	Common Name
CCl_4	Carbon Tetrachloride
CCl_3F	CFC-11
CCl_2F_2	CFC-12
$CClF_3$	CFC-13
CF_4	CFC-14
$CHCl_2F$	HCFC-21
$CHClF_2$	HCFC-22
$C_2Cl_3F_3$	CFC-113
$C_2Cl_2F_4$	CFC-114
C_2ClF_5	CFC-115
N_2O_5	Dinitrogen Pentoxide
HO_2NO_2	Peroxynitric Acid†
SF_6	Sulphur Hexafluoride
$ClONO_2$	Chlorine Nitrate

† Seriously incomplete

**Table V: Additional Cross-Section Species Needed by TES
(but no useful data available)**

Molecule	Common Name
C_2H_6	Benzene
C_2H_4	Ethylene
C_3H_8	Propane
$CH_3C(O)CH_3$	Acetone
CH_3OH	Methyl Alcohol
$CH_3C(O)NO_2$	Peroxyacetyl Nitrate (PAN)
HO_2NO_2	Peroxynitric Acid†
CH_3COOH	Acetic Acid
CH_3OOH	Methyl Hydroperoxide

† For bands not in HITRAN

4.4: Field Validation Requirements

There can never be any substitute for real field data both to validate the retrieval process and the spectral databases generated as just described. A common experience in such studies is the discovery that unexpected interferences occur in spectral regions that were believed to be either clear or at least well-understood.

Thus, while every effort will be made to generate realistic synthetic spectra for testing TES retrieval algorithms, synthetic data alone will not provide a sufficient test of those programs. Therefore, well in advance of launch, the TES team will require high quality, accurately calibrated, IR atmospheric emission data sets similar in quality to those of TES. Ideally, both limb and nadir spectra would be recorded along with correlative measurements for use in validating the inversions of atmospheric parameters (e.g., O_3 profile, pressure & temperature).

A major contributor to this effort is expected to be the Airborne Emission Spectrometer (AES) which has been specifically designed to emulate the TES downlooking modes from an aircraft. AES commenced operations in 1994 and is planned to continue throughout the EOS era.

For limb-viewing tests, MIPAS (to be launched in 2000) will provide data at similar resolution to TES.

THIS PAGE INTENTIONALLY LEFT BLANK

5: SYSTEM & MEASUREMENT REQUIREMENTS

5.1: Introduction

Based upon the detailed scientific objectives discussed in §3, it is possible to define requirements in the areas of:

- Spectrometer type
- Spectral coverage, resolution and accuracy;
- Spatial coverage and resolution;
- Temporal coverage and resolution;
- Dynamic range and radiometric accuracy;
- Operations;
- System parameters;
- Data system and products.

5.2: Spectrometer Type

Spectral lines formed in the troposphere have a shape and width that is determined by the atmospheric pressure. Thus they become narrower as the altitude increases until the random motions of the molecules dominates (so-called "Doppler broadening"). The situation is illustrated in Fig. 3, where it can be seen that this cross-over occurs in the lower stratosphere (i.e. near the top of the range of interest to TES).

The absorption coefficient for a purely Doppler-broadened line is

$$\kappa_D(\nu - \nu_0) = \frac{S(\nu_0)\exp[-ln2\{(\nu - \nu_0)/\alpha_D\}^2]}{\alpha_D\sqrt{(\pi \, ln2)}}$$

(5.1)

where S is the line strength (tabulated), ν is frequency (cm^{-1}), ν_0 is the frequency of the line center and α_D, the Doppler width, is given by

$$\alpha_D = (\nu_0/c)\sqrt{2 \cdot ln2 \cdot kT/M}$$
$$= 3.581x10^{-7}\nu_0\sqrt{T/M} \quad cm^{-1}$$

(5.2)

33

The absorption coefficient of pressure broadened lines κ_L is reasonably well described by the Lorentz Function:

$$\kappa_L(\nu-\nu_0)=\frac{S(\nu_0)\cdot\alpha_L}{\pi\cdot[(\nu-\nu_0)^2+\alpha_L^2]}$$

(5.3)

where α_L is the broadening coefficient (defined as the *half-width* at half-maximum of the function). α_L, which is directly proportional to pressure, is determined empirically through laboratory investigations and is tabulated at STP because it also has a weak (and often unknown) temperature dependence (roughly as $T^{\frac{1}{2}}$).

Now, it is a curious (but explicable) property of α_L that its value is nearly independent of species and frequency (wavelength) and takes a value of about 0.05 cm^{-1} near the Earth's surface. Thus, when the product of κ and L is small (≤ 0.1; a so-called "weak line"), the full width at half maximum depth of the spectral line is $2\alpha_L$ (≈ 0.1 cm^{-1}) for all molecules anywhere in the spectrum.

The absorption A ($= 1$ - transmission) of the gas is related to the absorption coefficient by:

$$A(\nu-\nu_0) = 1- \exp[-\kappa(\nu-\nu_0).L]$$

(5.4)

where L is the number of molecules of the particular species in the line of sight (at constant temperature and pressure).

In a later section (§5.4), it is shown that the optimum recovery of information from a spectrum occurs when the instrument spectral resolution matches the width of the spectral features and it is precisely those weak features (i.e., those near the limit of detectability) that we must be able to observe because the fractional concentrations of the important species to be measured are very low (parts per trillion in some cases). There is only one class of spectrometer that meets the requirements of broad spectral coverage (see next section) and frequency-independent spectral resolution - a Fourier Transform Spectrometer (FTS, see Appendix A).

*** TES will therefore be an FTS ***
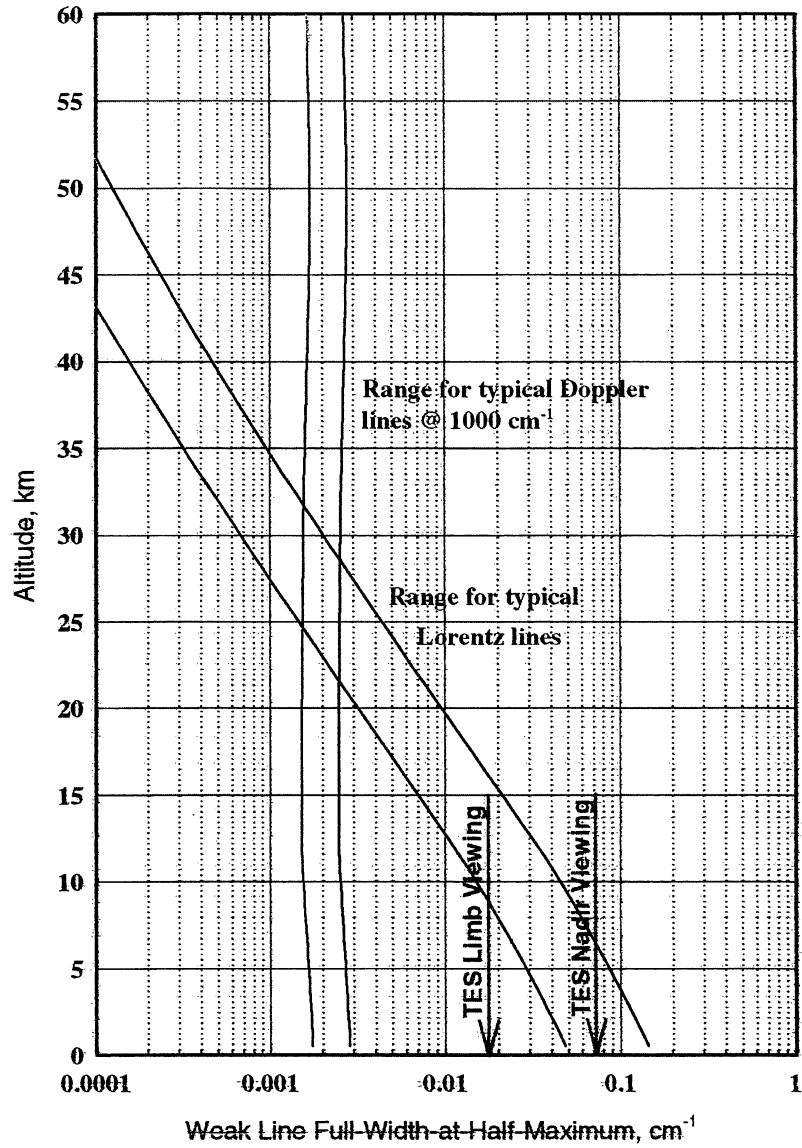
Fig. 3: Variation of typical spectral linewidths with altitude

5.3: Spectral Coverage

Tropospheric spectra are very dense and complex. "Window" regions are rare and, in any case, are used for analysis of the surface. The large suite of molecules listed in Tables I & II have absorption/emission features throughout the infrared. Furthermore, the tables are incomplete: some molecules of known interest are missing and it is certain that new ones will be added as the mission progresses. It, therefore, follows that *continuous* spectral coverage is mandatory. *Simultaneous* coverage is also required in that the more molecules that can be measured in a single sequence, the better, because it is often the chemistry of *families* of molecules that is important, not the individual species. However, considerations of signal-to-noise ratio (SNR) and data rate indicate that sequential coverage in selected bands 200 - 300 cm^{-1} wide is to be preferred, permitting four different detector technologies (in the sense of chemical composition) to be used, each optimized for a different spectral region. The detector arrays are labeled 1A, 1B, 2A & 2B and their associated filters by an added index.

Table VI shows the spectral coverage needed to measure ozone and its precursors. It is obvious that the *minimum* requirement is for coverage between 650 and 3050 cm^{-1} (3.2 - 15.4 μm) and, should detector technology advance in time, extension down to 600 cm^{-1} (16.7 μm) would improve our capability for measuring atmospheric temperature (a crucial parameter).

The simplest type of FTS is based on the classical Michelson interferometer. It does, however, have an important defect: half of the incoming signal is returned to the source. A better configuration introduced by P. Connes in 1964 avoids this problem (see Fig. 4) by separating the light-paths so that there are 2 input and 2 output ports. It is readily shown that the interferograms at the output ports contain the *difference* between the two input signals and, further (by conservation of energy), that the output interferograms are complementary. TES will employ this configuration and the detector arrays will be assigned to the outputs in such a manner as to provide the largest possible frequency gap between them because the dichroic reflectors required further to split the beams will have relatively "slow" transitions between efficient reflection and transmission. Table VII shows how this may be accomplished for the two outputs: the dichroics must therefore have their cross-overs set at 1525 cm^{-1} in output 1 and at 1000 cm^{-1} in output 2, although the tolerances are quite loose ($\pm$25 cm^{-1}). However, in order to conserve the maximum efficiency, each filter should have a peak transmittance of at least 80% and be operated at 65 kelvin in collimated normal-incidence light. These requirements that should be relatively simple to achieve since the filters are quite broad. Furthermore, for test purposes, each filter wheel must have both "fully open" and "fully closed" positions. Table VI shows a set of filters that accomplishes the measurement requirements and Table IX shows the principal species available in each filter band.

Considerations of signal-to-noise ratio dictate that downlooking coverage can encompass the complete 650 - 3050 cm^{-1} range, whereas, at the limb, the coverage will be limited to 650 - 2450 cm^{-1}.

36

Table VI: Spectral Coverage Requirements for Ozone & its Precursors

Species	Spectral Region cm^{-1}	μm
Ozone (O_3)	970 - 1180	8.47 - 10.31
Nitric Oxide (NO)	1800 - 1950	5.13 - 5.56
Nitrogen Dioxide (NO_2)	750 - 850	11.76 - 13.33
	1590 - 1615	6.19 - 6.29
Nitric Acid (HNO_3)	860 - 920	10.87 - 11.63
Water Vapor (H_2O)	1200 - 1800	5.56 - 8.33
Carbon Monoxide (CO)	2060 - 2200	4.55 - 4.85
Methane (CH_4)	1530 - 1570	6.37 - 6.54
	2950 - 3050	3.28 - 3.39

For atmospheric temperature:

Carbon Dioxide (CO_2)	2200 - 2450	4.08 - 4.55
	650 - 800	12.50 - 15.38

Table VII: Spectral Coverage Requirements by Detector Array

Output	Array I.D.	Lower Bound (cm^{-1})	Upper Bound (cm^{-1})
1	A	1900	3050
	B	820	1150
2	A	1100	1950
	B	650	900
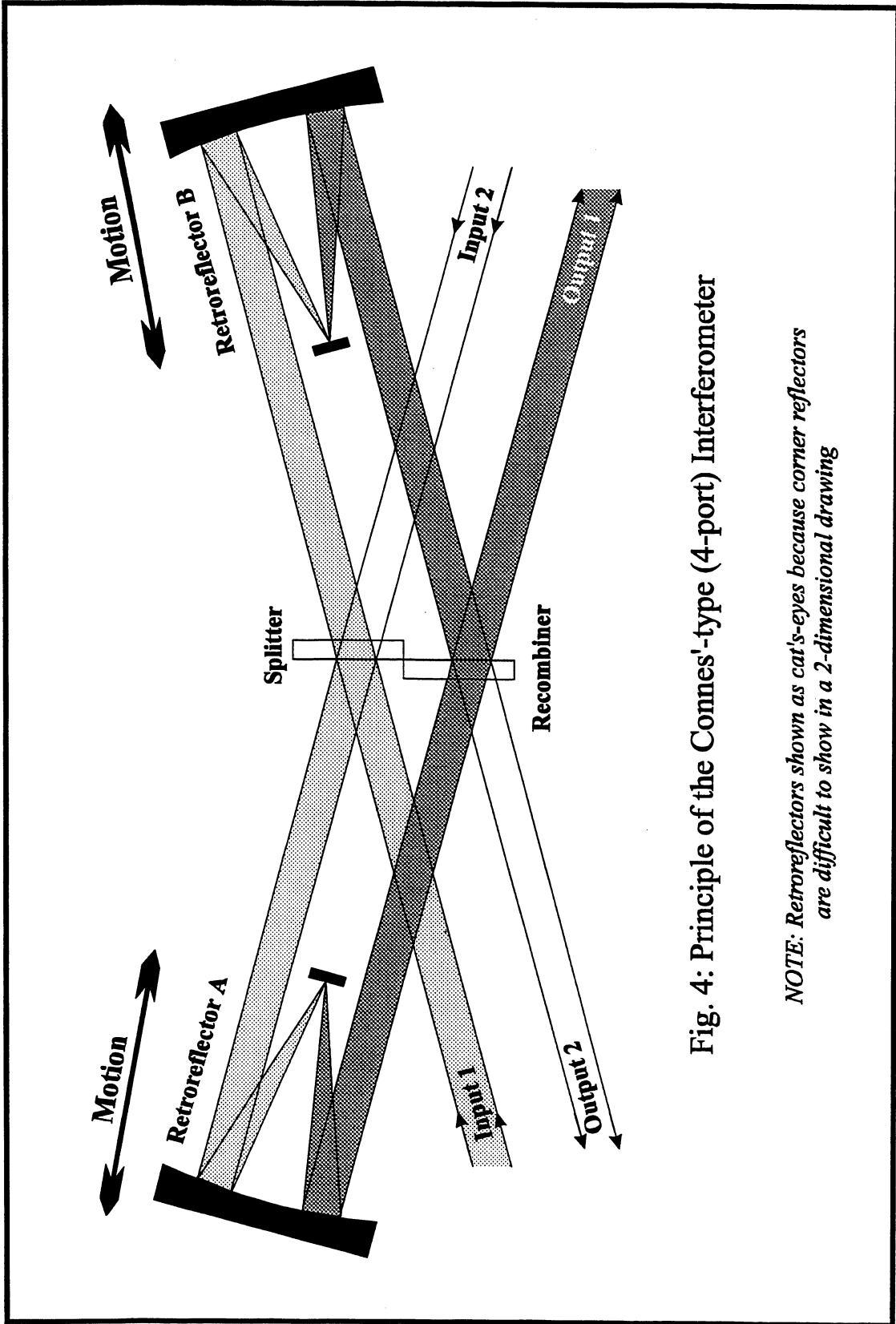
Fig. 4: Principle of the Connes'-type (4-port) Interferometer

NOTE: Retroreflectors shown as cat's-eyes because corner reflectors
are difficult to show in a 2-dimensional drawing

38

It should also be noted that an appropriate portion of the optical and electronic system must be capable of transmitting and detecting the 1.06 μm beam from the Nd:YAG control laser and do so with a reasonable modulation index (> 50% is the requirement).

5.3.1: Filter Specifications

The passband requirements on the optical filters are dictated by two conflicting considerations: a) the bands must be wide enough to permit the required molecular bands (which are typically 100 - 200 cm^{-1} wide) to be observed with as few breaks as possible; b) the bands must be narrow enough to control the instrumental background. Furthermore, we must resort to undersampling of the interferograms in order to minimize the data rate, which also places stringent limits on the allowable width of the passbands. This topic is expanded on in §5.16. Accordingly, each of the filters must adhere to the requirements shown in Table VII (values given are the frequencies of 50% of peak transmittance):

Table VIII: Optical Filter Specifications

Filter I.D.	Lower Half-Power Frequency (cm^{-1})	Upper Half-Power Frequency (cm^{-1})	
1A1	1900 (+0, -50)	2250 (-0, +50)	
1A2	2200 (+0, -50)	2450 (-0, +50)	
1A3	2425 (+0, -50)	2650 (-0, +50)	
1A4	2600 (+0, -50)	2850 (-0, +50)	
1A5	2800 (+0, -50)	3050 (-0, +50)	
1B1	820 (+0, -50)	1050 (-0, +50)	
1B2	950 (+0, -50)	1150 (-0, +50)	
2A1	1100 (+0, -50)	1325 (-0, +50)	
2A2	1300 (+0, -50)	1550 (-0, +50)	
2A3	1500 (+0, -50)	1750 (-0, +50)	
2A4	1700 (+0, -50)	1950 (-0, +50)	
2B1:	650 (+0, -50)	900 (-0, +50)	(see footnote[1])

---

[1] In the event that long-wave (600 cm^{-1}) detectors become available in time, the low frequency limit of Filter 2B1 will also be reduced to 600 cm^{-1}

Table IX: FILTER BANDS & SPECIES COVERAGE

Filter ID	Filter Half-Power Points, cm⁻¹		Temperatures	Species
Array 1A (1900 - 3050 cm⁻¹)				
1A1	1900	2250	T_b	O_3, CO, N_2O, NO, OCS, CH_3D
1A2	2200	2450	T_a	CO_2, N_2
1A3	2425	2650	T_b	N_2O
1A4	2600	2850	T_b	HDO
1A5	2800	3050	T_b	CH_4, HCl, O_3
Array 1B (820 - 1150 cm⁻¹)				
1B1	820	1050	T_b	HNO_3, NH_3, CFC11, CFC12, SF_6, O_3, C_2H_4
1B2	950	1150	T_b	O_3, NH_3, CFC11, CFC12, N_2O
Array 2A (1100 - 1950 cm⁻¹)				
2A1	1100	1325	T_b	O_3, N_2O, HNO_3, CFC12, SO_2, CH_4, $CH_3C(O)CH_3$, H_2O_2
2A2	1300	1550		O_3, HNO_3, CH_4
2A3	1500	1750		H_2O, NO_2
2A4	1700	1950		H_2O, NO
Array 2B (650 - 900 cm⁻¹)				
2B1	650	900	T_a	CO_2, HNO_3, CFC11, NO_2, C_2H_2, HCN

Notes: T_a = Atmospheric Temperature Profile; T_b = Surface Brightness Temperature

Revised 2/11/99

5.3.2: Filter Wheels

Engineering considerations have dictated that motions of the four filter wheels must be limited to single steps (i.e., to an adjacent position). As a consequence, and based on the Mission Plan (§7), the ordering of the filters in the wheels is not simply sequential (see Table X and Figs. 5 & 6).

*** This ordering is essential and must be adhered to ***

Table X: Filter Wheel Layouts

Position	Array 1A	Array 1B	Array 2A	Array 2B
0	1A4	1B2*†	2A4†	2B1*†
1	1A5	1B1*†	2A1*†	Closed
2	1A1*†	Closed	2A3	Closed
3	1A2*	Closed	2A2	Closed
4	1A3	Closed	Closed	Closed
5	Closed	Closed	Closed	Closed
6	Open	Open	Open	Open
7	Closed	Closed	Closed	Closed

* = Global Survey nadir position
† = Global Survey limb position

Fig. 5: Dewar 1 Filter Wheel Layouts
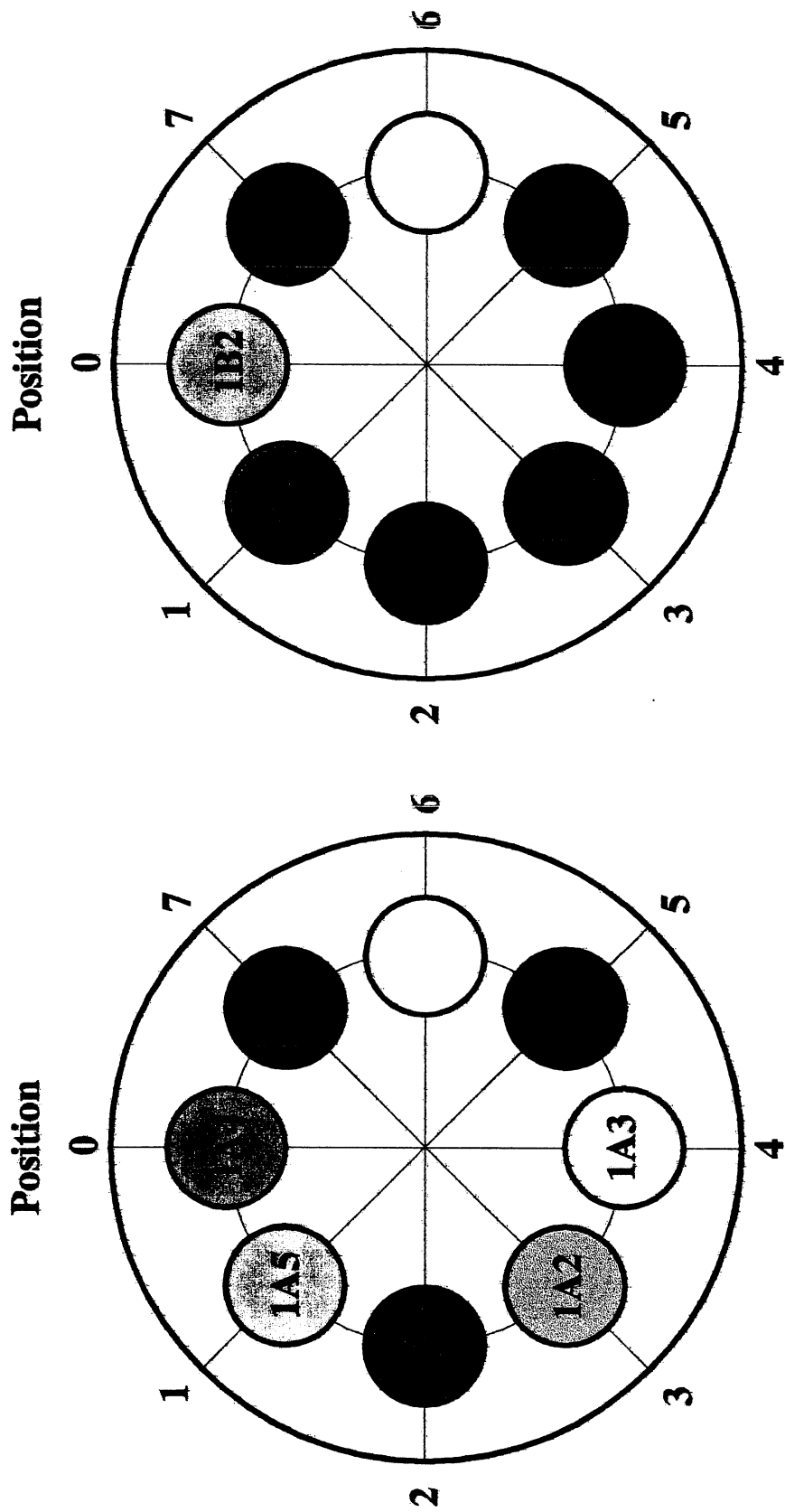
ARRAY 1A

ARRAY 1B

Fig.6: Dewar 2 Filter Wheel Layouts
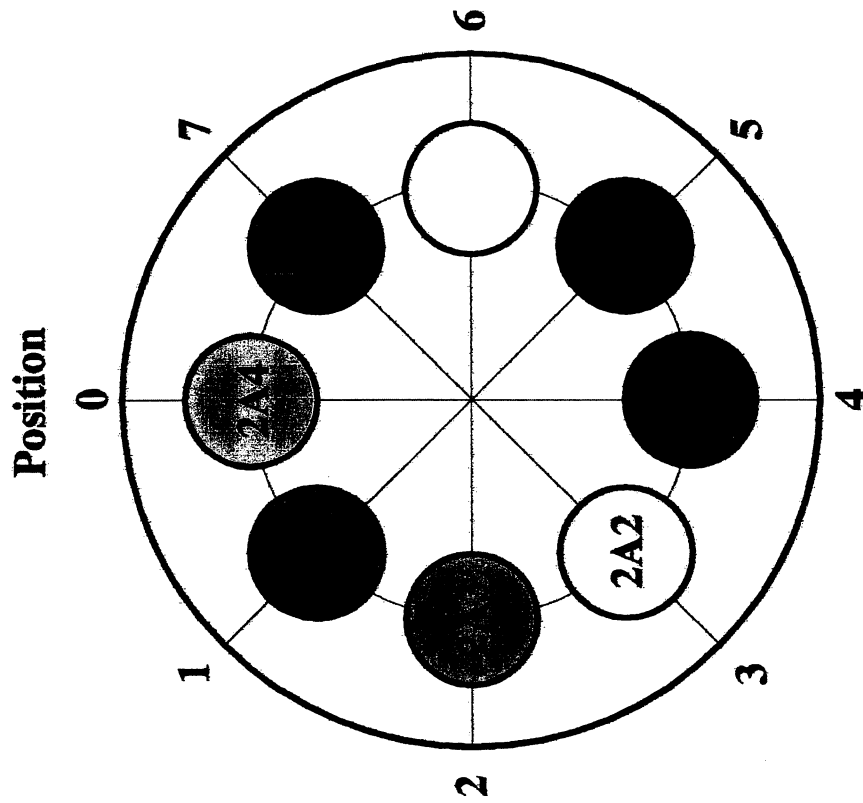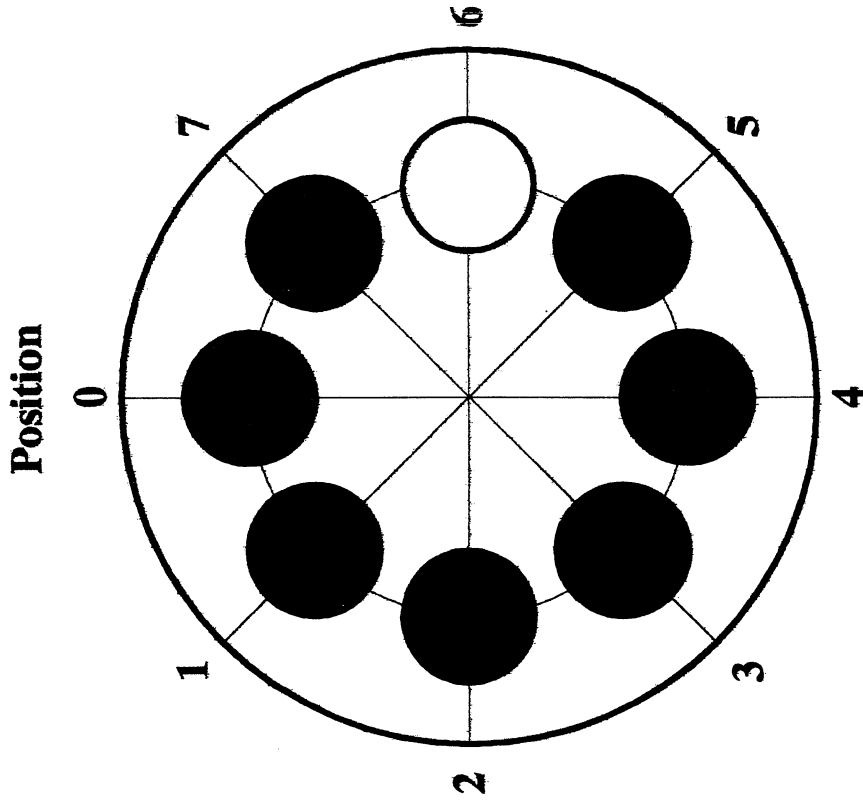
ARRAY 2A

ARRAY 2B

5.4: Spectral Resolution

It is demonstrable (*via* the Optimum Filter Theorem and actual trial retrieval experiments; see Appendix A.8) that the maximum information throughput of a spectrometer occurs when the spectral resolution matches the inherent width of the spectral features to be studied. As discussed in §5.2, in the Earth's lower atmosphere weak spectral features have a full width at half maximum (FWHM) of about 0.10 cm^{-1} (1 cm^{-1} ≡ 30 GHz). As the altitude increases, the pressure decreases (roughly exponentially) and the spectral lines become narrower. At 10 km, the lines are about 0.025 cm^{-1} wide (see Fig. 3).

Accordingly, TES will have a maximum spectral resolution not worse than 0.025 cm^{-1}. The resolution will be adjustable under software control so that downlooking observations into the lower atmosphere can be accomplished at 0.1 cm^{-1} resolution. For an FTS, these requirements demand a maximum optical path difference (OPD) of 33.8 cm. The baseline concept for TES further requires that this path difference be available in either sense. The lower, downlooking resolution of 0.1 cm^{-1} will be accomplished with a reduced OPD of 8.45 cm (again, in either sense).

5.5: Spectral Accuracy

5.5.1: Introduction. The retrieval algorithms to be applied to the TES spectra assume that the frequency scale has almost arbitrary accuracy (the goal is ± 0.00025 cm^{-1}). There are, unfortunately, a number of effects that can cause the measured frequencies to be in error. These are:

- All detectors (pixels) are off-axis;
- All pixels have a finite field-of-view;
- Aberrations and diffraction modify the ray paths;
- Drifts of the control laser cause scale changes;
- Interferogram sampling errors induce frequency errors;
- Source-spectrometer radial velocities induce Doppler shifts.

The phenomena are discussed in the following sections; however, it is worth remarking that the scale changes induced by real or apparent laser frequency changes can be "back-calibrated" so that, in the Level 1B data processing, a different effective laser frequency will be assigned to each pixel.

5.5.2: Off-axis effects. Fig. 7 shows the relative frequency shift as a function of off-axis pixel number, using the approximation developed in Appendix A.6. The effect is significant, approaching 0.1 cm^{-1} for the outermost detector elements at 3050 cm^{-1}. A more accurate analysis requires numerical integration and knowledge of the wavefront errors and detector non-uniformities (next topic).

44
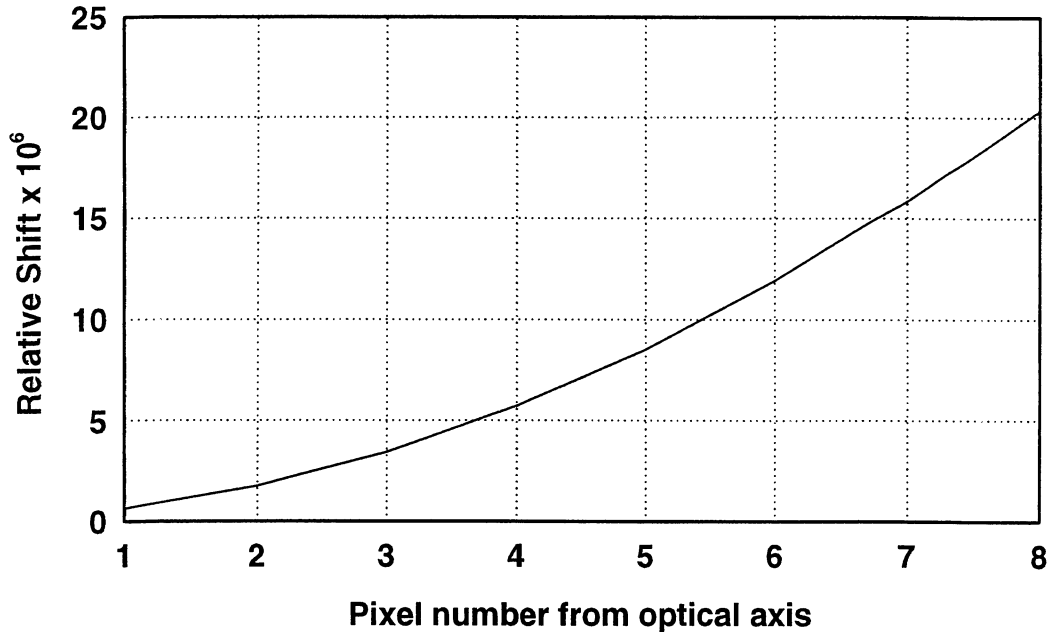
Fig. 7: Relative Frequency Shift as a Function of Off-Axis Pixel Number

5.5.3: Field-of-view effects. As suggested above, finite field-of-view effects (see Appendix A.6) cannot properly be distinguished from the off-axis frequency shifts. Accordingly, a computer program has been developed that "traces" 500 monochromatic rays through each pixel (75 μrad grid) and averages the outcome in the form of a theoretical interferogram. Figs. 8a & 9a show the results for Pixels 1 & 8 near 2450 cm^{-1} (the highest frequency for the high resolution, limb-viewing, case). It is evident that significant self-apodization[2] occurs for the off-axis pixels. At lower resolution (i.e., the downlooking case) or lower frequencies the plots would look much more like a cosine-wave of constant amplitude (the ideal case).

Figs. 8b & 9b show the Fourier Transforms of 8a & 9a, (the Instrumental Line Shape [ILS]) and a sinc function representing the "ideal" solution of an on-axis, zero field-of-view, ray of the same frequency. The shifts, broadening and asymmetry are clearly evident (the broadening is quantified and displayed as the sum of the ideal (sinc) halfwidth and the impact of the off-axis effect; the symmetry factor is simply the ratio of the depths of the two closest minima). Note that no additional apodizations have been applied; it is possible, however, to develop

---

[2] Apodization is, in general, any procedure used to damp out oscillations in the wings of the Instrumental Line Shape function (the impulse response). It can either be applied deliberately during data analysis or it may occur naturally, in which case it is termed "self-apodization". Apodization is always accompanied by a loss of spectral resolution.

45

functions to symmetrize the ILS (a highly desirable feature) while maintaining the resolution. Such functions are based on the envelope of a monochromatic interferogram computed at the central frequency of each filter. However, in no case is the unapodized resolution worse than requirements. The analytic derivation of these correction functions has been discussed at length in the Level 1B ATBD (JPL D- 16479; K. Bowman & H. Worden).

5.5.4: Aberrations and Diffraction. These cause the effective off-axis angles somewhat to differ from the simple analyses presented above. The effect is partially calculable (by ray tracing) but must be supplemented by laboratory calibrations using known spectral sources.

A related (although causally different) effect is induced by detector spatial non-uniformities. Ray-tracing assigns an equal energy weight to each ray. Obviously, a badly aberrated ray falling on a detector "bad" spot is less important than one falling on a "hot" spot. Again, only laboratory calibrations can account for such effects.

5.5.5: Control laser frequency. The absolute frequency of a Nd:YAG laser is temperature dependent so an uncertainty can arise which can only be removed by back-calibration against well-known atmospheric features. The stability requirement is $\pm$ 7.5 MHz (peak-to-peak) in any 16 second interval. The wavelength of a Nd:YAG laser is rather longer than desirable (approx. 1.06415 μm $\equiv$ 9397.171 cm^{-1}) but it has been deemed inappropriate to sample at half-wavelength intervals (i.e., on both negative-going *and* positive-going zero crossings because of the danger of periodic sampling errors (next topic)

5.5.6: Interferogram sampling errors. The relative position of the interferogram samples must be known (and constant) to 2 nm RMS for random errors and to 1 nm peak-to-peak for periodic errors. Larger errors introduce both amplitude uncertainties into the spectra and second-order frequency shifts. The problem will be solved by proper instrument design.
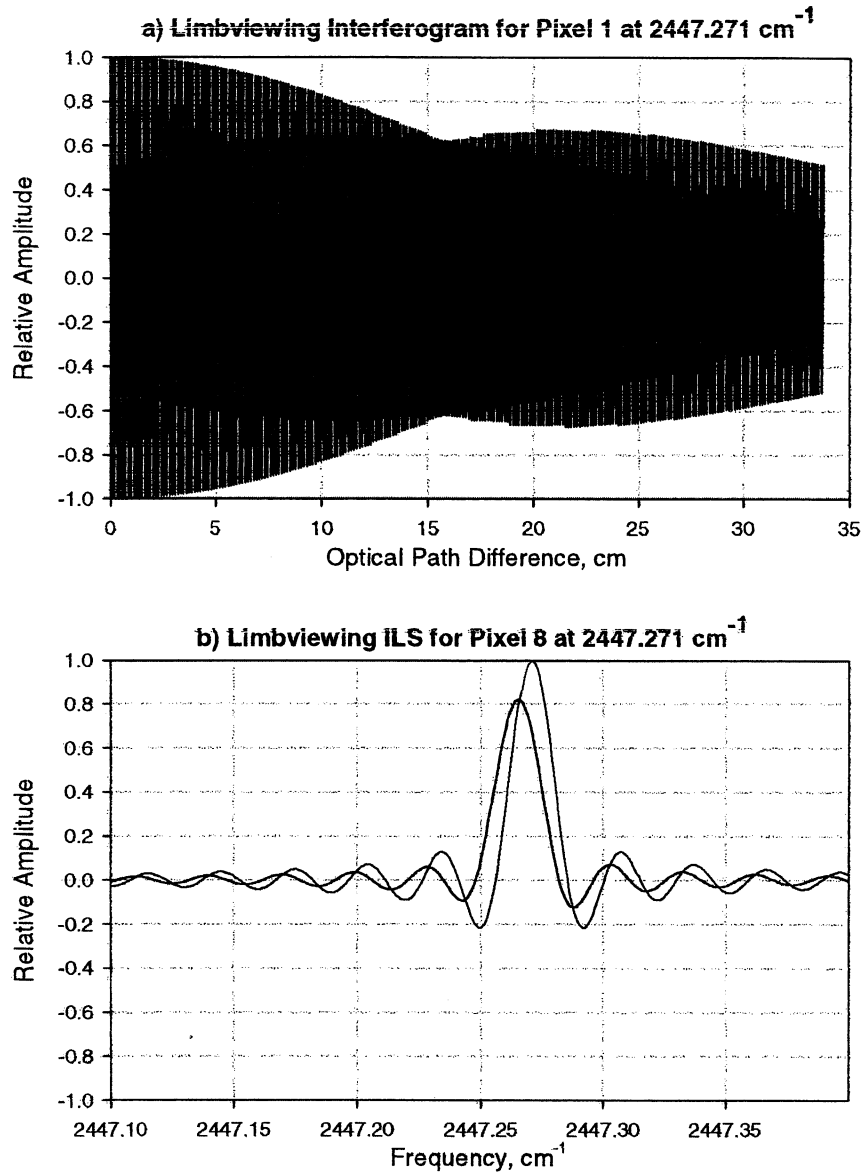
Fig. 8: a) High-resolution theoretical (limb-viewing) monochromatic interferogram for Pixel 1 (the closest to the axis) near 2450 cm^{-1}; b) Black - Resultant ILS, Red - Ideal On-Axis Sinc Function

47
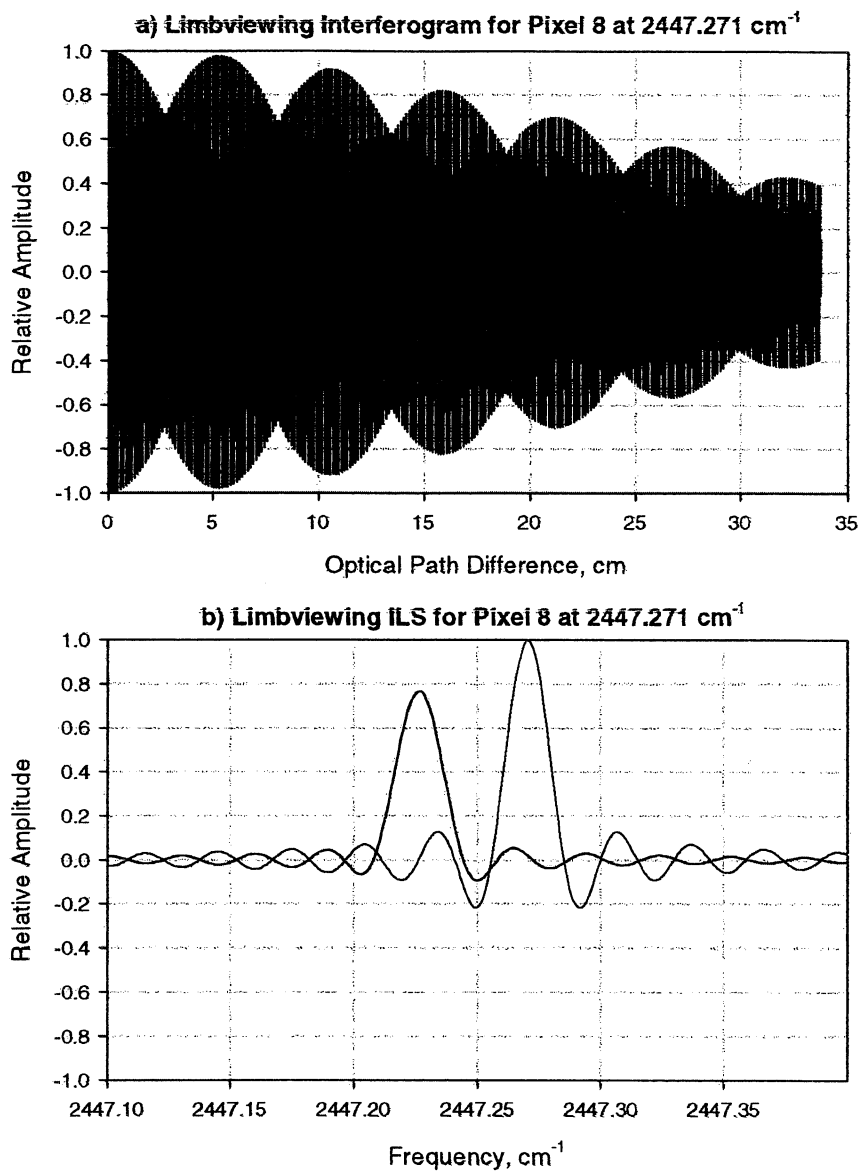
Fig. 9: a) High-resolution theoretical (limb-viewing) monochromatic
interferogram for Pixel 8 (the furthest from the axis) near 2450 cm⁻¹, note the
increased self-apodization compared to 8a; b) Black - Resultant ILS, Red - Ideal
On-Axis Sinc Function

48

5.5.7: Control laser fringe amplitude stability. The previous topic also places constraints on the allowable variation in control laser fringe amplitude. A change in amplitude induces a phase shift into the fringes, which has two impacts that are readily calculated: the positional accuracy of 1 nm is essentially 0.1% of the control fringe spacing (in OPD). A shift of this amount corresponds to an amplitude change of 0.5%, which is therefore the fringe-to-fringe stability requirement. An end-to-end (in OPD) "droop" or total variation in amplitude also results in an apparent change in laser frequency - about 0.02 cm^{-1} for a droop of a factor of two. This is not a problem provided that the droop does not change substantially between calibrations.

5.5.8: Doppler shifts. For any viewing direction not perpendicular to the spacecraft velocity vector, a component of Doppler shift will be introduced (e.g., for TES trailing-limb observations). The effect is largely calculable from the spacecraft ephemeris and pointing data, but additional effects can occur due to winds. The effect is clearly seen in the ATMOS data and must be removed by empirical line-fitting.

The data required are the 3 axes of spacecraft attitude, the time of observation (the time to cross 1 narrow angle pixel - 70 milliseconds - accuracy suffices here) and the spacecraft ephemeris, all of which are expected to be available either directly within the science data stream or from the Flight Dynamics office at GSFC.

NADIR PROJECTION

Flight Path

7.5 mrad

0.75 mrad

In-track swath ~ 13.2 mrad

5.3 km

~ +4.2 km

Optic Axis

0.53 km

~ -4.2 km

LIMB PROJECTION

Flight Path perpendicular to page

7.5 mrad

0.75 mrad

~ 33 km altitude

16 km aimpoint

2.3 km

0 km altitude

23 km
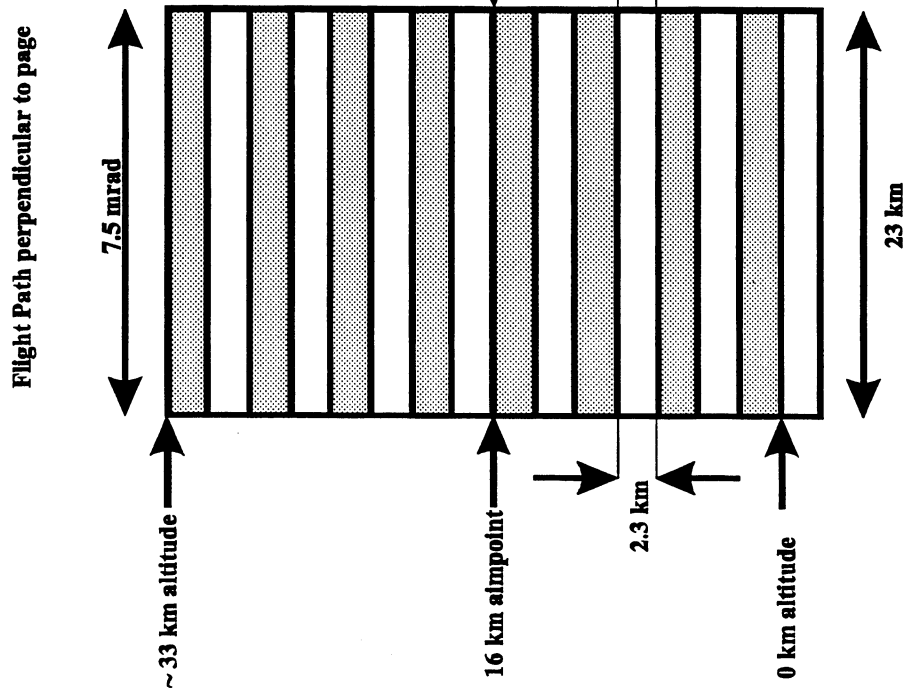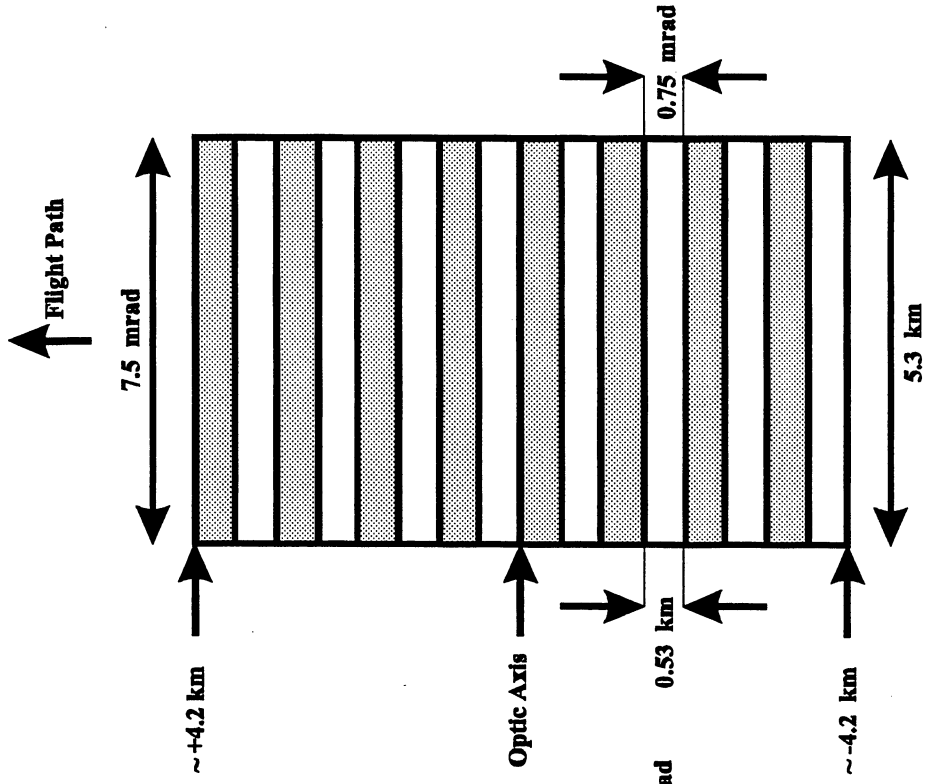
Vertical FOV ~ 13.2 mrad

Fig. 10: TES Detectors Projected to the Nadir and Limb

50

5.6: Spatial Resolution

TES will operate in two different ways: as a downlooking (near nadir) sounder and as a limb sounder (Fig. 10). When downlooking, TES offers good horizontal spatial resolution (see below) but limited height resolution: details of radiative transfer show that a nadir sounder is limited in height resolution to about 1/2 - 1 scale height. For a uniformly mixed species such as N_2O, the scale height[3] in the lower atmosphere is about 8 km. However, many problems in atmospheric physics and chemistry demand rather better height resolution. For such problems, limb sounding is the preferred approach because the height resolution is defined by the optical properties of the spectrometer, not the atmosphere. For TES, we have specified that the height resolution for limb observations should be 2.3 km. Since, for the EOS orbit, the range to the tangent point (the point of closest approach of the light path to the Earth's surface) is about 3100 km, it immediately follows that the IFOV in the vertical axis must be 0.75 mrad. In order to enhance the signal-to-noise ratio, however, the IFOV in the horizontal axis (i.e., parallel to the Earth's limb) can be much greater. For TES, we have chosen 7.5 mrad, giving each detector element a 10:1 aspect ratio (Fig. 10) and a 23 km horizontal resolution at the limb. This is not a serious problem because the resolution along the line of sight is, of course, ill-determined and large (many tens of kilometers). Such a detector geometry, from the 705 km EOS orbit, translates to a nadir resolution of about 0.5 x 5 km.

5.7: Spatial Coverage (Instantaneous)

The limits on instantaneous spatial coverage are intimately connected to the limits on spectral resolution discussed in §5.4 & §5.5. That is (to repeat), as one adds detectors to the arrays to increase the spatial coverage, the spectral properties deteriorate. As developed in Appendix A.5, the absolute limits on coverage are

$$L_r \le 2 \cdot R^2 \cdot \delta v / (v_{max} \cdot \delta L_r) \quad \text{in the interferometer radial axis, and} \tag{5.3}$$

$$\delta L_t \le 2 \cdot R \cdot \sqrt{(2 \cdot \delta v / v_{max})} \quad \text{in the tangential direction,} \tag{5.4}$$

where

δv	= required spectral resolution
v_{max}	= highest spectral frequency to be observed
L_r	= spatial coverage (radial axis)
δL_r	= required spatial resolution (radial axis)
δL_t	= required spatial resolution (= coverage, tangential axis)
R	= range from sensor to ground or limb tangent point

---

[3] Scale height is the altitude range over which the partial pressure declines by a factor 1/e.

Given the requirements of the previous sections, we may immediately infer that, at the limb ($\delta v = 0.025$ cm^{-1}; $v_{max} = 2450$ cm^{-1}; $\delta L_r = 2.3$ km; $R = 3100$ km), $L_r \leq 84$ km. In fact, prudence (and resources) suggests limiting the coverage to no more than a fraction of this theoretical limit (to 33 km).

In the tangential axis, the computation suggests that a width (at the limb) of 28 km could be used. Again, for prudence, we have selected the smaller value of 23 km, thus giving the detector elements a 10:1 aspect ratio as previously discussed.

The coarser spectral resolution (0.1 cm^{-1}) when downlooking, despite the higher frequency limit (3050 cm^{-1}), would permit a much larger array to be used (up to 100 elements) but, again, considerations of resources force us to a maximum of 16 elements. From a 705 km orbit, then, the nadir spatial resolution will be 5.3 x .53 km with a coverage of 5.3 x 8.4 km. It should also be noted that, as previously discussed, four separate and optically-conjugated 1x16 linear detector arrays are required to provide both the spectral coverage *and* the spatial coverage.

In order to preserve the uniformity of spatial resolution, the effective width of the pixels should be identical to 10% or better.

5.8: Spatial Coverage (Field of Regard)

Overall spatial coverage for TES is provided by a 2-axis pointing mirror. The angular range must be sufficient to fulfill both a requirement of making downlooking observations anywhere within a 45° semi-angle cone centered on the nadir (+Z) axis and at the limb in the trailing (-X) direction. The field-of-regard requirement at the trailing limb is for a nadir angle of 72°, which permits observation of cold space above any sensible atmosphere. Note that actual limb atmospheric observations are made at a smaller angle: 64.52° for a nominal orbit, a spherical Earth and a 16 km altitude aimpoint. The computation of the actual value for any given observation is part of Mission Operations planning.

It should also be noted that these angles make no allowance for the finite field-of-view of TES (7.5 x 12 mrad $\equiv$ 0.4° x 0.7°). The TES envelope must accommodate this field without obscuration in any of the observation directions.

A further, and crucial, requirement is that the pointing mirror must be commandable so that the line-of-sight can be aimed at specific locations on the ground defined by latitude and longitude. Provisional pointing algorithms and the resultant footprint are described in Appendix F. *It should be noted that these entail commandable and variable rates in both the pitch and roll axes of the gimbal.*

As a consequence of the requirement that the projection of the arrays at the trailing limb be vertical with the long axis of the pixels parallel to the horizon, it follows that the nadir projection will be such that the narrow axis will lie in the ground track (see Fig. 10). The commanding capability of the pointing mirror permits us to "stack" these footprints end-to-end for up to 885 km while the line-of-sight remains within 45° of nadir ("Transect Mode"; see Table XIII). Alternatively, we can employ a "Step-and-Stare" mode wherein spot samples are obtained in which the interval between successive samples increases (the "Step") as the integration time (the "Stare") increases (Table XII). A variant of this forms the basis for our Global Surveys (Standard Data Product generation).

Off-nadir, in any direction other than along the ground track, the footprint is rotated by an amount equal to the gimbal roll angle, which is itself roughly equal to the nadir angle at closest approach (see Appendix F).

5.9: Temporal Coverage

The requirements on temporal coverage are, in turn, based on the needs of the science team and the tropospheric chemistry community:

- Global Surveys must be made sufficiently often so that seasonal changes in atmospheric dynamics and chemistry are clearly evident. The baseline orbit for EOS (see Table XI) has a 16-day repeat period, so these surveys will be made for commensurate periods such as "4 days on, 4 days off". Indeed, the data rate and volume calculations presented later assume this specific scenario;

- More localized observations (those we term "Intensive Campaigns" and "Special Events"; see §7) may be performed sporadically but, in general, demand a capability for pointing at predetermined locations (e.g., a volcano) either for as long as possible or in a manner that permits reconstruction of the spatial variations in the phenomena. These would be, of course, Special Products.

The temporal coverage of any given location is determined by the EOS orbital parameters and the allowable range of the TES pointing mirror. For downlooking observations, it has been determined that look angles should be limited to no more than 45° from nadir in order to reduce problems of atmospheric inhomogeneity. Geometry shows (Appendix E) that these requirements result in an available coverage time of up to 221 seconds. This time can be used either to enhance sensitivity at a single location (i.e., extended integration) or to search for some limited time variability, but for such a long-term observation a pointing stability within 1 pixel should suffice. The EOS orbit and TES geometric viewing properties are shown in Tables XI & XII.

Additional requirements stem from the nature of the EOS mission. Although TES is currently being planned to operate at about a 50% annual duty cycle to conserve resources both in space and on the ground, it is an EOS Mission Requirement that TES be operable for 5 years on orbit plus an additional 2 years pre-flight for test and calibration. Based on the Provisional Mission Plan (§7), this implies that the TES scan mechanism must be capable of performing at least 10,000,000 start-stop cycles (strokes or scans) and must be capable of being turned on and off on command.

Table XI: ASSUMED EOS ORBITAL PARAMETERS

Altitude (mean)	705	km	
Inclination	98.21	deg	(Sun-synchronous, frozen)
Eccentricity	0.0012		
Ascending Node	1:45 p.m.	±15 min	
Repeat Period	16	days	
Nodal Period	5933.05	sec	
Orbits/Day	14 9/16		
Orbits/16 days	233		
Orbital Speed (mean)	7.50	km/sec	
Ground Speed (mean)	6.743	km/sec	
Ground Speed (max)	6.757	km/sec	(N. Hemisphere)
Ground Speed (min)	6.718	km/sec	(S. Hemisphere)

Orbit Plane Rotation 1.1408×10^{-5} deg/sec westwards

Longitude Drift $4.178075 \times 10^{-3} \cdot \cos(LAT)$ deg/sec westwards

Ground-Track Drift = Orbit Plane Rotation + Longitude Drift

Equatorial Longitude Change	361.971	deg/day
	24.8564	deg/orbit

Approximate launch parameters (from TRW):

Time from launch to orbit:	69 min
First nodal crossing:	38° east longitude

Table XII: DOWNLOOKING STEP-AND-STARE PARAMETERS
(In-track)

Nadir View Angle (Deg, ±)	Target Zenith Angle (Deg, ±)	Minimum In-Track Distance (km)	Total Observation Time (seconds)	Number of Downlooking Scans
1.43	1.59	35.2	5.2	1
2.85	3.17	70.2	10.4	2
4.27	4.74	105.3	15.6	3
5.69	6.32	140.6	20.8	4
11.32	12.49	280.6	41.6	8
16.54	18.43	420.9	62.4	12
21.52	24.04	561.0	83.2	16
26.13	29.28	701.5	104.0	20
30.33	34.11	841.8	124.8	24
34.12	38.53	981.9	145.6	28
37.53	42.57	1122.2	166.4	32
40.56	46.24	1262.5	187.2	36
43.27	49.57	1402.7	208.0	40

Notes (see also Appendix E):

1)   **Minimum In-Track Distance** is the smallest distance between successive samples and assumes a pointing mirror slew time ≤ 1.2 seconds

2)   **Number of Downlooking Scans** is an integer divide of the time column by 5.2

5.10: Temporal Resolution

The temporal resolution requirement on TES is compounded of many factors:

- The integration time for single observations must be long enough to:

  - achieve adequate signal-to-noise ratio;
  - avoid too high speeds and drive power levels for the FTS moving elements.

- The integration time must be short enough to:

  - keep view-angle changes to less than 2° (≡ 2% change in airmass @ 45°)
  - keep modulation frequencies well above any pointing-jitter-induced amplitude modulations;
  - avoid stressing the pointing system stability and accuracy.

Thus, while none of these factors is strictly quantitative, baseline scan times of 4 seconds for the downlooking observations and 16 seconds for limb observations have been chosen. In order to avoid excessive "dead time" due to system turn-around at the end of a scan, a goal of 1.2 seconds or less has been selected for this parameter. The only firm requirement is that the overall cycle time from the beginning of one sky calibration to the next must be 81.2 seconds, which is the time to cover just under 5° of latitude at the equator (as prescribed by the Level 1 Requirements). These times then lead to a speed requirement on the FTS that the *rate-of-change of optical path difference* must be 4.2235 ±0.2 cm/sec. The *physical* speed of the moving elements is one-quarter of this value - 1.0559 cm/sec. These speeds are unchanged for all observation types and must be constant to better than 3% peak-to-peak to avoid problems of frequency shifts within the electronic filter bandpasses.

5.11: Dynamic Range

It is a property of an FTS that the dynamic range of the signals to be recorded is very large, exacerbated by the strong variability of the signals themselves. The most serious consequence is the potential for non-linearity. The linearity (knowledge) requirements for an FTS are quite severe: 1% or better end-to-end. This requires extreme precautions both in signal chain design and in calibration; in-flight calibration is mandatory.

Calculations of dynamic range for TES show a requirement for 16 bit digitization (but note that under no circumstances must the input to the A-D converter exceed this limit, "overflow" destroys the interferogram).

In addition, the highly variable nature of the expected inputs require that several stages of calibrated, adjustable, gain must be provided prior to the A-D converter(s).

56

5.12: Radiometric Accuracy

The requirements for radiometric accuracy are intimately involved in considerations of data retrieval accuracy, signal-to-noise ratio and integration time.

TES is required to retrieve, from the spectral data, the concentration and distribution of all the molecular species making a significant contribution to the received radiance. The basic approach is to match, using one of several possible algorithms, the received data with a numerical model which contains the physical and chemical properties of the atmosphere as constrained variables. Implicit in this approach is the assumption of exact knowledge of the absorption coefficients for every significant transition of every molecule. However, the computation of the absorption coefficients is liable to several sources of error because:

a)   the absorptions/emissions are not monochromatic but are spread over a finite spectral width in a shape that depends on the molecule, the particular transition, temperature, pressure, and the presence of other molecules, all in an exceedingly non-linear fashion;

b)   the strengths of the absorptions/emissions are based on laboratory measurements which are, themselves, prone to errors. The current state-of-the-art in this discipline is 1% RMS accuracy, and that for only a very limited number of species.

The impact of radiometric error can be quantified as follows:

For an isolated weak line (as defined in §5.2), the area under the line is $W = SL$ where S is the line strength and L is the column density of the species. Thus a radiometric error of x% induces a similar error in the determination of the column density. If S is known to 1%, it follows that the radiometric accuracy should also be 1% if it is not to be the dominant source of systematic error. However, this applies only to spectral regions where solar reflection is insignificant (generally below 2500 cm^{-1}). At higher frequencies, errors in knowledge of the solar irradiance itself will dominate, so the radiometric accuracy requirement can be relaxed to 2% for the range 2250 - 3050 cm^{-1}. Note that it is an EOS Mission Requirement that radiometric calibrations be traceable to standards maintained by institutions such as NIST.

All of the foregoing is irrelevant if the spectral signal-to-noise ratio (SNR) is inadequate. Note, however, that 1% accuracy does not necessarily translate to an SNR requirement of 100:1 or better. Most molecules have transitions at many different frequencies (sometimes thousands), most of which will be present in the TES data. Proper utilization of all the available data can permit 1% retrievals to be achieved with substantially poorer SNR. Experience suggests that adequate retrievals can be achieved with an SNR of 30:1 but it is certainly true that 100:1 or better SNR simplifies the process. There is, of course, no upper limit on SNR imposed by the scientific requirements.

5.13: Cross-Talk

Cross-talk between detectors can occur in several different ways: by optical aberrations, diffraction, scattering (stray light), carrier diffusion between pixels and electrical coupling between signal chains. In view of the fact that the radiance gradients between adjacent pixels at the limb are comparable to the signals themselves, it follows that the overall system cross-talk between adjacent pixels should be 10% or less.

5.14: Expected Performance

Expected performance is based on a radiometric model for TES (Appendix C). Parameters to be installed into the model are based on a "grass roots" analysis of the current design in which each surface is assigned a temperature, reflectance/transmittance and emittance based either on measurements or by analogy to similar systems (Table XIII). Source radiances are derived from detailed spectroradiometric simulations of likely measurement scenarios using line-by-line computer codes. The required input data are shown in Table XIII; the results appear in Tables XIV & XV. For several scenarios involving each filter, the tables show the estimated mean source radiance, the noise equivalent source radiance (NESR), the band-average signal-to-noise ratio, the peak photocurrent, the interferogram dynamic range, the total photon flux density falling on the detector and, in the last column, a code indicating the dominant noise source(s). These tables reflect the general goal that the TES system be source-photon-shot-noise limited for all reasonable scenarios. Detector requirements that meet this goal are shown in Table XIII(b) but the reader is cautioned that the results shown in Tables XIV and XV are totally model-dependent and will require revision when actual performance data become available. *However, compared to the previous revision of this document (Version 5.0), the results are conservative.* For example, individual mirror reflectances have been set to 0.97 and detector quantum efficiencies to their minimum specification. This is more like the "end of life" performance. Values closer to the tables in Version 5.0 are more representative of the "at launch" performance.

Recognizing, however, that technology limitations may make these goals unrealizable, the actual spectroscopic requirements are that a signal-to-noise ratio of *at least* 30:1 is necessary for adequate retrievals. In those cases where it appears that single scans provide inadequate signal-to-noise, resort must be had to multiple scans and scan averaging. In addition, when downlooking, pixel averaging may be used to the same effect.

Table XIII(a): TES SYSTEM PARAMETERS (Assumed)

Sub-System	Element/Parameter	Value(s)	Units
Pointing System	Temperature	290.0	Kelvins
	Effective Emittance	0.06	-
	Transmittance	0.94	-
Spectroradiometer	Temperature	180.0	Kelvins
	Effective Emittance	0.32	-
	Transmittance*	0.26	-
	Modulation Index	0.7	-
	Étendue	9.448×10^{-5}	$cm^2.sr$
	OPD Scan Rate	4.2235	$cm^2.s^{-1}$
	Total Useful Integration Time	4.0 or 16.0	s
	Spectral Resolution	0.1 or 0.25	cm^{-1}
Detector/Filters etc.	Element Temperature	65.0	Kelvins
	Housing Temperature	65.0	Kelvins
	Transmittance	0.56	-
	Effective Emittance	1.0	-
	Element Size	0.075 x 0.75	mm
Miscellaneous	Solar Zenith Angle	0.0, 45.0 or 180.0	degrees
	Surface Albedo	0.15 or 1.0	-

* Includes a factor of 0.5 for single-ended operation and 0.75 for obscuration

Table XIII(b): Derived Detector Requirements

Array I.D.	Frequency Coverage From (cm⁻¹)	To (cm⁻¹)	Q.E.	Approx. Dynamic Impedance	Background Flux Density (phot/sec/cm²)	Required D* @ 65K (Zero Bkgrnd) (cm·√Hz/watt)
1A	1900	3050	≥0.7	1000 MΩ	$1 \times 10^{11} - 2 \times 10^{15}$	$> 7 \times 10^{11}$
1B	820	1200	≥0.65	2 MΩ	$1 \times 10^{15} - 2 \times 10^{16}$	$> 5 \times 10^{11}$
2A	1100	1950	≥0.65	4 MΩ	$8 \times 10^{13} - 1 \times 10^{16}$	$> 6 \times 10^{11}$
2B	650	900	≥0.6	10 kΩ	$5 \times 10^{15} - 3 \times 10^{16}$	$> 2 \times 10^{11}$

Note: all detectors are PV HgCdTe; Q.E. = Quantum Efficiency

Table XIV: Downlooking Signal, Noise & Dynamic Range Estimates

Source Conditions	Mean Source Radiance (W/cm²/sr/cm⁻¹)	Noise Equiv. Source Radiance (W/cm²/sr/cm⁻¹)	Average Spectral SNR	Peak Photocurrent (Nanoamps)	Interferogram Dynamic Range	Total Photon Flux Density (Ph/cm²/sec)	Limit
FILTER 1A1 (1900 - 2250 cm⁻¹)							
N, T_b = 180K	6.66-10	2.08-9	<1	0.3	40	5.22+12	F
N, T_b = 300K	5.07-7	9.57-9	57	7	5642	1.11+14	S
N, T_b = 340K	1.64-6	1.67-8	103	22	10190	3.41+14	S
D, T_b = 340K, θ = 45°, A = 0.15	1.64-6	1.69-8	104	22	10290	3.48+14	S
D, T_b = 340K, θ = 0°, A = 1.0	1.95-6	1.82-8	112	25	11110	4.03+14	S
FILTER 1A2 (2200 - 2450 cm⁻¹)							
N, T_b = 180K	1.27-10	1.16-9	0	0.08	10	1.25+12	F
N, T_b = 300K	2.15-7	5.48-9	41	2	3420	2.91+13	S
N, T_b = 340K	7.98-7	1.03-8	80	6	6660	1.03+14	S
D, T_b = 340K, θ = 45°, A = 0.15	8.40-7	1.06-8	82	7	6830	1.09+14	S
D, T_b = 340K, θ = 0°, A = 1.0	1.19-6	1.25-8	97	10	8110	1.52+14	S
FILTER 1A3 (2425 - 2650 cm⁻¹)							
N, T_b = 180K	3.02-11	7.81-10	0	.03	3	4.58+11	F
N, T_b = 300K	1.01-7	3.71-9	28	.7	2230	1.12+13	S
N, T_b = 340K	4.22-7	7.43-9	58	3	4630	4.48+13	S
D, T_b = 340K, θ = 45°, A = 0.15	4.71-7	7.83-9	62	3	4890	4.98+13	S
D, T_b = 340K, θ = 0°, A = 1.0	8.84-7	1.06-8	84	6	6670	9.21+13	S

N = Night; D = Day

Limit code (significant noise sources): S = source; F = foreoptics; I = interferometer; D = detector system

Revised 2/27/99

Table XIV (cont.): Downlooking Signal, Noise & Dynamic Range Estimates

Source Conditions	Mean Source Radiance (W/cm²/sr/cm⁻¹)	Noise Equiv. Source Radiance (W/cm²/sr/cm⁻¹)	Average Spectral SNR	Peak Photocurrent (Nanoamps)	Interferogram Dynamic Range	Total Photon Flux Density (Ph/cm²/sec)	Limit
FILTER 1A4 (2600 - 2850 cm⁻¹)							
$N, T_b = 180K$	3.36-12	6.19-10	0	.01	1	2.32+11	F
$N, T_b = 300K$	5.08-8	2.89-9	18	0.4	1540	5.86+12	S
$N, T_b = 340K$	2.37-7	6.09-9	40	1.7	3360	2.61+13	S
$D, T_b = 340K, \theta = 45°, A = 0.15$	2.92-7	6.74-9	44	2.0	3720	3.20+13	S
$D, T_b = 340K, \theta = 0°, A = 1.0$	7.61-7	1.08-8	71	5.2	5980	8.18+13	S
FILTER 1A5 (2800 - 3050 cm⁻¹)							
$N, T_b = 180K$	2.09-12	4.74-10	0	-	-	9.87+10	F,D
$N, T_b = 300K$	2.41-8	2.07-9	12	0.3	1020	2.59+12	S
$N, T_b = 340K$	1.26-7	4.60-9	28	0.8	2360	1.29+13	S
$D, T_b = 340K, \theta = 45°, A = 0.15$	1.89-7	5.60-9	34	1.2	2890	1.92+13	S
$D, T_b = 340K, \theta = 0°, A = 1.0$	7.22-7	1.08-8	67	4.5	5610	7.19+13	S

N = Night; D = Day

Limit code (significant noise sources): S = source; F = foreoptics; I = interferometer; D = detector system

Revised 2/28/99

61

Table XIV (cont.): Downlooking Signal, Noise & Dynamic Range Estimates

Source Conditions	Mean Source Radiance (W/cm²/sr/cm⁻¹)	Noise Equiv. Source Radiance (W/cm²/sr/cm⁻¹)	Average Spectral SNR	Peak Photocurrent (Nanoamps)	Interferogram Dynamic Range	Total Photon Flux Density (Ph/cm²/sec)	Limit
FILTER 1B1 (820 - 1050 cm⁻¹)							
N, T_b = 180K	5.53-7	1.01-8	59	20	4730	5.65+14	I,F,S
N, T_b = 300K	1.11-5	2.54-8	442	198	35540	3.60+15	S
N, T_b = 340K	1.90-5	3.24-8	590	329	47410	5.83+15	S
FILTER 1B2 (950 - 1150 cm⁻¹)							
N, T_b = 180K	3.12-7	7.92-9	42	11	3130	2.76+14	F,I,S
N, T_b = 300K	9.02-6	2.24-8	407	124	30520	2.21+15	S
N, T_b = 340K	1.64-5	2.95-8	559	219	41930	3.84+15	S
FILTER 2A1 (1100 - 1325 cm⁻¹)							
N, T_b = 180K	1.31-7	6.58-9	22	6.0	1720	1.43+14	F,I,S
N, T_b = 300K	6.35-6	2.13-8	304	86	24130	1.50+15	S
N, T_b = 340K	1.26-5	2.94-8	435	165	34560	2.85+15	S
FILTER 2A2 (1300 - 1550 cm⁻¹)							
N, T_b = 180K	3.89-8	4.99-9	9	2.8	730	5.95+13	F.I
N, T_b = 300K	3.71-6	1.86-8	206	48	17220	8.25+14	S
N, T_b = 340K	8.31-6	2.72-8	311	103	26090	1.77+15	S

N = Night

Limit code (significant noise sources): S = source; F = foreoptics; I = interferometer; D = detector system

Revised 2/28/99

Table XIV (cont.): Downlooking Signal, Noise & Dynamic Range Estimates

Source Conditions	Mean Source Radiance (W/cm²/sr/cm⁻¹)	Noise Equiv. Source Radiance (W/cm²/sr/cm⁻¹)	Average Spectral SNR	Peak Photocurrent (Nanoamps)	Interferogram Dynamic Range	Total Photon Flux Density (Ph/cm²/sec)	Limit
FILTER 2A3 (1500 - 1750 cm⁻¹)							
N, T_b = 180K	1.17-8	3.64-9	4	1.3	302	2.43+13	F
N, T_b = 300K	2.11-6	1.49-8	146	24	12230	4.09+14	S
N, T_b = 340K	5.28-6	2.31-8	234	57	19570	9.82+14	S
FILTER 2A4 (1700 - 1950 cm⁻¹)							
N, T_b = 180K	3.34-9	2.66-9	1	.6	119	1.03+13	F
N, T_b = 300K	1.14-6	1.16-8	102	12	8530	1.97+14	S
N, T_b = 340K	3.21-6	1.91-8	172	31	14440	5.30+14	S
FILTER 2B1 (650 - 900 cm⁻¹)							
N, T_b = 180K	1.13-6	1.34-8	90	40	7570	1.34+15	I,S,F
N, T_b = 300K	1.38-5	2.85-8	490	296	40850	6.07+15	S
N, T_b = 340K	2.17-5	3.47-8	626	454	52450	8.99+15	S

N = Night

Limit code (significant noise sources): S = source; F = foreoptics; I = interferometer; D = detector system

Table XV: Limbviewing Signal, Noise & Dynamic Range Estimates

Source Conditions	Mean Source Radiance (W/cm²/sr/cm⁻¹)	Noise Equiv. Source Radiance (W/cm²/sr/cm⁻¹)	Average Spectral SNR	Peak Photocurrent (Nanoamps)	Interferogram Dynamic Range	Total Photon Flux Density (Ph/cm²/sec)	Limit
FILTER 1A1 (1900 - 2250 cm⁻¹)							
Tropical Model, 0.6 km T.H.	8.8-8	8.92-9	11	1.5	2180	2.42+13	S,F
S.A.W. Model, 0.6 km T.H.	3.4-8	6.45-9	6	0.8	1190	1.26+13	S,F
Tropical Model, 10 km T.H.	1.5-8	5.28-9	3	0.5	650	8.46+12	F,S
S.A.W. model, 10 km T.H.	6.6-9	4.67-9	2	0.4	330	6.59+12	F,S
FILTER 1A2 (2200 - 2450 cm⁻¹)							
Tropical Model, 0.6 km T.H.	1.3-8	3.52-9	4	0.2	660	2.97+12	S,F
S.A.W. Model, 0.6 km T.H.	6.2-9	2.95-9	2	0.1	380	2.07+12	F,S
Tropical Model, 10 km T.H.	1.3-8	3.52-9	4	0.2	660	2.97+12	S,F
S.A.W. model, 10 km T.H.	6.2-9	2.95-9	2	0.1	380	2.07+12	F,S
FILTER 1B1 (820 - 1050 cm⁻¹)							
Tropical Model, 0.6 km T.H.	7.4-6	4.27-8	176	136	28320	2.54+15	S
S.A.W. Model, 0.6 km T.H.	4.1-6	3.38-8	124	80	19980	1.59+15	S
Tropical Model, 10 km T.H.	8.1-7	2.15-8	40	25	6440	6.4+14	S,I,F
S.A.W. model, 10 km T.H.	6.2-7	2.05-8	32	21	5190	5.84+14	I,S,F

Peak SNR should be 2-3 times greater than the mean; S.A.W. = Sub-Arctic Winter

Limit code (significant noise sources): S = source; F = foreoptics; I = interferometer; D = detector system

Revised 3/1/99

Table XV (cont.): Limbviewing Signal, Noise & Dynamic Range Estimates

Source Conditions	Mean Source Radiance (W/cm²/sr/cm⁻¹)	Noise Equiv. Source Radiance (W/cm²/sr/cm⁻¹)	Average Spectral SNR	Peak Photocurrent (Nanoamps)	Interferogram Dynamic Range	Total Photon Flux Density (Ph/cm²/sec)	Limit
FILTER 1B2 (950 - 1150 cm⁻¹)							
Tropical Model, 0.6 km T.H.	4.0-6	3.16-8	129	59	19340	1.10+15	S
S.A.W. Model, 0.6 km T.H.	1.9-6	2.40-8	82	32	12220	6.34+14	S,F
Tropical Model, 10 km T.H.	1.1-6	2.03-8	56	21	8420	4.55+14	S,F,I
S.A.W. model, 10 km T.H.	9.6-7	1.96-8	51	19	7630	4.23+14	S,F,I
FILTER 2A1 (1100 - 1325 cm⁻¹)							
Tropical Model, 0.6 km T.H.	2.5-6	2.84-8	91	37	14430	6.65+14	S
S.A.W. Model, 0.6 km T.H.	1.3-6	2.21-8	61	21	9740	4.03+14	S,F
Tropical Model, 10 km T.H.	5.0-7	1.65-8	32	11	5080	2.26+14	S,F,I
S.A.W. model, 10 km T.H.	4.4-7	1.60-8	29	10	4620	2.13+14	S,F,I
FILTER 2A2 (1300 - 1550 cm⁻¹)							
Tropical Model, 0.6 km T.H.	5.3-7	1.66-8	34	9	5670	1.64+14	S,F
S.A.W. Model, 0.6 km T.H.	3.6-7	1.47-8	26	7	4380	1.29+14	S,F
Tropical Model, 10 km T.H.	4.0-7	1.51-8	28	7	4710	1.37+14	S,F
S.A.W. model, 10 km T.H.	2.8-7	1.36-8	22	6	3680	1.12+14	S,F

Peak SNR should be 2-3 times greater than the mean; S.A.W. = Sub-Arctic Winter

Limit code (significant noise sources): S = source; F = foreoptics; I = interferometer; D = detector system

Revised 3/1/99

Table XV (cont.): Limbviewing Signal, Noise & Dynamic Range Estimates

Source Conditions	Mean Source Radiance (W/cm²/sr/cm⁻¹)	Noise Equiv. Source Radiance (W/cm²/sr/cm⁻¹)	Average Spectral SNR	Peak Photocurrent (Nanoamps)	Interferogram Dynamic Range	Total Photon Flux Density (Ph/cm²/sec)	Limit
FILTER 2A3 (1500 - 1750 cm⁻¹)							
Tropical Model, 0.6 km T.H.	1.6-7	1.07-8	16	2.9	2680	5.24+13	S,F
S.A.W. Model, 0.6 km T.H.	1.2-7	9.88-9	13	2.5	2180	4.49+13	S,F
Tropical Model, 10 km T.H.	1.4-7	1.03-8	15	2.7	2440	4.87+13	S,F
S.A.W. model, 10 km T.H.	1.2-7	9.88-9	13	2.5	2180	4.49+13	S,F
FILTER 2A4 (1700 - 1950 cm⁻¹)							
Tropical Model, 0.6 km T.H.	1.2-7	9.05-9	14	1.7	2360	2.99+13	S,F
S.A.W. Model, 0.6 km T.H.	6.3-8	7.48-9	9	1.2	1510	2.04+13	S,F
Tropical Model, 10 km T.H.	8.1-8	8.01-9	11	1.3	1810	2.34+13	S,F
S.A.W. model, 10 km T.H.	4.4-8	6.87-9	7	1.0	1160	1.72+13	F,S
FILTER 2B1 (650 - 900 cm⁻¹)							
Tropical Model, 0.6 km T.H.	6.8-6	4.31-8	161	156	26910	3.47+15	S
S.A.W. Model, 0.6 km T.H.	4.9-6	3.85-8	131	117	21880	2.76+15	S,I
Tropical Model, 10 km T.H.	3.2-6	3.38-8	98	83	16460	2.12+15	S,I
S.A.W. model, 10 km T.H.	2.7-6	3.22-8	87	72	14610	1.93+15	S,I,F

Peak SNR should be 2-3 times greater than the mean; S.A.W. = Sub-Arctic Winter

Limit code (significant noise sources): S = source; F = foreoptics; I = interferometer; D = detector system

Revised 3/1/99

5.15: Operations

5.15.1: Global Surveys. Present plans call for TES to make alternating downlooking and limb measurements for 4 days & nights every 8 days at about 500 km intervals. All survey measurements will be made in-track (limb views at the trailing limb). Concatenation of downlooking and limb views is delayed by about 7 minutes because the limb is some 3000 km behind the spacecraft (see Table XVIII). Each downlooking observation set is preceded by a "cold space" and "hot (340 K) black body" calibration measurement, one filter combination (see §5.3) at a time (so-called "embedded" calibrations).

Global Surveys will cover ±82° of latitude (determined by the orbit inclination). The time interval between starts of the measurement groups (called "sequences") is required to be 81.2 seconds. Downlooking and calibration observations employ 16 seconds of this interval; limb views 48 seconds with the remainder used for scan reset and turn-around. 73 such sequences will be acquired on every orbit, with the start triggered by passage of the southern apex (the most southerly point) of the orbit (the overall timing includes about a 5 second contingency to accommodate ephemeris errors and orbit changes).

The temporal phasing of the views is shown in Figs. 11a & b. Immediately before and after each 4-day collection, 2 orbits will be used to make continuous blackbody and space-view calibrations of 40 scan sequences using every combination of filter and foreoptics. These data will be used both to verify and improve the embedded calibrations and also as a monitor of instrument health/contamination status.

The Global Surveys will encompass the full suite of molecules shown in Table I and constitute the primary database for models from which inferences about the present and future state of the Earth's lower atmosphere will be drawn. The resultant data volume is, however, very large: every 4/8 days about 2 million individual interferograms containing more than 1 Tb will be generated, yet an obvious requirement is that TES cannot afford to become backlogged since it will be impossible ever to catch up. Clearly, state-of-the-art computing power will be mandatory, together with a fully automated analytic system.

In the intervening periods, TES will be available for two other types of observation which we term "Intensive Campaigns" and "Special Events" plus more extensive calibrations than are possible during the Global Surveys.

5.15.2: Intensive Campaigns. Downlooking Intensive Campaigns will involve TES generating transects of a limited, preselected, number of molecules within relatively small areas (the Eastern U.S., for example). In this mode, the pointing mirror is employed to "stack" the individual line images (Fig. 12) along-track for a distance that can be as great as 885 km. The pointing angles, spatial resolution and cumulative coverage are shown in Table XVa-c. Alternatively, TES can be used in a "step-and-stare" mode (similar to that used in Global Surveys) in which observations are made at periodic intervals with the *caveat* that the longer a given spot is observed, the further down-track is the next point. This is also illustrated in Fig. 12.

Limbviewing intensive campaigns involve investigations of the stratospheric effects of volcanos and biomass burning, plus intercomparison campaigns with the other CHEM platform instruments - HiRDLS and MLS.

5.15.3: Special Events. Special Events are primarily targets of opportunity (e.g., volcanic eruptions) and ground-truth calibrations. The common factor is that they occur over very limited areas. TES would therefore stare at a particular location for as long as possible given the orbital speed and the angular limits on the pointing mirror. The maximum is 208 seconds ($\approx$40 scans), during which time we may choose to enhance SNR for trace species not normally measured during routine operations or search for some limited time variability. The EOS orbit is such that we could revisit most sites (with a different viewing angle) in 2 days.

5.15.4: Definitions. In order to identify data sets, a hierarchical series of counters has been established:

Run Counter: A "run" is an identifiable block of data such as a 4-day Global Survey or the 2+ orbits of bracketing continuous calibrations or any one of the Special Products observations. The run counter continuously increments for the life of the mission.

Sequence Counter: A "sequence" is a sub-set of a run such as the 81.2 second group of "2 calibrations + 2 nadir + 3 limb" observations or a once-through cycle of Special Product observations. The sequence counter is reset at the beginning of every run.

Scan Counter: A "scan" is a transition of the interferometer carriage from one limit to the other, taking 4 seconds for a nadir view and 16 seconds for a limb view. The scan counter is reset at the beginning of every sequence.
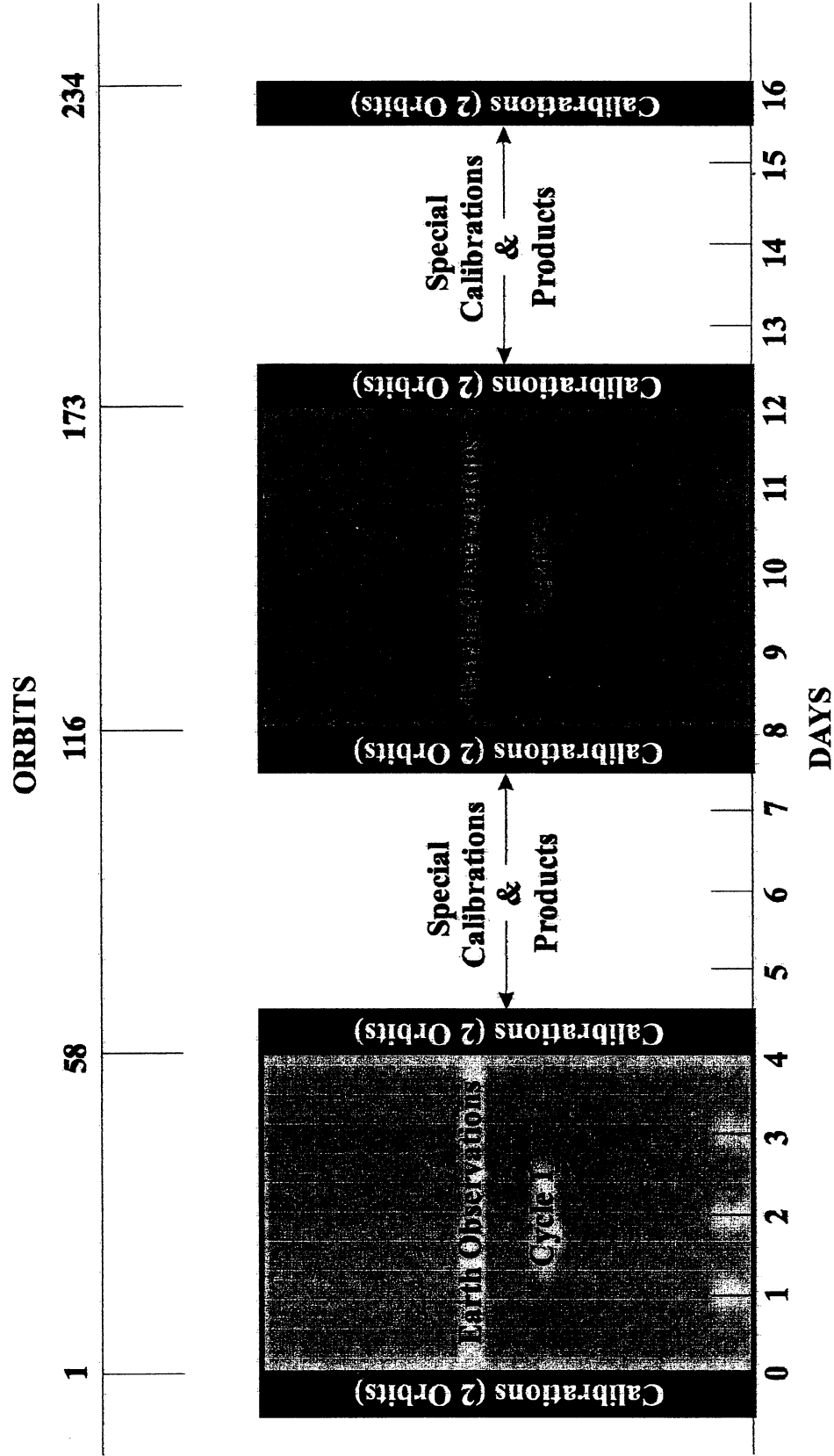
GLOBAL SURVEY MODE 16-DAY SEQUENCE

Fig. 11(a): Overview of the Global Survey Mode

71

NADIR & LIMB GLOBAL SURVEY STRATEGY

Nadir & Limb bracketting pairs

Relative Time (seconds)

0   100   200   300   400   500   600   700   800

81.2 Seconds

77.0 Seconds

SP	BB				L1		L2		L3	SP
4.0	2.6	4.0	2.6	4.0	1.24.0	4.2	16.0	1.2	16.0	1.2	16.0	4.2

Reset & Turnaround

Seconds

Reset & Turnaround
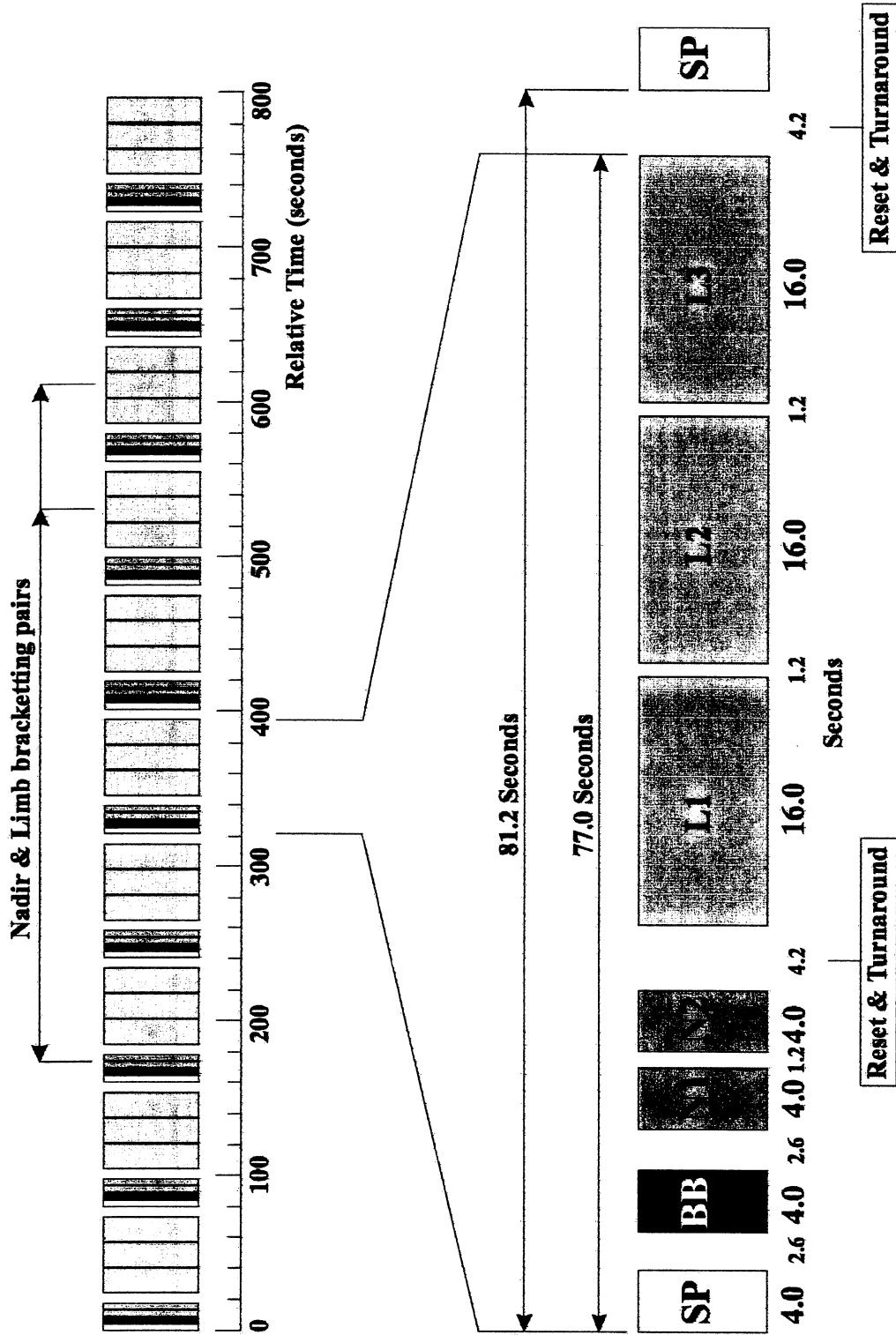
Fig.11(b): Phasing of Limb and Nadir observations in Global Surveys

72
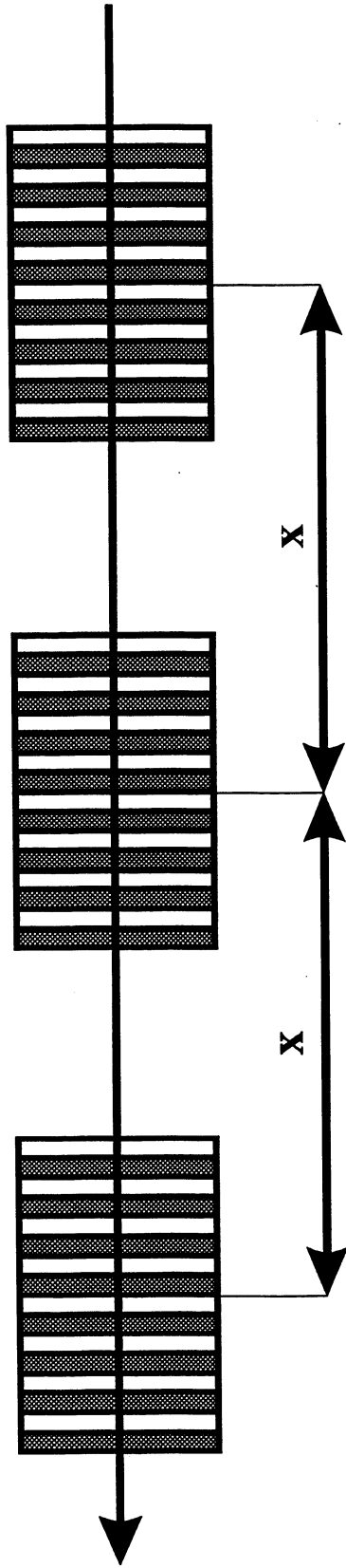
STEP-and-STARE $\left\{ \begin{array}{l} 0 < X < 1490 \text{ km} \\ \text{for } 5 < t < 221 \text{ sec} \end{array} \right.$

TRANSECT:

Footprints are exactly contiguous in a line up to 885 km long

Fig. 12: TES Step-and-Stare and Transect Mode

Table XVI(a): Transect Mode Parameters - Single Scans

Scan No.	Nadir Angle (deg)	Foot-Print (km)	Cumul. Cov. (Km)	Start Time (sec)
1	45.00	20.53	20.53	0.0
2	44.51	20.04	40.57	5.2
3	43.98	19.54	60.11	10.4
4	43.43	19.04	79.14	15.6
5	42.84	18.53	97.67	20.8
6	42.22	18.02	115.70	26.0
7	41.56	17.52	133.22	31.2
8	40.86	17.02	150.23	36.4
9	40.12	16.51	166.75	41.6
10	39.33	16.02	182.76	46.8
11	38.50	15.53	198.29	52.0
12	37.62	15.04	213.33	57.2
13	36.69	14.56	227.89	62.4
14	35.70	14.09	241.98	67.6
15	34.66	13.64	255.62	72.8
16	33.56	13.19	268.81	78.0
17	32.40	12.76	281.57	83.2
18	31.18	12.34	293.91	88.4
19	29.89	11.94	305.85	93.6
20	28.53	11.55	317.40	98.8
21	27.10	11.18	328.58	104.0
22	25.61	10.83	339.41	109.2
23	24.04	10.50	349.92	114.4
24	22.40	10.20	360.11	119.6
25	20.70	9.91	370.03	124.8
26	18.93	9.65	379.68	130.0
27	17.09	9.41	389.09	135.2
28	15.19	9.20	398.29	140.4
29	13.23	9.01	407.30	145.6
30	11.22	8.85	416.16	150.8
31	9.16	8.72	424.88	156.0
32	7.06	8.61	433.49	161.2
33	4.93	8.53	442.02	166.4
34	2.78	8.48	450.51	171.6
35	0.62	8.46	458.97	176.8
36	-1.55	8.47	467.43	182.0
37	-3.71	8.50	475.94	187.2
38	-5.86	8.56	484.50	192.4
39	-7.98	8.66	493.16	197.6
40	-10.07	8.77	501.93	202.8
41	-12.12	8.92	510.85	208.0
42	-14.12	9.09	519.95	213.2
43	-16.07	9.29	529.24	218.4
44	-17.96	9.52	538.76	223.6
45	-19.78	9.77	548.53	228.8
46	-21.54	0.05	558.58	234.0
47	-23.23	10.35	568.93	239.2
48	-24.85	10.67	579.60	244.4
49	-26.40	11.01	590.61	249.6
50	-27.88	11.38	601.99	254.8
51	-29.29	11.76	613.75	260.0
52	-30.63	12.16	625.92	265.2
53	-31.90	12.58	638.50	270.4
54	-33.11	13.02	651.52	275.6
55	-34.26	13.47	664.99	280.8
56	-35.34	13.93	678.92	286.0
57	-36.37	14.41	693.33	291.2
58	-37.34	14.89	708.23	296.4
59	-38.26	15.39	723.62	301.6
60	-39.13	15.89	739.51	306.8
61	-39.95	16.41	755.92	312.0
62	-40.72	16.92	772.84	317.2
63	-41.45	17.44	790.28	322.4
64	-42.13	17.96	808.23	327.6
65	-42.78	18.48	826.71	332.8
66	-43.39	19.00	845.71	338.0
67	-43.96	19.52	865.23	343.2
68	-44.51	20.04	885.27	348.4

Table XVI(b): Transect Mode Parameters- Double & Triple Scans

Double Scans				Triple Scans			

Sample No.	Nadir Angle (Deg)	Foot-Print (km)	Cumul. Cov. (km)	Start Time (sec)	Sample No.	Nadir Angle (Deg)	Foot-Print (km)	Cumul. Cov. (km)	Start Time (sec)
1	45.00	20.53	20.53	0.0	1	45.00	20.53	20.53	0.0
2	43.27	18.89	39.42	10.4	2	41.95	17.81	38.35	15.6
3	41.32	17.34	56.77	20.8	3	38.31	15.42	53.77	31.2
4	39.13	15.89	72.66	31.2	4	34.00	13.36	67.13	46.8
5	36.67	14.55	87.21	41.6	5	28.92	11.66	78.79	62.4
6	33.92	13.33	100.55	52.0	6	23.03	10.31	89.10	78.0
7	30.86	12.24	112.78	62.4	7	16.35	9.33	98.42	93.6
8	27.46	11.27	124.05	72.8	8	9.00	8.71	107.13	109.2
9	23.72	10.44	134.49	83.2	9	1.23	8.46	115.60	124.8
10	19.64	9.75	144.25	93.6	10	-6.61	8.59	124.19	140.4
11	15.25	9.21	153.45	104.0	11	-14.16	9.10	133.29	156.0
12	10.58	8.81	162.26	114.4	12	-21.13	9.98	143.27	171.6
13	5.71	8.56	170.82	124.8	13	-27.34	11.24	154.51	187.2
14	0.72	8.46	179.28	135.2	14	-32.73	12.88	167.39	202.8
15	-4.29	8.52	187.80	145.6	15	-37.33	14.89	182.28	218.4
16	-9.22	8.72	196.52	156.0	16	-41.21	17.27	199.54	234.0
17	-13.98	9.08	205.60	166.4	17	-44.47	20.01	219.55	249.6
18	-18.49	9.59	215.19	176.8					
19	-22.70	10.25	225.44	187.2					
20	-26.58	11.06	236.50	197.6					
21	-30.11	12.00	248.50	208.0					
22	-33.31	13.09	261.60	218.4					
23	-36.18	14.32	275.91	228.8					
24	-38.75	15.67	291.58	239.2					
25	-41.04	17.14	308.73	249.6					
26	-43.08	18.73	327.46	260.0					
27	-44.89	20.42	347.88	270.4					

5.16: Interferometer System Parameters

5.16.1: Introduction. All the foregoing place some specific additional requirements on the TES interferometer. Some of these were briefly mentioned earlier, but demand more complete explanation.

5.16.2: Interferogram sampling. A critical element in the operation of a Fourier Transform Spectrometer is proper control of the interferogram sampling. First and foremost, an FTS is not amenable to the use of an external clock for sampling because fairly massive optical elements must be moved and it is difficult to control the rate-of-change of optical path difference (RCOPD; nominally 4.2235 cm/sec for TES) to better than a few tenths of a percent. The solution is to allow the FTS to generate its own clock.

The means universally employed is to illuminate the optical system with light from a frequency-stabilized laser and to sense the output with detectors separate from the main infrared detectors. For a truly monochromatic input and a constant RCOPD, the output is a sinewave of constant frequency.

Now, it is easily demonstrated that if the RCOPD is V cm/sec, then the frequency f in Hz of the sinewave emanating from a detector is related to the optical frequency v cm^{-1} by

$$f = V \cdot v \quad \text{Hz} \tag{5.5}$$

Assuming that a Nd:YAG laser is used for control, $v_1 \approx 9397.171$ cm^{-1} and, for the case of TES, $V = 4.2235$ cm/sec, the clock frequency generated by the laser is 39,689 Hz *with the proviso that this frequency is only as accurate as the RCOPD stability*.

Although there are many different ways of exploiting this output, they are all substantially equivalent to detecting zero-crossings of the sinewave (not necessarily every one). The theory of interferogram sampling is explained in Appendix D, but Table XVI(a) shows the allowed spectral intervals as a function of step length in fringes (K) and alias order (J), and Table XVI(b) shows the same data converted to kHz through the transformation equation. These transformed data are to be used for signal-chain design purposes *only*.

5.16.3: Filter bandpass control. A crucial requirement for the type of undersampling discussed in Appendix D is that the entirety of the transmitted bandpass *must* be contained within the limits prescribed by Table XVI. However, real filters inevitably have some out-of-band "leakage" and this must be carefully controlled. In order to maintain the goal of 1% radiometric accuracy, it follows that the *cumulative* out-of-band (i.e., out-of-alias) leakage of any of the filters should be less than 1%. Note, however, that added factors such as detector cut-offs can be used to advantage in order to meet this requirement. That is, the requirement is on the *effective* bandpass rather than on the physical filter itself.

Table XVIII(a): ALLOWED SAMPLING INTERVALS FOR A Nd:YAG LASER-CONTROLLED FTS

(Assumes $\nu_{\text{Nd:YAG}} = 9397.171$ cm^{-1})

SAMPLING INDEX

K / J	1	2	3	4	5	6	7	8	9	10	11	12	13	14	15
(0)	0.0	0.0	0.0	0.0	0.0	0.0	0.0	0.0	0.0	0.0	0.0	0.0	0.0	0.0	0.0
1	4698.6	2349.3	1566.2	1174.6	939.7	783.1	671.2	587.3	522.1	469.9	427.1	391.5	361.4	335.6	313.2
2		4698.6	3132.4	2349.3	1879.4	1566.2	1342.5	1174.6	1044.1	939.7	854.3	783.1	722.9	671.2	626.5
3			4698.6	3523.9	2819.2	2349.3	2013.7	1762.0	1566.2	1409.6	1281.4	1174.6	1084.3	1006.8	939.7
4				4698.6	3758.9	3132.4	2684.9	2349.3	2088.3	1879.4	1708.6	1566.2	1445.7	1342.5	1253.0
5					4698.6	3915.5	3356.1	2936.6	2610.3	2349.3	2135.7	1957.7	1807.1	1678.1	1566.2
6						4698.6	4027.4	3523.9	3132.4	2819.2	2562.9	2349.3	2168.6	2013.7	1879.4
7							4698.6	4111.3	3654.5	3289.0	2990.0	2740.8	2530.0	2349.3	2192.7
8								4698.6	4176.5	3758.9	3417.2	3132.4	2891.4	2684.9	2505.9
9									4698.6	4228.7	3844.3	3523.9	3252.9	3020.5	2819.2
10										4698.6	4271.4	3915.5	3614.3	3356.1	3132.4
11											4698.6	4307.0	3975.7	3691.7	3445.6
12												4698.6	4337.2	4027.4	3758.9
13													4698.6	4363.0	4072.1
14														4698.6	4385.3
15															4698.6

Frequencies in cm^{-1}

ALIAS ORDER

SAMPLING INDEX

Table XVII(b): ALLOWED SAMPLING INTERVALS FOR A Nd:YAG LASER-CONTROLLED FTS

(Assumes $\nu_{Nd:YAG}$ = 9397.171 cm^{-1} and Rate of Change of OPD = 4.2235 cm/sec)

SAMPLING INDEX

K \ J	1	2	3	4	5	6	7	8	9	10	11	12	13	14	15
(0)	0.0	0.0	0.0	0.0	0.0	0.0	0.0	0.0	0.0	0.0	0.0	0.0	0.0	0.0	0.0
1	19.8	9.9	6.6	5.0	4.0	3.3	2.8	2.5	2.2	2.0	1.8	1.7	1.5	1.4	1.3
2		19.8	13.2	9.9	7.9	6.6	5.7	5.0	4.4	4.0	3.6	3.3	3.0	2.8	2.6
3			19.8	14.9	11.9	9.9	8.5	7.4	6.6	5.9	5.4	5.0	4.6	4.2	4.0
4				19.8	15.9	13.2	11.3	9.9	8.8	7.9	7.2	6.6	6.1	5.6	5.3
5					19.8	16.5	14.2	12.4	11.0	9.9	9.0	8.3	7.6	7.1	6.6
6						19.8	17.0	14.9	13.2	11.9	10.8	9.9	9.1	8.5	7.9
7							19.8	17.4	15.4	13.9	12.6	11.6	10.6	9.9	9.3
8								19.8	17.6	15.8	14.4	13.2	12.2	11.3	10.6
9									19.8	17.8	16.2	14.9	13.7	12.7	11.9
10										19.8	18.0	16.5	15.2	14.1	13.2
11											19.8	18.2	16.7	15.5	14.5
12												19.8	18.2	16.9	15.9
13													19.8	18.3	17.2
14														19.8	18.5
15															19.8

Frequencies in kHz (Approximate)

SAMPLING INDEX

76

5.16.4: Sampling accuracy. The required accuracy of location of sampling points is severe although, strictly speaking, it is the *knowledge of the spacing* between points that is most critical. The absolute location (so-called linear phase error) is a secondary issue that can be dealt with in the data processing as part of the phase correction operation.

Two types of error must be avoided - periodic and random. Periodic errors (such as those that will occur if sampling is attempted at both laser zero-crossings) generate "ghosts" within the spectral interval. Detailed computation and simulation suggests that periodic variations in the sampling interval must be kept to less than 10 Å (1 nm) peak-to-peak. The tolerance for random error is a little greater - 20 Å (2 nm) RMS. **Bear in mind that both these numbers represent only a few atomic diameters!** It is in this requirement that the most serious difficulties of Fourier Transform Spectrometry lie.

5.16.5: Scan centering. It is important that ZPD lie in the middle of the travel range of the scan mechanism, because the resultant spectral resolution will be determined by the size of the *smaller* of the two Maximum Path Differences (MPD). The requirement is that the scan mechanical mid-point be ZPD to ± 1 mm.

Since it is often observed that the output of an FTS depends on the direction of travel of the scan mechanism, an additional requirement is that the housekeeping data stream permits the determination of the scan direction (e.g., by outputting the ICS encoder readings).

5.16.6: Scan capability. As explained earlier (§5.4), the two basic TES resolutions require scan ranges (in OPD) of -33.8 to +33.8 cm and -8.5 to +8.5 cm for limb and downlooking observations respectively (the tolerance on these locations is ± 1 mm). Once ZPD has been established, the system can be offset to one or other position of maximum path difference and the scan started using the ICS encoder reading. Note that an additional "pad" in the scan range must be provided to allow for acceleration and deceleration.

In addition, during integration and test, it is very useful to be able to make rapid, repetitive, scans just through the region of ZPD (plus and minus a few tenths of a mm) while observing a bright source and to examine the output on a CRT. Obvious gross errors are immediately evidenced by asymmetry of the interferogram - ideally, after digitization, it should look somewhat like (but not identical to) Fig. 13.
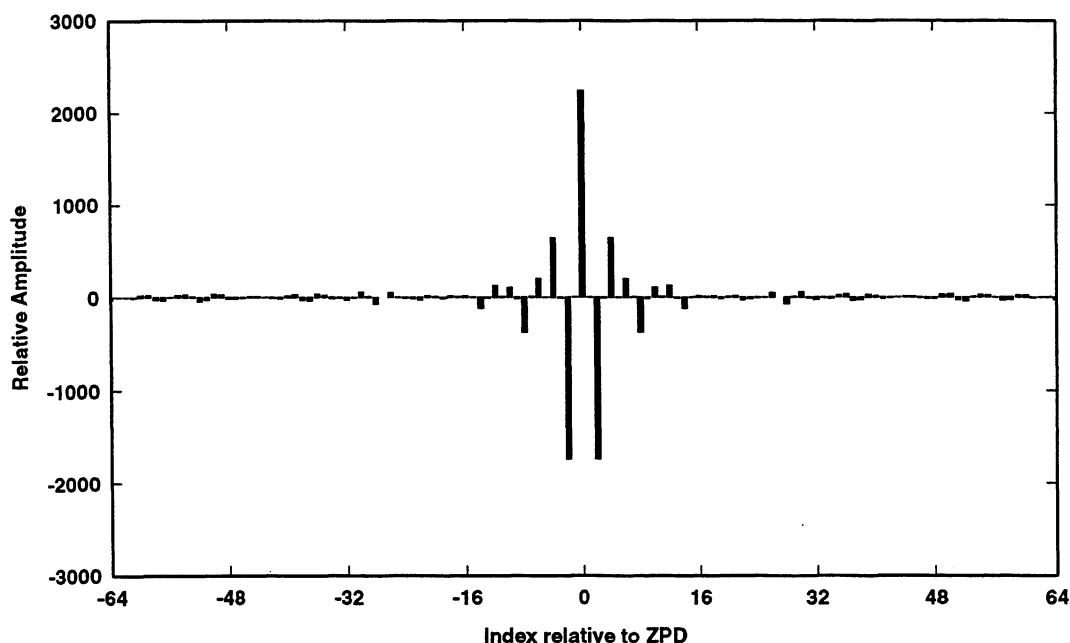
Fig. 13: An ideal (sampled) interferogram near Zero Path Difference (ZPD)

5.16.7: Modulation index. A critical parameter to be measured is the modulation index, an indicator of the ability of the instrument to act as an interferometer. For an ideal system, the modulation index is simply 4RT, where R is the beamsplitter reflectance and T is the transmittance. When R = T = 0.5 (i.e., no absorption), 4RT = 1.0; 100% modulation index[4]. Perfect modulation manifests itself as a signal that (at any path difference for a monochromatic input; at ZPD for a broad-band input) alternates between complete darkness and the same intensity as the input signal (with due allowance for transmission losses). Note that, depending on the beamsplitter and the direction of incidence, the ZPD signal can be either a maximum or a minimum - either is acceptable. The measurement is made just as described: by comparison of the modulation amplitude to zero and the unmodulated input signal. Since TES is AC coupled, this measurement will require a modulated (chopped or pulsed) source (see Appendix F for a detailed methodology).

---

[4] For consistency with other documentation, the 4RT product itself will be termed *modulation efficiency*

78

The importance of the modulation index is that it directly multiplies the system signal-to-noise ratio by reducing the signal *without* reducing the photon shot noise. The requirement is that the Modulation Index be ≥ 0.7 over the entire range 650 - 3050 cm^{-1}. Factors which impact modulation index are:

a) Imperfect beamsplitter/recombiner coatings. It is impossible to achieve the ideal of R = T = 0.5 over more than a limited frequency range. Fortunately, the product 4RT is relatively insensitive to changes in R and T. For example, R = 0.4; T = 0.6 still provides 4RT = 0.96. More serious is absorption and scattering within the coatings. Metalized beamsplitters, for instance, for which one might typically find R = T = A = 0.33 (R + T + A = 1 by definition), provide 4RT = 0.44, a substantial loss of efficiency. Good dielectric beamsplitter/recombiner coatings are essential (i.e., metallic coatings are unacceptable).

b) Imperfect wavefronts. The ideal Michelson interferometer assumes interference between perfectly plane and parallel waves. Any differential distortion between wavefronts manifests itself as a loss of modulation index. In effect, each element of the wavefront behaves as if it had a slightly different path difference from its neighbors; the interferogram is "washed out". Common distortions of the wavefronts (i.e., those shared by both interfering beams) are less important unless they become severe curvatures (comparable to the field-of-view of a single pixel). It is always the *path difference* between the two interfering beams of the interferometer that matters, not the path lengths.

c) Beam shear. If the beams from the two retroreflectors of the FTS are not perfectly superimposed at the recombiner surface, modulation is reduced in two ways. First, the mere fact that parts of each beam are not superimposed means that no interference occurs. The loss is directly proportional to the missing overlap area. Second, if the incoming wavefronts are not perfectly plane, the shear causes the beams to behave as though differential distortion was present as in b), above.

Beam shear occurs when the mechanical axes of the retroreflectors are not coincident with the optical axis. Thus the separations of the incoming and outgoing beams will differ in the two arms and the outgoing beams will not overlap at the recombiner. The solution is proper design and, above all, attention to detail during the assembly process.

5.16.8: Phase dispersion. Phase dispersion manifests itself as an asymmetry in the interferogram. There are two types: linear and non-linear. Linear phase dispersion is not a true dispersion - it simply occurs as a result of the sample points being asymmetric with respect to ZPD. As noted earlier, provided that the *spacing* of the samples is properly maintained, linear effects are readily removed during data processing. Non-linear phase dispersion can also be removed during processing, *provided that it is not too severe* ($\leq 90°$). It has two origins - optical and electronic. Optical phase dispersion occurs primarily in the beamsplitter/recombiner, whose optical thicknesses are frequency-dependent. That is, the ZPD point is slightly different for each frequency. The cure is to ensure that the splitter and

recombiner are as near identical as possible. To that extent, they are self-compensating. Electronic phase dispersion occurs because all analog electronic systems (which includes the actual detector elements) have a finite frequency response, which can result in frequency-dependent phase-shifts. The solution is, of course, to approximate a "linear-phase" system by proper design. Nevertheless, some residuals will occur. Sources of such residuals are the largely uncontrollable capacitance of the detector elements and the inherent characteristics of electronic band-pass filters.

The two types of non-linear phase shift can be distinguished during testing by careful analysis of the interferograms. Electronic dispersion should be independent of the direction of travel of the FTS retroreflectors; optical dispersion reverses as the scan reverses. There is, however, a *caveat*: small dispersive effects occur due to induced lateral shifts in the retroreflectors (because bearings must always have a finite clearance) as the moving elements are being "pushed" or "pulled". This is yet another reason why the scan direction must be recorded.

5.16.9: Channeling. A phenomenon unique to an FTS is channeling, which manifests itself as a near-sinusoidal modulation of the spectral continuum (typically a few percent peak-to-peak). While channeling is generated within the instrument and ought, therefore, to be removable by calibration (or some numerical tricks in data processing), it is universally found that a) removal never works properly; b) channeling changes with the instrument environment (primarily temperature) and c) channeling changes with the character of the source under investigation; point sources generate much stronger channeling than do extended ones.

The origin of channeling is optical interference between the back and front surfaces of transmissive elements (beamsplitter, windows, filters, etc.) in the optical path (or even between elements). Firm requirements are therefore 1) that all transmissive elements be wedged and 2) that there be no paths by which "back surface" light can reach a detector. While antireflection coatings are helpful, they are not a complete solution because they usually cannot cover the wide (5:1) frequency range over which TES must operate. The goal is to keep any residual channeling (post-calibration) to less than 1% (p-p) of the signal.

In the same context, care must be taken to ensure that no light from the control laser reaches the infrared detectors. The laser is so much more powerful than the infrared light to be detected that even scattered laser light can penetrate minute pinholes in the filters and overwhelm the infrared signal.

The wedging of elements must be done with caution because of the potential for angular dispersion of the spectral frequencies. If the wedge angle between back and front faces of any element is α, the parasitic reflected beam is deviated through an angle $\approx 2 \cdot \alpha$. However, the transmitted beam is also deviated by an angle θ in the same sense, where

$$\theta \approx [n(\nu) - 1] \cdot \alpha \quad \text{for small values of } \alpha \qquad (5.7)$$

For common materials such as KBr and Ge, [n(v) - 1] changes by 6 - 8% over the TES operating range, so "overkill" in wedging is to be avoided. Obviously, since the TES detector arrays are rectangular, the unwanted beams should be sent in a direction perpendicular to the long axis of the arrays. Some relief from the effects of dispersion can be obtained by judicious alternation of the wedge directions (i.e., the wedging effect should be compensating rather than cumulative). However, detailed ray tracing will be required to ensure that multiple reflections between transmissive elements are avoided.

Two further points: the filters, being the transmissive elements closest to the detectors, must be very carefully mounted. Furthermore, account must be taken of the fact that the substrates will have different refractive indices. *Therefore, the wedge angle will not be the same for all filters*. The second point involves the beam splitter and recombiner. Their wedges must be parallel rather than antiparallel so that each ray passes through the same amount of material, remembering that a ray which enters a retroreflector closest to its internal axis also emerges closest to the axis.

5.16.10: Pointing location. When downlooking, the pointing location as defined by the system optical axis **(Note that there is no detector actually on-axis)** will be determined from coordinates derived from the spacecraft ephemeris and attitude. At the limb, there is an additional constraint: the optical axis (boresight) must be aimed at the 16 km altitude point (to ±1 pixel with respect to a reference geoid). This permits the "negative" Pixel 8 to overlap the horizon and the "positive" Pixel 8 to be centered at 33.3 km. Knowledge of the true boresight direction is determined in ground data processing.

The basic pointing range requirements are that the line-of-sight from TES be pointable through a cone of semi-angle 45° and to -72° with respect to spacecraft nadir in-track. This will enable all downlooking and limb science objectives to be met and also permit a "cold space" view for calibration purposes. In addition, the pointing mirror must be able to rotate to view all on-board calibration sources.

The range (refracted & unrefracted), tangent height and airmass as a function of nadir angle is shown in Table XVIII. Note that these data (especially at tangent heights less than 30 km) are strongly influenced by the temperature-pressure profile of the atmosphere. That is, to some extent the observation point (downlooking and limb) is unpredictable. Furthermore, refraction at very low tangent heights induces a spatial dispersion into the ray paths - the IFOV in the vertical direction will be slightly enlarged.

_____

Notes to Table XVIII (next page):
a) Calculations are for a spherical Earth and the US Standard Atmosphere;
b) "Range" is measured *along* the light path;
c) This is the unrefracted grazing ray

Table XVIII: Refracted & Unrefracted Viewing Geometry from 705 km (a)

Nadir Angle (Deg)	Unrefracted Tangent Height, km	Refracted Tangent Height, km	Relative Air Mass	Refracted Range (km) (b)	Unrefracted Range (km) (b)
0	0	0	1.0017	705.0	705.0
10	0	0	1.0208	717.1	717.1
20	0	0	1.0826	755.8	755.8
30	0	0	1.2038	829.6	829.7
40	0	0	1.4285	959.3	959.3
45	0	0	1.6145	1059.4	1059.5
50	0	0	1.8994	1200.4	1200.5
55	0	0	2.3974	1414.0	1414.0
60	0	0	3.6004	1794.3	1794.4
61	0	0	4.1242	1916.6	1916.8
62	0	0	4.9488	2073.0	2073.3
63	0	0	6.5567	2292.8	2293.6
63.25	0	0	7.2691	2366.3	2367.3
63.5	0	0	8.2746	2453.1	2454.6
63.75	0	0	9.8584	2561.1	2563.5
64	0	0	12.9795	2710.8	2716.5
64.1	0	0	15.5318	2797.0	2807.5
64.2	0	0	21.1988	2929.1	2967.4
64.22	0	0	23.6577	2971.4	3080.6 (Note c)
64.25	1.6	0	34.3449	3102.4	3077.2
64.26	2.2	0.53	71.5170	3132.5	3076.1
64.27	2.7	1.16	66.5358	3129.2	3074.9
64.28	3.3	1.79	61.8149	3124.4	3073.8
64.29	3.8	2.42	57.4897	3120.8	3072.7
64.3	4.3	3.03	53.2294	3116.9	3071.6
64.35	7.0	6.07	36.4229	3099.8	3066.0
64.4	9.7	9.01	24.4722	3085.5	3060.5
64.45	12.3	11.88	15.9312	3073.5	3054.9
64.5	15.0	14.71	10.1163	3060.9	3049.3
64.52	16.0	(nominal aimpoint)			
64.55	17.7	17.47	6.5205	3051.4	3043.7
64.6	20.3	20.19	4.2167	3043.2	3038.1
64.65	23.0	22.88	2.7606	3035.8	3032.6
64.7	25.6	25.55	1.8165	3029.1	3027.0
64.75	28.3	28.21	1.2017	3022.8	3021.4
64.8	30.9	30.85	0.8045	3016.8	3015.8
64.85	33.5	33.49	0.5382	3010.9	3010.2
64.9	36.13	36.12	0.3629	3005.1	3004.6
64.95	38.7	38.74	0.2498	2999.3	2999.0
65	41.4	41.36	0.1731	2992.7	2993.4
65.5	67.2	67.24	0.0062	2937.3	2937.3
66	92.6	92.63	0.0001	2881.0	2880.9
67	141.9	141.92	0	2767.6	2767.6
67.1	146.7	146.74	0	2756.2	2756.2
67.16	149.6	149.63	0	2749.3	2749.3
67.69	175.	175.	0	2688.3	2688.8
68.23	200.	200.	0	2626.6	2627.0
68.79	225.	225.	0	2563.1	2562.5
69.35	250.	250.	0	2497.7	2497.9
70.0	278	278	0	2422.5	2422.5
71.0	319	319	0	2306.	2306.
72.0	349				

5.16.11: Pointing stability. An FTS requires extreme pointing stability because signal modulation induced by pointing jitter is indistinguishable from interferogram modulation. That is, the jitter-induced signal can overwhelm the required signal and render the results worthless. The situation is exacerbated at the limb because the radiance gradients can be very severe - as much as a factor of two across the width of a *single* pixel. Trial limb retrievals with simulated 1 km peak-to-peak jitter ($\equiv$ 320 μrad) result in errors that exceed a factor of two. Such jitter is totally unacceptable. Accordingly, the following "not to exceed" requirements have been placed on the pointing (referenced to the boresight vector):

Pitch (i.e. perpendicular to the horizon):	75 μrad peak-to-peak
Roll:	1 mrad peak-to-peak
	($\equiv$ 1.1 mrad about the spacecraft X-axis)
Yaw:	750 μrad peak-to-peak

The budgeting of these values between the spacecraft and the TES Pointing Control System is an engineering consideration and is therefore not discussed here.

5.15.12: Contamination. TES is a cryogenic instrument: most of the optics being maintained at 180 K and the filters, cold stops and focal planes at 65 K. Consequently, it is unavoidable that over a period of time condensible vapors will deposit themselves on critical surfaces. The most likely contaminants are water vapor, carbon dioxide and organic species (lubricants, encapsulation & insulator materials, paints, etc) as they evaporate and/or decompose in the space environment; although it should be noted that at 65K even nitrogen and oxygen condense. The contamination will manifest itself a) by reducing the system SNR (less signal will be transmitted *and* more background emitted, a double impact) and b) by imposing unwanted absorption features on the spectra.

The first line of defense is avoidance: the interior of TES must be as clean as possible prior to launch. TES must also be provided with appropriate, deployable, covers for use when events such as thruster firings occur.

*** Note, therefore, that TES must never be operated except under a hard vacuum ***

When avoidance fails (as it will), TES will be outgassed by permitting it to warm up to spacecraft ambient, or even a little higher. The warm-up, cool-down, cycle will probably take many hours to accomplish. The criterion for performing the outgassing will be either that the spectra have scientifically unacceptable absorptions due to specific contaminants or the signal from the calibration sources declines by 5%.

5.17: Signal Chain & Data System

5.17.1: Introduction. TES has 64 independent detectors. That is, although the detectors are to be constructed as 1 x 16 arrays (each element 0.075 x 0.75 mm) with minimum inter-element "dead" space, each element will have a separate signal chain. **This is a TES requirement, not an option, because:**

- Multiplexed focal planes are sampled by a clock. As discussed earlier, this is not permissible for a Fourier Transform Spectrometer;

- Multiplexed focal planes have a very limited dynamic range and are subject to saturation. As discussed earlier, an FTS has strong linearity requirements;

- Multiplexed focal planes have very limited frequency response. TES requires full response to 18 kHz.

- Using independent signal chains offers valuable fault-tolerance to the system. Multiplexed focal planes are much less fault-tolerant.

5.17.2: Optical filter selection. The filter bands tabulated earlier were selected on the basis of: a) scientific utility; b) optimization of signal-to-noise ratio vs. spectral bandpass (information content); c) optimization of fit to allowed spectral bands (aliases) defined by the Nd:YAG control laser frequency and the FTS inter-sample step length (an integral number of Nd:YAG wavelengths) with appropriate allowance for filter "tail-off" and noise definition; d) minimization of data rate and volume.

5.17.3: Electrical filter selection. It is evident from the transformation equation (5.5) that it is, in principle, redundant to employ both optical and electrical filtering. Indeed, if the OPD scan rate were perfectly constant and reproducible, it would be possible to eliminate the optical filters entirely! Unfortunately, the cut-off of all plausible electrical filters is too slow to permit this (an optical interference filter is a direct analog of a 20 - 30 pole electrical filter, which would be most difficult to realize). Nevertheless, electrical filtering is essential unless it can be guaranteed that detector and signal chain noise is always negligible compared to photon shot noise. Since experience shows that this is rarely the case, the TES signal chains will incorporate switchable or tunable electrical filters whose response matches (to a reasonable degree) that of the optical filters. The design must ensure that OPD scan rate variations do not corrupt the signal through amplitude modulation (to 3% peak-to-peak), which implies that the electrical filter bandwidth must be somewhat larger than is desirable.

Now, electrical filters, by definition, impose frequency-dependent phase shifts on the signal. As discussed earlier (§ 5.16), *linear* phase dispersion is equivalent to a position shift of the interferogram and is trivially corrected in data processing. What must be avoided are major ($> \pi/2$) *deviations* from linearity. This should not be difficult to accomplish.

5.17.4: Single-scan data rates & volumes. With these precepts in mind, it is possible to construct another table based on the data of Table XVI that defines the total data rates and volumes for each filter, remembering that downlooking observations use a scan time of 4 seconds, whereas limb observations require 16 seconds. The results are shown in Table XIX. The corresponding electrical requirements are shown in Table XX.

5.17.5: Permissible science data error rate. We wish to establish a goal of 99% recovery of uncorrupted interferograms. Since as little as a single 1 bit error can invalidate an interferogram, it follows that a substantial degree of error-correction encoding will be essential, given that the average Global Survey limb interferogram contains about 1 Mb.

Table XIX: FILTER BAND INTERFEROMETRIC PROPERTIES, DATA RATES & VOLUMES (per array)

Filter ID	Filter Half-Power Points, cm⁻¹		Sampling Step	Sampling Alias	Alias Boundaries cm⁻¹		Sampling Rate kHz	Short Scans Rate Mbps	Short Scans Volume Mb	Long Scans Rate Mbps	Long Scans Volume Mb
Array 1A (1900 - 3050 cm⁻¹)											
1A1	1900	2250	8	4	1761	2348	4.959	1.269	5.078	1.269	20.31
1A2	2200	2450	9	5	2087	2609	4.408	1.128	4.514	1.128	18.06
1A3	2425	2650	12	7	2348	2740	3.306	0.846	3.385	na	na
1A4	2600	2850	8	5	2348	2935	4.959	1.269	5.078	na	na
1A5	2800	3050	9	6	2609	3131	4.408	1.128	4.514	na	na
							Average:	1.128	4.512	1.200	19.19
Array 1B (820 - 1150 cm⁻¹)											
1B1	820	1050	8	2	587	1174	4.959	1.269	5.078	1.269	20.31
1B2	950	1150	11	3	854	1281	3.607	0.923	3.693	0.923	14.77
							Average:	1.096	4.384	1.096	17.54
Array 2A (1100 - 1950 cm⁻¹)											
2A1	1100	1325	10	3	939	1409	3.967	1.016	4.062	1.016	16.25
2A2	1300	1550	8	3	1174	1761	4.959	1.269	5.078	1.269	20.31
2A3	1500	1750	10	4	1409	1879	3.967	1.016	4.062	1.016	16.25
2A4	1700	1950	9	4	1566	2087	4.408	1.128	4.514	1.128	18.06
							Average:	1.107	4.429	1.107	17.72
Array 2B (650 - 900 cm⁻¹)											
2B1	650	900	9	2	522	1044	4.408	1.128	4.514	1.128	18.06
						COMPOSITE (4-BAND) AVERAGE:		4.459	17.836	4.531	72.51
						PER-FILTER AVERAGE:		1.115	4.459	1.127	18.04
						WORST-CASE PEAK VALUES:		4.935	19.740	4.935	78.96

Revised 7/15/97

Table XX: FILTER BAND SPECTRAL & ELECTRICAL PROPERTIES

Filter ID	Filter Half-Power Points, cm⁻¹		Sampling Step	Alias	Alias Boundaries cm⁻¹		Sampling Rate kHz	Alias Boundaries Lower kHz	Upper kHz	1dB Electrical Bandwidth Lower kHz	Upper kHz
Array 1A (1900 - 3050 cm⁻¹)											
1A1	1900	2250	8	4	1761	2348	4.959	7.44	9.92	8.03	9.50
1A2	2200	2450	9	5	2087	2609	4.408	8.82	11.02	9.29	10.35
1A3	2425	2650	12	7	2348	2740	3.306	9.92	11.57	10.24	11.19
1A4	2600	2850	8	5	2348	2935	4.959	9.92	12.40	10.98	12.04
1A5	2800	3050	9	6	2609	3131	4.408	11.02	13.22	11.83	12.88
Array 1B (820 - 1150 cm⁻¹)											
1B1	820	1050	8	2	587	1174	4.959	2.48	4.96	3.46	4.44
1B2	950	1150	11	3	854	1281	3.607	3.61	5.41	4.01	4.86
Array 2A (1100 - 1950 cm⁻¹)											
2A1	1100	1325	10	3	939	1409	3.967	3.97	5.95	4.65	5.60
2A2	1300	1550	8	3	1174	1761	4.959	4.96	7.44	5.49	6.55
2A3	1500	1750	10	4	1409	1879	3.967	5.95	7.93	6.33	7.39
2A4	1700	1950	9	4	1566	2087	4.408	6.61	8.82	7.18	8.24
Array 2B (650 - 900 cm⁻¹)											
2B1	650	900	9	2	522	1044	4.408	2.20	4.41	2.75	3.80

THIS PAGE INTENTIONALLY LEFT BLANK

6: CALIBRATION REQUIREMENTS

6.1: Introduction

An emission-mode instrument such as TES is critically dependent on its calibrations, both preflight and inflight. If the inflight radiometric calibration system fails, TES spectra cannot be converted to radiance units and the primary objective of extracting quantitative abundance profiles of tropospheric gases will be defeated.

6.2: General Requirements

TES requires three types of calibration to be performed both pre-flight and in-flight: radiometric, spatial and spectral.

6.2.1: Radiometric. Detailed analysis through spectral simulations suggest that, in order not to compromise abundance retrievals, the line-of-sight temperature profile must be known to 2K or better. At the longer wavelengths (beyond $4\mu m$), this requires a radiometric calibration accuracy of 1% (see §6.3.3). In addition, an FTS can be seriously impacted by system non-linearity. Modeling of likely non-linearities in detectors and data systems (especially the analog-digital converters, ADC's) shows that the end-to-end system non-linearity must be known to 1% or better. It should also be noted that an EOS Mission requirement is that radiometric calibrations be traceable to NIST standards or their equivalent.

6.2.2: Spatial. Since TES employs four independent, but optically-conjugated, detector arrays, proper registration of the data from each requires that the relative pixel positions be known to 1% in both axes. In addition, the pixel-to-pixel sensitivity variations must be mapped to 0.5% or better in order not to impact the radiometric accuracy.

6.2.3: Spectral. Although an FTS is generally regarded as "self-calibrating" in the spectral domain, this is less true for an imaging FTS where the off-axis pixels are subject to an effective frequency shift and distortion of the instrumental line shape. These effects must be mapped prior to launch using both monochromatic sources and gas cells. During flight, any changes will be monitored from the atmospheric spectra themselves.

6.3: Detailed Requirements

6.3.1: Approach. In order for TES to meet its scientific goals and to permit intercomparisons with other instruments, an extensive series of preflight and inflight calibrations is planned. The basic calibration requirements were outlined in §6.2 and it is evident that state-of-the-art radiance sources and calibration techniques will be essential. The first task will be to model each element of the system and to compare the empirical calibrations to the model on a component-by-component basis.

The methodology for radiometric calibration is similar to that for a filter radiometer. A blackbody source, radiometrically accurate to 0.1 K, uniform to 1% and large enough to overfill the instrument field-of-view by at least 25%, illuminates the instrument. Spectra are acquired *in vacuo* using every combination of filters and detector elements over a range of at least ambient to 340 K, generating a set of look-up tables that characterize the system gain and offset over the complete spectral and dynamic range and permitting conversion of Data Numbers (DN) to the physical units of watts/cm^2/sr/cm^{-1}. The utilization of these tables, together with the spatial and spectral calibrations, is an inherent part of the Level 1B data processing (§8.2).

TES calibrations will be maintained throughout its operational life through the use of specialized on-board hardware. The tables, as they are updated, will be an important resource for judging the performance of the system and for identifying any degradation. Thus, every calibration set will be archived at the DAAC both before and after launch. In addition, we plan to validate both the radiometry and the conversions to geophysical parameters (Level 2 processing) through a series of field tests (see below).

6.3.2: Preflight Calibrations. All system-level calibrations must be performed with TES at its inflight operating temperatures. This will require a thermal vacuum chamber with LN_2-cooled walls large enough to accommodate all the necessary calibration hardware. In addition, the chamber must be provided with solar-simulation lamps to investigate the impact of changing solar illumination on system stability and an Earth-shine simulator to exercise the radiative cooling.

Radiometric. Radiometric calibration data will be obtained for each detector of each focal plane. The linearity and stability of the instrument response through expected in-orbit temperature cycles will also be determined. The calibration determined from the laboratory blackbody source will be compared to the calibration using the on-board source(s). Several sequences of data will be collected at each intensity level, and the entire cycle repeated to collect multiple inputs for each calibration point. These latter data are used as inputs to the calibration uncertainty analysis, along with estimated errors on blackbody accuracy. Note that the desired 1% accuracy is required only at frequencies below 2500 cm^{-1}. Above 2500 cm^{-1} (i.e., Filters 1A3 - 1A5), a reduced accuracy is acceptable, declining to 3% at 3050 cm^{-1}.

It should further be noted that scan averaging must be done with caution. In general, only scans obtained in the same direction of travel should be combined.

Signal-to-Noise Ratio. The system signal-to-noise ratio will be determined with as many redundant techniques as possible. For example, part of the retrieved signal is expected to be zero (that portion out of the electrical and optical passband). The noise in this region can be compared to the signal within the passband, for one measure of SNR (assuming additive noise). In addition, multiple spectra, obtained from alternate scans obtained while viewing a radiometrically stable source, can be averaged for mean and deviation. Systematic noise

sources, for example those caused by electrical interference and optical channeling, will be determined by comparison to predicted spectral output. In addition, the system response to a very cold stimulus (i.e., « 220 K) will be characterized in order to determine both the noise "floor" and the system self-emission.

Spectral Calibration. In order successfully to employ synthetic spectral fitting techniques to the data, the decalibrated frequency accuracy should be better than 1% of the spectral resolution (± 0.00025 cm^{-1}). The inherent stability of the Nd:YAG control laser is much better than this; however, thermal drifts of the frequency are a known problem. Preflight calibration scans will be made using gas cells containing well-studied gases (e.g., CO_2, CO, N_2O) at low pressure to verify both the spectral stability and the impact on off-axis pixels of systematic frequency shifts and instrumental profile distortion (see §5.5 and Appendix A). In flight, actual atmospheric spectra will play a similar role.

Spatial Characterization. The angular response, off-axis rejection and inter-array registration of each pixel must be carefully determined. Off-axis rejection is particularly important for limb observations because the rapid change in source radiance in the mid-troposphere (up to 40% per km) can seriously impact both spectral analysis and radiometric accuracy. Thus the requirement on off-axis rejection is that no more than 10% of the radiation nominally impinging on the next pixel can "leak" onto the target pixel.

The approach of choice is to illuminate the system with pencil beams small compared to a pixel. While this could be done using the pointing mirror, better control could be had by the use of a 2-dimensional moving aperture at the focus of a collimator (a so-called "target projector") equipped with a broad-band source (which need not, itself, be calibrated).

Modulation Index. The interferometer Modulation Index is most readily determined by illuminating the system with monochromatic beams (a set of diode lasers, for example) and recording the fringe amplitude as compared to the signal seen with 100% amplitude modulation of the source with the system held at a fixed path difference (see Appendix F for a detailed description). The goal is 1% accuracy at the selected frequencies.

6.3.3: In-Orbit Calibrations.

Radiometric. An on-board blackbody source (capable of temperature excursions between ambient and 340 K) and deep space viewing will be implemented. The blackbody will be a cavity about 6.5 cm in diameter (to fill a 5 cm beam) provided with appropriate heaters and temperature sensors.

Most radiometric calibrations will be 2-point (space and 340 K), providing a gain and offset, taken at 0.1 cm^{-1} resolution. During Global Surveys, one of the filter sets will be calibrated every 81.2 seconds. Since there are 2 such sets (see Tables XX & XXI), a complete sequence will be acquired every 162 seconds. Requirements are derived as follows:

91

Let G(v) be the calibration gain (slope) and O(v) the offset. The relationship between the source radiance R(v) and the measured signal S(v) is simply:

$$R(v) = G(v) \cdot S(v) + O(v) \tag{6.1}$$

The unknown gain and offset are determined by observing calibration sources at two different temperatures T_1 and T_2. If we can assume that the sources behave as perfect black bodies, their radiance is given by the Planck function:

$$P(v,T) = \frac{c_1 \cdot v^3}{\exp(\frac{c_2 \cdot v}{T}) - 1} \tag{6.2}$$

where $c_1 = 1.1910439 \times 10^{-12}$ and $c_2 = 1.438769$ for a result in watts/cm^2/sr/cm^{-1} (August 1993 values from *Physics Today*). Thus

$$G(v) = \frac{P_1(v,T_1) - P_2(v,T_2)}{S_1(v) - S_2(v)} \tag{6.3}$$

and

$$O(v) = P_1(v,T_1) - G(v) \cdot S_1(v) \tag{6.3a}$$

Note that the denominator of Eqn. 6.3 contains the difference between two empirically-determined quantities. That is, they are both noisy and their difference is even noisier (roughly by a factor of $\sqrt{2}$). Furthermore, it is normal to ensure that T_1 is at a higher temperature than any potential real target, so P_1 will also be the largest signal ever measured. The resultant ratio G(v) will therefore be noisier yet, especially near the edges of the filters. When the offset O(v) is determined, the gain is multiplied by the observed signal and the resultant noise is uncorrelated with that of the gain - even more noise in the calibrated target data! It goes without saying that we wish to avoid compromising the target data by adding unnecessary extra noise in the calibration process - the "rule of thumb" being that the SNR of the calibration constants should be at least 3 times better than that of the target data (more is better). At least 10 calibration sequences are necessary to achieve this.

From time-to-time, a multipoint calibration (at least 10 scans at each of 10 temperatures plus a space view) will be performed using every filter. This will test slope, offset and system linearity. Early in the mission, however, these will be performed frequently.

Intermittently (once or twice per year), a set of full-resolution (0.025 cm^{-1}) calibration scans will be made using the blackbody at 340 K. This will test the assumption that no sharp spectral features have appeared from contaminants or residual outgassing that would compromise the routine calibrations.

Spatial. A hot-wire source parallel to the long axis of the detectors will be swept across the arrays using the pointing mirror with TES operating in its low-resolution (downlooking) mode. Since spectral data are not an issue here, the scans can be made through an open position in the filter wheels to enhance the signal. Single scans will be made at 10 positions across each element. The outcomes will be: a) a 1-dimensional mapping of the detector responsivity; b) the pixel-to-pixel registration in the crucial short direction; c) the off-axis rejection and inter-element cross-talk by interrogation of unilluminated pixels. The measurement should be made once or twice per year (again, more frequently earlier in the mission).

Spectral. Spectral calibrations in orbit will be performed by careful modeling of sharp lines of well-known species such as CO_2, CO and N_2O. With isolated lines and good signal-to-noise ratio, positions to 1% of the resolution (i.e., ± 0.00025 cm^{-1} at the limb; ± 0.001 cm^{-1} in the nadir) can be achieved. These calibrations will be most concerned with the *linearity* of the frequency scale, since the absolute frequencies are subject to a large variety of poorly-quantifiable shifts (§5.5). Indeed, the spectra will be used to quantify these shifts rather than the other way round.

6.3.4: Field Validation. In order to validate TES temperature and molecular species retrievals, a series of field experiments using AES and other instruments will be planned for the first and third years of data collection. The validations will be accomplished by a suite of ground-based and airborne instruments, operated simultaneously with EOS overflights. Although it is not possible to duplicate exactly the geometry and conditions of the EOS observation, the validating observations will be made to obtain measurements of parameters which do not vary over the scale of the TES footprint and are, more or less, invariant in time. Accessible sites (which should include large bodies of water) will be selected which are substantially uniform over an area at least as large as the TES footprint.

Ground-based measurements.

Spectrometer. A high resolution "solar occultation" spectrometer such as the JPL Mk.IV system would be valuable to provide accurate column densities over the site. By investigation of line shapes, some limited altitude profiling can also be accomplished. A passive microwave spectrometer might also be useful for this purpose (on a limited range of species).

Radiosonde. A radiosonde should be employed to obtain accurate values of the temperature and moisture profiles during the overflight.

Ozonesonde. An ozonesonde should be a regular feature of such experiments.

Radiometer. A narrow-band (~ 10 nm) infrared radiometer operating over the same wavelength range as TES will be useful in establishing the correct values of surface radiance. Such instruments are widely available.

Thermometers. Accurate values of the surface temperatures, along with the radiometric temperatures derived from other instrumentation, can be used to derive values for the surface emissivity.

Reflectometers and reflectance standards. The reflected solar component of radiance is important in the short wavelength limit of TES. A measure of the surface reflectivity will provide data to verify the accurate retrieval of the reflected solar intensity. A candidate instrument is the JPL Field-Portable Reflectance Spectrometer.

Airborne instrumentation.

Balloon-borne spectrometer. Although little profiling of molecular species abundances can be accomplished with a ground-based spectrometer, a spectrometer floating at 40 km (e.g., on a balloon gondola) can obtain profiles down to the surface and column densities above the instrument. It is recognized that balloon-borne experiments are costly and difficult to control (i.e., the instrument flight-path is hard to predict), but such an instrument and instrument platform could usefully emulate the TES data set. Candidate systems are the University of Denver SCRIBE and the Goddard SFC SIRIS spectrometer. However, both of these systems are quite old and would probably require considerable refurbishment.

Radiometers. An airborne spectroradiometer would allow us to map the TES footprint more efficiently and more accurately than point measurements collected at the surface. Such an instrument would fly at low altitudes to map the surface upwelling radiance at spatial scales more appropriate for comparison to the satellite data.

6.3.5: Correlative Measurements. A related topic to validation is correlative measurements, the main difference being that correlative measurements are on-going, rather than sporadic. The entire suite of instruments discussed under validation is also pertinent here but of particular value would be the Airborne Emission Spectrometer (AES) flying on the NASA P3, C140 or DC8 because of its similarity to TES (for downlooking observations). Such a program would be particularly useful for results comparisons under partially-cloudy conditions (since the aircraft can fly below the clouds) and could result in improved algorithms for space data retrieval: as much as 50% of TES data is expected to be cloud-contaminated. Another advantage of such a flight program would be to identify locations that would benefit from the long-term monitoring capability of the spaceborne system.

We should also encourage continuous operation of such *in situ* devices as ozone lidars and ozonesonde flights. In particular, we hope that a global network of ozonesondes can be created and maintained throughout the EOS era.

7: PROVISIONAL MISSION PLAN

7.1: Introduction

Before proceeding to the Ground Data System Concepts (§8), it is necessary to estimate what rates and volumes of science data are to be handled, based on the information developed in §5. For this a provisional Mission (Operations) Plan must be outlined. Such a plan also plays a significant role in the determination of spacecraft resource requirements.

As discussed in §5.15, the primary TES mode is a periodic Global Survey of tropospheric ozone and its precursors. Interspersed with these acquisitions may be occasional Intensive Campaigns primarily aimed at regional phenomena that are reasonably predictable and sporadic Special Events - localized phenomena often called "targets of opportunity".

The periodic Global Survey generates the TES Standard Products (Table I), which are also the highest priorities for global tropospheric chemistry. At the same time, the Global Survey data are searched for unexpected or sporadic species and flagged if there appears to be a difference between the actual and the expected spectrum. The generation of these flags is part of the standard processing but their analysis is a Special Product (i.e., studies performed by the Science Team at their own facilities). The results of Intensive Campaigns and Special Events would also be Special Products.

7.2: Global Surveys

Global Surveys are the basic TES operating mode. Tables XXI & XXII show a mix of filters that accomplishes the goal of a complete survey of tropospheric ozone chemistry, together with the associated data rates and volumes. As discussed in §5.15, following a pair of "embedded" calibration scans (cold space and the internal hot blackbody, see Table XXIII), 2 nadir observations followed by 3 trailing-limb observations will be made every 81.2 seconds for 4 days (58 orbits), followed by 4 days of other types of measurement. With an interval of 81.2 seconds, pairs of nadir and limb views will observe roughly the same airmass with a delay of 422 seconds (because of the 3100 km range to the limb). The phasing is illustrated in Fig.11b. The start of each 4 day cycle will be triggered by the predicted time of the crossing of the southern apex (the most southerly point of the orbit) to ensure that the data sets observe the same geographic locations. Note, however, that the two sets obtained in a 16-day interval (the orbit repeat time) are separated by about 2° in equatorial longitude.

An important ingredient of the Mission Plan is the 2 orbits of continuous calibration that precede and follow each of the 4 day sets ("bracketing" calibrations, see Table XXIV) in which every combination of filters are exercised repeated sequences of 40 observations of cold space and the hot blackbody (Fig. 11a). These are the principal system diagnostics: the function of the embedded calibrations is primarily to track any changes that may occur during the 4-day surveys. The resultant combination produces the data volumes shown in Table XXV.

95

All basic calibrations are obtained at low (4 second scan) resolution because it is expected that no sharp features (less than 0.1 cm^{-1}) will be present in the calibration data. Consequently, by simple analytic extension, we should be able to expand these calibrations to match the higher resolution limb views without loss of accuracy. In order to ensure that this assumption is, indeed, true, we shall occasionally produce a set of calibration data at high (16 second scan) resolution (see §7.7). Thus the bracketing calibrations not only of aid the calibration of the atmospheric data but also serve as our fundamental database against which instrument performance will be judged.

It should also be noted that embedded calibrations are obtained in pairs so that we have close-in-time sets of "forward" and "reverse" scans for each because of the likelihood of a dependence on scan directions. The phasing is shown in Table XXVI.

Table XXI: GLOBAL SURVEY NADIR OBSERVATION FILTER MIX

ARRAY I.D.

Scan No.		1A	1B	2A	2B	Totals
1	Filter	1A1	1B2	2A1	2B1	
	Range (cm^{-1})	1900 - 2250	950 - 1150	1100 - 1325	650 - 900	
	Rate (Mbps)	1.269	0.923	1.016	1.128	4.336
	Volume (Mb)	5.078	3.693	4.062	4.514	17.34
2	Filter	1A1	1B2	2A1	2B1	
	Range (cm^{-1})	1900 - 2250	950 - 1150	1100 - 1325	650 - 900	
	Rate (Mbps)	1.269	0.923	1.016	1.128	4.336
	Volume (Mb)	5.078	3.693	4.062	4.514	17.34
Total Interferograms:		32	32	32	32	128

Principal Species Measured:

O_3, CO, CH_4, H_2O

T_{atmos}, T_{surf}, e_{surf}

Average data rate (per scan):	4.336 Mbps
Average data volume (per scan):	17.34 Mb
Total volume (2 x 4 sec scans):	34.69 Mb
Average volume per interferogram:	271 kb

Revised 3/21/99

Table XXII: GLOBAL SURVEY LIMB OBSERVATION FILTER MIX

ARRAY I.D.

Scan No.		1A	1B	2A	2B	Totals
1	Filter	1A1	1B1	2A1	2B1	
	Range (cm^{-1})	1900 - 2250	820 - 1050	1100 - 1325	650 - 900	
	Rate (Mbps)	1.269	1.269	1.016	1.128	4.682
	Volume (Mb)	20.31	20.31	16.26	18.06	74.91
2	Filter	1A1	1B2	2A4	2B1	
	Range (cm^{-1})	1900 - 2250	950 - 1150	1700 - 1950	650 - 900	
	Rate (Mbps)	1.269	0.923	1.128	1.128	4.448
	Volume (Mb)	20.31	14.77	18.06	18.06	71.17
3	Filter	1A1	1B2	2A4	2B1	
	Range (cm^{-1})	1900 - 2250	950 - 1150	1700 - 1950	650 - 900	
	Rate (Mbps)	1.269	0.923	1.128	1.128	4.448
	Volume (Mb)	20.31	14.77	18.06	18.06	71.17
Total Interferograms:		48	48	48	48	192

Principal Species Measured:

O_3, CO, CH_4, NO, NO_2, HNO_3, H_2O

T_{atmos}

Average data rate (per scan):	4.526 Mbps
Average data volume (per scan):	72.42 Mb
Total volume (3 x 16 sec scans):	217.25 Mb
Average volume per interferogram:	1.132 Mb

Revised 3/21/99

Table XXIII: GLOBAL SURVEY EMBEDDED CALIBRATIONS FILTER MIX

ARRAY I.D.

Type (2 scans each)		1A	1B	2A	2B	Totals
1	**Filter**	1A1	1B1	2A1	2B1	
Space	**Range (cm⁻¹)**	1900 - 2250	820 - 1050	1100 - 1325	650 - 900	
&	**Rate (Mbps)**	1.269	1.269	1.016	1.128	4.682
B-B	**Volume (Mb)**	5.076	5.076	4.062	4.512	18.728
2	**Filter**	1A1	1B2	2A4	2B1	
Space	**Range (cm⁻¹)**	1900 - 2250	950 - 1150	1700 - 1950	650 - 900	
&	**Rate (Mbps)**	1.269	0.923	1.128	1.128	4.448
B-B	**Volume (Mb)**	5.076	3.692	4.512	4.512	17.792

Total Interferograms per type: 32   32   32   32   128

Average data rate (per scan):   4.565 Mbps

Average data volume (per scan):   18.26 Mb

Total volume (4 x 4 sec scans):   73.04 Mb

Average volume per interferogram: 285 kb

Revised 3/21/99

Note:

Scan types alternate. Hence filters 1A1 & 2B1 are calibrated every 81.2 seconds, 1B1/1B2 & 2A1/2A4 every 162.4 seconds

Table XXIV: GLOBAL SURVEY BRACKETING CALIBRATIONS FILTER MIX

Scans		1A	1B	2A	2B	Totals
1-10 B-B	Filter	1A1	1B1	2A1	2B1	
	Range (cm⁻¹)	1900 - 2250	820 - 1050	1100 - 1325	650 - 900	
	Rate (Mbps)	1.269	1.269	1.016	1.128	4.682
	Volume (Mb)	5.076	5.076	4.062	4.512	18.728
11-20 Space	Filter	1A1	1B1	2A1	2B1	
	Range (cm⁻¹)	1900 - 2250	820 - 1050	1100 - 1325	650 - 900	
	Rate (Mbps)	1.269	1.269	1.016	1.128	4.682
	Volume (Mb)	5.076	5.076	4.062	4.512	18.728
21-30 B-B	Filter	1A1	1B2	2A4	2B1	
	Range (cm⁻¹)	1900 - 2250	950 - 1150	1700 - 1950	650 - 900	
	Rate (Mbps)	1.269	0.923	1.128	1.128	4.448
	Volume (Mb)	5.076	3.692	4.512	4.512	17.792
31-40 Space	Filter	1A1	1B2	2A4	2B1	
	Range (cm⁻¹)	1900 - 2250	950 - 1150	1700 - 1950	650 - 900	
	Rate (Mbps)	1.269	0.923	1.128	1.128	4.448
	Volume (Mb)	5.076	3.692	4.512	4.512	17.792
Total Interferograms:		640	640	640	640	2560

ARRAY I.D.

Average data rate (per scan): 4.565 Mbps

Average data volume (per scan): 18.26 Mb

Total volume per sequence(40 x 4 sec scans): 730.4 Mb

Average volume per interferogram: 285 kb

Revised 3/21/99

100

Table XXV: GLOBAL SURVEY MISSION PLAN

(Standard Product)

ACQUISITION: Take Global Survey (Nadir and Trailing Limb plus embedded calibrations) measurements every 81.2 seconds ($\pm 82°$ of latitude) for 4 days (58 orbits) plus 2+ orbits of continuous (bracketing) calibration data immediately before and after

NADIR MODE: repeatedly stare at selected in-track ground locations (2 short scans per sequence)
LIMB MODE: make 3 consecutive long scans immediately following the nadir scans
EMBEDDED & BRACKETING CALIBRATIONS: exercise all employed filters viewing cold space and the hot blackbody

Repeat at 8-day intervals → 46 surveys/"year" (1 "year" = 368 days)

ORBIT DATA: Exactly 233 orbits per 16 days (14 9/16 per day). Nodal period is 5933.05 seconds.
All sequences triggered by the (predicted) time of southern apex passage.
All measurements made at the same latitudes on each orbit.

∴ 81.2 seconds ≈5° of latitude at the equator

∴ 73 sequences/orbit. ∴ 4,234 sequences/survey → 194,764 sequences/"year"

SAMPLING: (Excluding bracketing cals)

DATA RATES: (Average per scan)

NADIR MODE:	4.336 Mbps
LIMB MODE:	4.526 Mbps
EMBEDDED & BRACKETING CALS:	4.565 Mbps

DATA VOLUME:

NADIR MODE: 128 interferograms/sequence (34.69 Mb).
541,952 interferograms/survey (146.88 Gb)
24,929,792 interferograms/"year" (6.76 Tb)

LIMB MODE: 192 interferograms/sequence (217.25 Mb)
812,928 interferograms/survey (919.8 Gb)
37,394,688 interferograms/"year" (42.31 Tb)

Table XXV (cont): GLOBAL SURVEY MISSION PLAN

EMBEDDED CALIBRATIONS:

Phased in pairs of "forward" & "reverse" scans

128 interferograms/sequence (36.52 Mb).
541,952 interferograms/survey (154.63 Gb)
24,929,792 interferograms/"year" (7.11Tb)

BRACKETING CALIBRATIONS:

Use same filter combinations as for Embedded Calibrations, but in blocks of 10 scans each of Blackbody and Cold Space (i.e., each sequence consists of 40 scans). Each sequence occupies 4[(10 x (4 + 1.2)) + 2.6] = 218.4 seconds. In 2 orbits the run therefore can contain 54 sequences (with about 72.5 seconds to spare).

Two such runs accompany each 4-day Global Survey.

Data also used to determine contamination state (5% decline in response = "contaminated")

VOLUMES:

2560 interferograms/sequence (730.4 Mb)
138,240 interferograms/run (39.44 Gb)
276,480 interferograms/survey (78.9 Gb)
12,718,080 interferograms/"year" (3.63 Tb)

DATA OPERATIONS: LEVEL 1:

Interferograms → Spectra (Volume 1:1; 60 Tb/"year" each)

LEVEL 2:

Spectra → Concentration Profiles of Standard Products (see Table I)
(7 per sequence) + atmospheric temperature profile + surface temperatures (~32) + land surface emissivity (~32)
Each profile (from merged limb & averaged nadir data): 16 points, 32 bits/point = 512 bits/profile

Volume = 6144 bits/sequence

194,764 sequences/year

∴ Annual volume = 1,558,112 profiles (1.2 Gb)

102

Table XXVI: Global Survey Embedded Calibrations Phasing

Orbit #	Seq. #	View	Filters				Scan Dir.
N	0	Sp	1A1	1B1	2A1	2B1	F
		BB	1A1	1B1	2A1	2B1	R
		N1	1A1	1B2	2A1	2B1	F
		N2	1A1	1B2	2A1	2B1	R
		L1	1A1	1B1	2A1	2B1	F
		L2	1A1	1B2	2A4	2B1	R
		L3	1A1	1B2	2A4	2B1	F
	1	Sp	1A1	1B1	2A1	2B1	R
		BB	1A1	1B1	2A1	2B1	F
	2	Sp	1A1	1B2	2A4	2B1	F
		BB	1A1	1B2	2A4	2B1	R
	3	Sp	1A1	1B2	2A4	2B1	R
		BB	1A1	1B2	2A4	2B1	F
	4	Sp	1A1	1B1	2A1	2B1	F
		BB	1A1	1B1	2A1	2B1	R
	5	Sp	1A1	1B1	2A1	2B1	R
		BB	1A1	1B1	2A1	2B1	F
	.						
	70	Sp	1A1	1B2	2A4	2B1	F
		BB	1A1	1B2	2A4	2B1	R
	71	Sp	1A1	1B2	2A4	2B1	R
		BB	1A1	1B2	2A4	2B1	F
	72	Sp	1A1	1B1	2A1	2B1	F
		BB	1A1	1B1	2A1	2B1	R
N+1	0	Sp	1A1	1B1	2A1	2B1	R
		BB	1A1	1B1	2A1	2B1	F
	1	Sp	1A1	1B2	2A4	2B1	F
		BB	1A1	1B2	2A4	2B1	R
	2	Sp	1A1	1B2	2A4	2B1	R
		BB	1A1	1B2	2A4	2B1	F
	3	etc.	etc.	etc.	etc.	etc.	etc.

Note 1: Complete sequence shown for first row only. Thereafter, just the embedded calibrations.
Note 2: Calibration pattern repeats every 4 orbits (orbit N+4 ≡ orbit N)

103

7.3: Intensive Campaigns

Intensive Campaigns either employ a "stacked scan" in-track downlooking mode to produce a transect across a regional phenomenon or a continuous series of limb observations of the upper troposphere/lower stratosphere or for intercomparisons with other limb sounders. Note that the specific scenarios outlined below a) are not the only possibilities and b) are by no means "cast in concrete". Again, they are only examples of how TES might be used in order to bound the spacecraft resource and subsequent data processing requirements. Note also that Intensive Campaigns and Special Events observations would not be permitted to interfere with Global Mode observations. Each observation set will be bracketed by a set of calibration scans similar to those for the Global Surveys.

7.3.1: Urban/Regional Pollution Event. The primary emphasis here will be on ozone, carbon monoxide and water vapor, requiring 3 scans at each point. The transect length can be up to 220 km long, occupying 250 seconds. It is expected that about 10 such events may occur each year around the globe and each one may be observed twice - unfortunately, a sun-synchronous polar orbit is unfavorable for synoptic monitoring. Table XXVII shows the filter mix and Table XXVIII the composite data rates and volumes.

7.3.2: Biomass Burning. Biomass burning involves several species which require 2 scans at each point. In this case, the transect length can be 348 km long, occupying 270 seconds. Since the primary areas of interest are tropical South America and Africa, only 2 events per year are assumed, each observed twice. Table XXIX shows the filter mix and Table XXX the composite data rates and volumes.

7.3.3: Stratospheric Effects of Biomass Burning. In conjunction with the foregoing, we may also undertake limb scans to measure lofting of the plume into the upper troposphere and lower stratosphere. As in Global Surveys, these would be delayed by some 7 minutes from the start of the transect. Table XXXI shows the filter mix and Table XXXII the composite data rates and volumes.

7.3.4: Stratospheric Effects of Volcanos. It is well-known that volcanos are a significant source of sulphate aerosols in the lower stratosphere. These aerosols, in turn, have measurable impacts on global mean temperatures, sometimes (e.g., Mt. Pinatubo) lasting for several months. The signatures of aerosols are fairly broad but are easily recognized (but much less easily *quantified*). Such events are relatively infrequent - an upper estimate would be once per year. Since the plumes tend to spread along latitude zones, the approach will be to make cross-plume limb transects ($\pm 10°$ along the orbit, say) on repeated orbits. The campaign would last until the plume dispersed. Table XXXIII shows the filter mix and Table XXXIV the composite data rates and volumes.

7.3.5: HiRDLS Intercomparisons. The High Resolution Dynamics Limb Sounder (HiRDLS) on CHEM is an infrared radiometer aimed at determining horizontal and vertical distributions of

various tracer gases in the lower and middle stratosphere. As such, it observes many of the same gases as TES except that HiRDLS exchanges spectral for spatial resolution (i.e., TES has high spectral resolution at the expense of modest vertical resolution and spot-samples the atmosphere. HiRDLS, by contrast, offers near-continuous horizontal coverage with very high vertical resolution). However, one of the consequences of the HiRDLS approach is that it is susceptible to the effects of unmodeled (or imperfectly modeled) interloper species. TES can provide HiRDLS with this information. In turn, the better vertical resolution (factor of 4-5) of HiRDLS will help TES to understand the impacts of vertical inhomogeneity on our retrievals. It has therefore been agreed that, occasionally, HiRDLS and TES (in its limb mode) will observe the same places at the same time in an effort to make a synergistic improvement in both data sets. Table XXXV shows the filter mix and Table XXXVI the composite data rates and volumes.

It is also likely that similar intercomparisons will be made with MLS and, if it is still operating, MIPAS on ENVISAT. However, these observations are currently unquantified.

Table XXVII: INTENSIVE CAMPAIGN - URBAN/REGIONAL POLLUTION EVENT FILTER MIX

ARRAY I.D.

Scan No.		1A	1B	2A	2B	Totals
1 & 6	Filter	1A1	1B2	2A2	2B1	
	Range (cm⁻¹)	1900 - 2250	950 - 1150	1300-1550	650 - 900	
	Rate (Mbps)	1.269	0.923	1.269	1.128	4.589
	Volume (Mb)	5.078	3.693	5.078	4.514	18.36
2 & 5	Filter	1A1	1B2	2A3	2B1	
	Range (cm⁻¹)	1900 - 2250	950 - 1150	1500-1750	650 - 900	
	Rate (Mbps)	1.269	0.923	1.016	1.128	4.336
	Volume (Mb)	5.078	3.693	4.062	4.514	17.34
3 & 4	Filter	1A5	1B2	2A1	2B1	
	Range (cm⁻¹)	2800 - 3050	950 - 1150	1100-1325	650 - 900	
	Rate (Mbps)	1.128	0.923	1.016	1.128	4.195
	Volume (Mb)	4.514	3.693	4.062	4.514	16.78
Total Interferograms:		48	48	48	48	192

Average data rate (per scan): 4.373 Mbps

Average data volume (per scan): 17.49 Mb

Total volume (3 x 4 sec scans): 52.48 Mb

Average volume per interferogram: 273 kb

Principal Species Measured:

O_3, CO, CH_4, N_2O, H_2O, SO_2

T_{atmos}, T_{surf}

*** If multiple (i.e., 4 or more) scans are made, filter order is reversed at the end of each cycle of 3 in order to avoid "more than 1 step" filter-wheel motions ***

Revised 10/13/98

Table XXVIII: URBAN/REGIONAL POLLUTION EVENT MISSION PLAN

(Special Product, Intensive Campaign in Triple-Scan Transect Mode)

ACQUISITION: Expect ~ 10 events/year.
At each location/region, use triple-scan transect mode (15.6 seconds/set). Up to 17 contiguous sets/sequence (51 scans) covering 220 km long x 5 km wide. Note that consecutive sets require a reversal of the filter mix.

Possible repeat 2 days later (synoptic monitoring is not possible from polar orbit)

ORBIT DATA: Transect mode is necessarily parallel to the ground track.

DUTY CYCLE: 100% for 250 seconds (4.3 % for 1 orbit)

SAMPLING: 16 pixels/set
272 pixels/transect (max)
Possible 5,440 pixels/year

DATA RATE: 4.373 Mbps (average/scan)

	Atmospheric Data	Calibration Data
ANNUAL ACQ. TIME:	4,080 sec	9,600 sec
DATA VOLUME:	192 interferograms/set (52.48 Mb)	3840 interferograms/set (1.05 Gb)
	3,264 interferograms/sequence (892.2 Mb)	7,680 interferograms/sequence (2.10 Gb)
	65,280 interferograms/year (17.8 Gb)	153,600 interferograms/year (42.0 Gb)

107

Table XXIX: INTENSIVE CAMPAIGN - REGIONAL BIOMASS BURNING FILTER MIX

ARRAY I.D.

Scan No.		1A	1B	2A	2B	Totals
1	Filter	1A1	1B2	2A1	2B1	
	Range (cm⁻¹)	1900 - 2250	950 - 1150	1100 - 1325	650 - 900	
	Rate (Mbps)	1.269	0.923	1.016	1.128	4.336
	Volume (Mb)	5.078	3.693	4.062	4.514	17.34
Total Interferograms:		16	16	16	16	64

Principal Species Measured:

H_2O, O_3, CO, HNO_3, NH_3, SO_2

T_{atmos}, T_{surf}, T_{plume}, T_{flame}

Average data rate (per scan):	4.336 Mbps
Average data volume (per scan):	17.35 Mb
Total volume (1 x 4 sec scan):	17.35 Mb
Average volume per interferogram:	271 kb

108

Table XXX: REGIONAL BIOMASS BURNING MISSION PLAN

(Special Product, Intensive Campaign in Single-Scan Transect Mode)

ACQUISITION: Expect ~ 2 events/year.
At each location, use single-scan transect mode: up to 68 contiguous single scans covering 885 km long x 5 km wide.

Possible repeat 2 days later.

ORBIT DATA: Transect mode is necessarily parallel to the ground track (i.e. N-S)

DUTY CYCLE: 100% for 348 seconds (5.9% for 1 orbit)

SAMPLING: 16 each 0.5 x 5 km pixels/scan
1,088 pixels/sequence (max)

Potential 4352 pixels/year

DATA RATE: 4.336 Mbps (average)

ANNUAL ACQ. TIME: 1088 sec

	Atmospheric Data	Calibration Data
	1088 sec	640 sec
DATA VOLUME:	64 interferograms/set (17.35 Mb)	1280 interferograms/set (347 Mb)
	4,352 interferograms/sequence (1.18 Gb)	2560 interferograms/sequence (694 Mb)
	17,408 interferograms/year (4.72 Gb)	10240 interferograms/year (2.78 Gb)

Table XXXI: LIMB CAMPAIGN - STRATOSPHERIC EFFECTS OF BIOMASS BURNING FILTER MIX

ARRAY I.D.

Scan No.		1A	1B	2A	2B	Totals
1	Filter	1A1	1B2	2A1	2B1	
	Range (cm^{-1})	1900 - 2250	950 - 1150	1100 - 1325	650 - 900	
	Rate (Mbps)	1.269	0.923	1.016	1.128	4.426
	Volume (Mb)	20.31	14.77	16.26	18.06	70.82
Total Interferograms:		16	16	16	16	64

Principal Species Measured:

H_2O, O_3, CO, HNO_3, HCN, CH_4, $CH_3C(O)CH_3$, C_2H_2, H_2O_2

T_{atmos}

Average data rate (per scan): 4.426 Mbps

Average data volume (per scan): 70.82 Mb

Total volume (1 x 16 sec scan): 70.82 Mb

Average volume per interferogram: 1.11 Mb

Table XXXII: STRATOSPHERIC EFFECTS OF BIOMASS BURNING MISSION PLAN

(Special Product, Intensive Limb Campaign)

PURPOSE: Large-scale biomass burning (e.g., southern Africa and the Amazon Basin plus occasional regional-scale wildfires such as occurred in Indonesia recently) can generate enough smoke and aerosols to penetrate to the upper troposphere and lower stratosphere. These aerosols can persist for long periods and be distributed around the entire globe with significant climatic impacts.

To a large extent, such events will be mapped during our Global Surveys. Nevertheless, there may be occasions when more continuous observations are warranted and this plan covers such a contingency.

FREQUENCY: Annual event (July - October)

Observe plume twice per orbit for a full day (14 orbits)

ASSUMPTIONS: The fires generate a large, South Atlantic, plume 5 - 10° of latitude wide

The basic plan is to make N-S limb (long scan) transects over about 20° of latitude centered on the plume, with the standard sets of short-scan calibrations (10 each of cold space and Blackbody) before and after.

TIMING: Time to cover 20° along the orbit ≈ 330 seconds = 19 long scans = 1 sequence

DATA RATE: 4.43 Mbps

ANNUAL ACQ. TIME: 8,512 sec

VOLUMES:

Atmospheric Data	Calibration Data
1216 interferograms/sequence (1.35 Gb)	2560 interferograms/sequence (708.2 Mb)
34048 interferograms/run (37.7 Gb)	71680 interferograms/run (19.8 Gb)
34048 interferograms/year (37.7 Gb)	71680 interferograms/year (19.8 Gb)

4,480 sec

Table XXXIII: LIMB CAMPAIGN - STRATOSPHERIC EFFECTS OF VOLCANOS FILTER MIX

ARRAY I.D.

Scan No.		1A	1B	2A	2B	Totals
1	Filter	1A1	1B1	2A1	2B1	
	Range (cm^{-1})	1900 - 2250	820 - 1050	1100 - 1325	650 - 900	
	Rate (Mbps)	1.269	1.269	1.016	1.128	4.682
	Volume (Mb)	20.30	20.30	16.26	18.05	74.91
Total Interferograms:		16	16	16	16	64

Principal Species Measured:

O_3, CO, N_2O, H_2O, SO_2, H_2SO_4, OCS, NO, HNO_3

T_{atmos}, Aerosol Opacity

Average data rate (per scan):	4.682 Mbps
Average data volume (per scan):	74.91 Mb
Total volume (1 x 16 sec scan):	74.91 Mb
Average volume per interferogram:	1.17 Mb

Table XXXIV: STRATOSPHERIC EFFECTS OF VOLCANIC ERUPTIONS MISSION PLAN

(Special Product, Intensive Limb Campaign)

PURPOSE: Large volcanic eruptions (e.g., Mt. Pinatubo) can have significant (and measurable) impacts on the upper troposphere and lower stratosphere, primarily because of the generation of dense sulphate aerosols (intermixed with liquid sulphuric acid droplets). These aerosols can persist for many months and be distributed around the entire globe with significant climatic impacts.

To a large extent, such events will be mapped during our Global Surveys. Nevertheless, there may be occasions when more continuous observations are warranted and this plan covers such a contingency.

FREQUENCY: Estimate 1 event per year

Observe plume twice per orbit for a full day (14 orbits)

ASSUMPTIONS: The volcano generates a globe-encircling plume 5 - 10° of latitude wide within the tropics (or at least below mid-latitudes - near-polar volcanos will require special handling)

The basic plan is to make N-S limb (long scan) transects over about 20° of latitude centered on the plume, with the standard sets of short-scan calibrations (10 each of cold space and Blackbody) before and after.

TIMING: Time to cover 20° along the orbit ≈ 330 seconds = 19 long scans = 1 sequence

DATA RATE: 4.68 Mbps

Atmospheric Data   **Calibration Data**

ANNUAL ACQ. TIME: 8,512 sec   4, 480sec

VOLUMES: 1216 interferograms/sequence (1.42 Gb)   2560 interferograms/sequence (708.2 Mb)
34048 interferograms/run (39.8 Gb)   71680 interferograms/run (19.8 Gb)
34048 interferograms/year (39.8 Gb)   71680 interferograms/year (19.8 Gb)

113

Table XXXV: HiRDLS INTERCOMPARISON LIMB OBSERVATION FILTER MIX

Scan No.		1A	1B	2A	2B	Totals
				ARRAY I.D.		
1 & 8	Filter	1A1	1B2	2A4	2B1	
	Range (cm^{-1})	1900 - 2250	950 - 1150	1700-1950	650 - 900	
	Rate (Mbps)	1.269	0.932	1.128	1.128	4.457
	Volume (Mb)	20.30	14.77	18.05	18.05	71.31
2 & 7	Filter	1A1	1B2	2A1	2B1	
	Range (cm^{-1})	1900-2250	950 - 1150	1100 - 1325	650 - 900	
	Rate (Mbps)	1.269	0.932	1.016	1.128	4.345
	Volume (Mb)	20.30	14.77	16.26	18.05	69.52
3 & 6	Filter	1A1	1B1	2A3	2B1	
	Range (cm^{-1})	1900-2250	820 - 1050	1500-1750	650 - 900	
	Rate (Mbps)	1.269	1.269	1.016	1.128	4.682
	Volume (Mb)	20.30	20.30	16.26	18.05	74.91
4 & 5	Filter	1A1	1B1	2A2	2B1	
	Range (cm^{-1})	1900-2250	820 - 1050	1300 - 1550	650 - 900	
	Rate (Mbps)	1.269	1.269	1.269	1.128	4.935
	Volume (Mb)	20.30	20.30	20.30	18.05	78.96
Total Interferograms:		64	64	64	64	256

Average data rate (per scan): 4.605 Mbps

Average data volume (per scan): 73.68 Mb

Total volume (4 x 16 sec scans): 294.7 Mb

Average volume per interferogram: 1.151 kb

Revised 3/21/99

Principal Species Measured:

O_3, CO, NO, NO_2, HNO_3, H_2O, N_2O, $ClONO_2$, CFC11, CFC12

T_{atmos}

*** Filter order reversed on alternate scan sets ***

114

Table XXXVI: HiRDLS INTERCOMPARISON MISSION PLAN

(Special Product, Intensive Limb Campaign)

PURPOSE: It has been agreed that, occasionally, HiRDLS and TES (in its limb mode) will observe the same places at the same time in an effort to make a synergistic improvement in both data sets.

ACQUISITION: The TES boresight will be raised to 32 km (nominal nadir angle 64.82°).

Because of concerns about rapidly-changing M1 mirror temperatures around the terminator, we shall avoid making measurements within ± 500 seconds of the temperature peak regions (which may be time-shifted from the actual terminator crossings).

Will be performed TBD (twice) per year.

TIMELINE:
1) With respect to the Southern Apex, calculate the time offset for avoidance of temperature peaks;

2) Configure for calibration (short) scans [~10 sec];

3) At time t=0, calibrate 10 scans each filter combination, B-B & Space [437 sec]

4) Configure for limb (long) scans [~ 10 sec]

5) Acquire 15 sets (4 scans/set) of limb data [1032 sec]

6) Configure for calibration [10 sec];

7) Calibrate [437 sec]; total time ~ 1926 sec;

8) Wait ~1000 sec

9) Repeat 3 - 7

DUTY CYCLE: 65% for 1 orbit

DATA RATE: 4.605 Mbps average

115

Table XXXV(cont): HiRDLS INTERCOMPARISON MISSION PLAN

Atmospheric Data

Calibration Data

ANNUAL ACQ. TIME: 4128 sec

1748 sec

VOLUME:

256 interferograms/set [4 long scans/set] (294.7 Mb)
15 sets/sequence
3840 interferograms/sequence (4.42 Gb)
2 sequences/run
9600 interferograms/run (8.84 Gb)
19,200 interferograms/year (17.68 Gb)

256 interferograms/set [4 short scans/set] (73.68 Mb)
20 sets/sequence
5120 interferograms/sequence (1.47 Gb)
4 sequences/run
20,480 interferograms/run (5.89 Gb)
40,960 interferograms/year (11.78 Gb)

116

7.4: Special Events

Special Events generally employ staring at a particular location, either to improve signal-to-noise or to search for some limited time variability (over a few minutes).

7.4.1: Volcanology. There are some 200 active volcanos in the world, a fraction of which emit copious amounts of gas (others, e.g., Mt. St. Helens, emit mostly ash and dust). The EOS Volcanology team has requested that TES monitor at least 10 of these about 12 times per year (Table XXXVII). The wide range of gases emitted requires that 4 scans be made to cover them. Table XXXVIII shows the filter mix and Table XXXIX the composite data rates and volumes.

Table XXXVII: VOLCANOS TO BE MONITORED

(Note: This is the current "top ten" list. It will change with time)

Name	Place	Latitude	Longitude
Colima	Mexico	19.42N	103.72W
Erebus	Antarctica	77.53S	167.15E
Etna	Sicily	37.73N	15.00E
Fuego	Guatemala	14.48N	90.88W
Kilauea	Hawaii	19.30N	155.11W
Lascar	Chile	23.37S	67.73W
Masaya	Nicaragua	11.98N	86.15W
Pacaya	Guatemala	14.38N	90.60W
Sakurajima	Japan	31.58N	130.67E
White Island	New Zealand	37.52S	177.18E

The data in this table were provided by Joy Crisp of JPL

7.4.2: Industrial Catastrophe. Certain major industrial catastrophes (e.g., Chernobyl, Bhopal) are sufficiently large-scale that TES may well be able to detect their gaseous emissions. Luckily, such events are infrequent so we estimate 1 per year. In this case, TES will exercise its search capability since the emitted gases are, in general, unpredictable. Table XL shows the filter mix and Table XLI the composite data rates and volumes.

Table XXXVIII: SPECIAL EVENT - VOLCANOLOGY FILTER MIX

		ARRAY I.D.				
Scan No.		1A	1B	2A	2B	Totals
1	Filter	1A2	1B2	2A1	2B1	
	Range (cm^{-1})	2200 - 2450	950 - 1150	1100 - 1325	650 - 900	
	Rate (Mbps)	1.128	0.923	1.016	1.128	4.195
	Volume (Mb)	4.514	3.693	4.062	4.514	16.78
2	Filter	1A1	1B1	2A1	2B1	
	Range (cm^{-1})	1900 - 2250	820 - 1050	1100 - 1325	650 - 900	
	Rate (Mbps)	1.269	1.269	1.016	1.128	4.682
	Volume (Mb)	5.078	5.078	4.062	4.514	18.73
3	Filter	1A5	1B2	2A1	2B1	
	Range (cm^{-1})	2800 - 3050	950 - 1150	1100 - 1325	650 - 900	
	Rate (Mbps)	1.128	0.923	1.016	1.128	4.195
	Volume (Mb)	4.514	3.693	4.062	4.514	16.78
4	Filter	1A1	1B1	2A1	2B1	
	Range (cm^{-1})	1900 - 2250	820 - 1050	1100 - 1325	650 - 900	
	Rate (Mbps)	1.269	1.269	1.016	1.128	4.682
	Volume (Mb)	5.078	5.078	4.062	4.514	18.73
Total Interferograms:		64	64	64	64	256

Principal Species Measured:

H_2O, CO, CO_2, HCl, SO_2, HNO_3, CH_4

T_{atmos}, T_{surf}, T_{plume}

Average data rate (per scan): 4.439 Mbps

Average data volume (per scan): 17.75 Mb

Total volume (4 x 4 sec scans): 71.02 Mb

Average volume per interferogram: 277 kb

Revised 10/13/98

118

Table XXXIX: VOLCANOLOGY MISSION PLAN

(Special Product, Targeted Special Event)

ACQUISITION: Expect ~ 10 targets/year. See Appendix F for pointing algorithms. At each volcano, use target staring mode. Stare for up to 208 seconds (function of off-nadir angle) → 40 scans/sequence (10 sets of 4 scans each).

Spatial resolution 0.5 x 5 km; footprint 8 x 5 km (nadir)

Repeat 2 days later if possible and again 16 & 18 days later. Revisit site twice more during the year.

ORBIT DATA: Volcanos anywhere within a nominal 705 km of ground track can be accessed some time within 0 - 8 days.

DUTY CYCLE: 100% for 208 seconds/volcano. 3.5%/volcano for 1 orbit

SAMPLING: 10 sets/sequence. Possibly 12 sequences/volcano. 10 volcanos/year.

Potential 1200 sequences/year (each comprising 16 pixels)

DATA RATE: 4.439 Mbps (average/sequence)

ANNUAL ACQ. TIME: 192,000 sec

	Atmospheric Data	Calibration Data
		768,000 sec

DATA VOLUME:

	Atmospheric Data	Calibration Data
	256 interferograms/set (71.02 Mb)	5120 interferograms/set (1.42 Gb)
	2560 interferograms/sequence (710 Mb)	10,240 interferograms/sequence (2.84 Gb)
	3,072,000 interferograms/year (852 Gb)	12,288,000 interferograms/year (3.41 Tb)

119

Table XL: SPECIAL EVENT - INDUSTRIAL CATASTROPHE FILTER MIX

Scan No.		1A	1B	2A	2B	Totals
ARRAY I.D.						
1 & 8	Filter	1A1	1B2	2A4	2B1	
	Range (cm^{-1})	1900 - 2250	950 - 1150	1700-1950	650 - 900	
	Rate (Mbps)	1.269	0.932	1.128	1.128	4.457
	Volume (Mb)	5.078	3.693	4.514	4.514	17.83
2 & 7	Filter	1A1	1B2	2A1	2B1	
	Range (cm^{-1})	1900-2250	950 - 1150	1100 - 1325	650 - 900	
	Rate (Mbps)	1.269	0.932	1.016	1.128	4.345
	Volume (Mb)	5.078	3.693	4.062	4.514	17.38
3 & 6	Filter	1A5	1B1	2A3	2B1	
	Range (cm^{-1})	2800-3050	820 - 1050	1500-1750	650 - 900	
	Rate (Mbps)	1.128	1.269	1.016	1.128	4.541
	Volume (Mb)	4.514	5.078	4.062	4.514	18.16
4 & 5	Filter	1A4	1B1	2A2	2B1	
	Range (cm^{-1})	2600 - 2850	820 - 1050	1300 - 1550	650 - 900	
	Rate (Mbps)	1.269	1.269	1.269	1.128	4.935
	Volume (Mb)	5.078	5.078	5.078	4.514	19.74
Total Interferograms:		64	64	64	64	256

Principal Species Measured:

O_3, CO, CO_2, H_2O, CH_4, Hydrocarbons, N_2O, HCl, SO_2

T_{atmos}, T_{surf}, T_{plume}

*** Filter order reversed on alternate scan sets ***

Average data rate (per scan): 4.570 Mbps

Average data volume (per scan): 18.28 Mb

Total volume (4 x 4 sec scans): 73.12 Mb

Average volume per interferogram: 286 kb

Revised 3/21/99

Table XLI: INDUSTRIAL CATASTROPHE MISSION PLAN

(Special Product, Targeted Special Event)

ACQUISITION: Expect ~1 event/year. See Appendix F for pointing algorithms. Requires "rapid response" capability. At each location, use target staring mode. Stare for up to 208 seconds (function of off-nadir angle) → 40 scans/sequence (10 sets of 4 scans each). Note that consecutive sets require a reversal of the filter mix.

Spatial resolution 0.5 x 5 km; footprint 8 x 5 km (nadir)

Repeat 2 days later if possible and again 16 & 18 days later.

ORBIT DATA: Locations anywhere within a nominal 705 km of ground track can be accessed some time within 0 - 8 days.

DUTY CYCLE: 100% for up to 208 seconds. 3.7% for 1 orbit.

SAMPLING: 10 sets/sequence. Potential 4 sequences/year.

DATA RATE: 4.570 Mbps (average/sequence)

Atmospheric Data	Calibration Data

ANNUAL ACQ. TIME: 640 sec   2560 sec

DATA VOLUME:
256 interferograms/set (73.12 Mb)   5120 interferograms/set (1.46 Gb)
2560 interferograms/sequence (731 Mb)   10240 interferograms/sequence (2.92 Gb)
10,240 interferograms/year (2.9 Gb)   40,960 interferograms/year (11.68 Gb)

121

7.5: Sporadic Calibrations

7.6.1: Linearity & Gain Calibration. Twice per year (much more frequently early in the mission), the blackbody will be cycled from ambient up to 340 K in 20 K steps with a complete suite of observations made as above. In addition, a space view will define the system "noise floor" and the system self-emission. The major reason for such an elaborate scheme is to verify the end-to-end system linearity and to measure the relative gains within each gain-switchable signal chain. At least one filter from each set will be employed - probably 1A1, 1B1, 2A1 & 2B1, since they are expected to receive the highest flux levels. Table XLIII shows the filter mix and Table XLIV the composite data rates and volumes. If required, non-linearity corrections will be applied to the interferograms in Level 1B processing.

7.6.2: Spatial Calibrations. Not currently quantified are the "hot wire" spatial calibrations because a) they are expected to be very infrequent (perhaps once or twice per year) and b) they should generate very little data. As stated earlier (§6.2), the data will be used to determine both the inter-array alignments and the off-axis rejection. The data will be used by the Science Team as part of the Level 2 retrieval process.

7.6.3: Global Survey Calibration Extension. Twice per year we shall compare the calibration of long and short scans. The results will primarily be used to ensure that the routine calibrations (done at low resolution) are not missing sharp instrumental or outgassing features. If these are observed, the Science Team will recommend that a decontamination cycle be performed. Table XLV shows the filter mix and Table XLVI the composite data rates and volumes.

7.6: Special Product Timing

Because individual Special Product observations are quite short (a few minutes at most), it would be inefficient to use embedded calibrations. We shall therefore obtain the needed calibrations before and after in a bracketing mode.

In order to construct a basis for a timeline, we need to know 1) the time of the atmospheric observations, 2) their duration and 3) the duration of the calibrations to be added on either end. From the analyses presented in Appendix F, the simplest approach for determining 1) is from the time of closest approach for targeted observations or the time of nadir passage for transects or the mid-range of limb campaigns. That is, these are the nominal mid-points (t_0) of the atmospheric observations.

The algorithm for determining the duration t_c of each calibration is

$$t_c = N[10(4 + t_i) + t_r + 10(4 + t_i) + t_r]$$

where N is the number of scans per set (defined in the "filter mix" tables), t_t is the turn-around time (currently estimated as 1.2 seconds) and t_r is the time to move from the blackbody to a space view (or *vice versa*, currently estimated as 2.6 seconds).

The results for each of the identified (atmospheric) Special Products are shown in Table XLII. Note that, in practice, it may be necessary to add a few seconds to the calibration times to allow for setup.

Table XLII: Special Product Timelines (Basis)

Mode	Special Product	Atmospheric Observation Start/End time $t_0 \pm$ (sec)	Calibration Duration added before & after (sec)
Transect	Biomass Burning	177	109
Transect	Urban/Regional Pollution	125	328
Limb Campaign	Stratospheric Effects of Volcanos	165	109
Limb Campaign	Stratospheric Effects of Biomass Burning	165	109
Limb Campaign	HiRDLS Intercomparison	516	437
Targeted	Volcanos	105	437
Targeted	Industrial Catastrophe	105	437

7.7: Summary

Table XLVI summarizes the science data rates and volumes for all types of observation on an annual basis (no overhead for embedded engineering data or error correction).

Table XLIII: LINEARITY & GAIN CALIBRATION FILTER MIX

ARRAY I.D.

Scan No.		1A	1B	2A	2B	Totals
1-10 Space	Filter	1A1	1B1	2A1	2B1	
	Range (cm⁻¹)	1900 - 2250	820 - 1050	1100 - 1325	650 - 900	
	Rate (Mbps)	1.269	1.269	1.016	1.128	4.682
	Volume (Mb)	5.078	5.078	4.062	4.514	18.73
11-20 B-B	Filter	1A1	1B1	2A1	2B1	
	Range (cm⁻¹)	1900 - 2250	820 - 1050	1100 - 1325	650 - 900	
	Rate (Mbps)	1.269	1.269	1.016	1.128	4.682
	Volume (Mb)	5.078	5.078	4.062	4.514	18.73
Total Interferograms:		320	320	320	320	1280

Average data rate (per scan): 4.682 Mbps

Average data volume (per scan): 18.73 Mb

Total volume per sequence (20 x 4 sec scans): 374.6 Mb

Average volume per interferogram: 146 kb

124

Table XLIV: LINEARITY & GAIN CALIBRATION MISSION PLAN

(Ancillary Special Product)

PURPOSE:

1) Measure non-linearity between input and output using known sources (the internal Black Body at several temperatures) and, if necessary, generate a correction function to be applied to atmospheric interferograms.

2) Measure the *relative* gains of the signal chains by observing the same Black Body temperature at adjacent gain settings (being careful to avoid saturation!).

ACQUISITION:

Twice per year each.

Time to generate a full run is indeterminate until the warming/cooling time constant of the B-B is known (i.e., individual data sequences can be timed, but not the interval between sequences).

No filter changes are required (use longest wavelength filter in each Focal Plane).

LINEARITY CALIBRATION:

Beginning at the maximum allowable temperature (TBD, 340 K), decrease the Black Body temperature in 10 K steps down to ambient (nominally 290 K). Acquire 1 sequence at each step, then reverse the temperature cycling back up to maximum. Assuming 6 temperature steps, a run will consist of 12 sequences.

VOLUMES:

1280 interferograms/sequence (374.6 Mb)
15,360 interferograms/run (4.495 Gb)
30,720 interferograms/year (8.99 Gb)

RELATIVE GAIN CALIBRATION:

With the gain set at its highest value, adjust the B-B temperature so that the A-D is near its upper limit (DN 65535). Acquire one step, acquire a second set; the two sets form a sequence. Increase the B-B temperature so that the A-D is near its upper limit. Reduce the gain 1 step, acquire a second set of scans. Reduce the gain 1 step, acquire a second set to complete the second set of scans. Acquire one set of scans. Reduce the gain 1 step, acquire a second set of scans. Reduce the relative gains of 4 settings). A-D is one again near its limit. Acquire one set of scans (i.e., 3 sequences are required to determine the relative gains of 4 settings). Repeat for the lowest gain setting (i.e., 3 sequences are required to determine the relative gains of 4 settings). Repeat for the lowest gain setting. *** Different temperature settings *may be needed for each Focal Plane, with the potential for quadrupling the Run time* ***

*** *Different temperature settings may be needed for each Focal Plane, with the potential for quadrupling the Run time* ***

ANNUAL ACQ. TIME: 960 sec

VOLUMES:

2560 interferograms/sequence (749.2 Mb)
7680 interferograms/run (2.25 Gb)
15,360 interferograms/year (4.50 Gb)

Table XLV: GLOBAL SURVEY CALIBRATION EXTENSION FILTER MIX

Scans		1A	1B	2A	2B	Totals
				ARRAY I.D.		
1-10 B-B	Filter	1A1	1B1	2A1	2B1	
	Range (cm⁻¹)	1900 - 2250	820 - 1050	1100 - 1325	650 - 900	
	Rate (Mbps)	1.269	1.269	1.016	1.128	4.682
	Volume (Mb)	20.31	20.31	16.26	18.06	74.91
11-20 Space	Filter	1A1	1B1	2A1	2B1	
	Range (cm⁻¹)	1900 - 2250	820 - 1050	1100 - 1325	650 - 900	
	Rate (Mbps)	1.269	1.269	1.016	1.128	4.682
	Volume (Mb)	20.31	20.31	16.26	18.06	74.91
21-30 B-B	Filter	1A1	1B2	2A4	2B1	
	Range (cm⁻¹)	1900 - 2250	950 - 1150	1700 - 1950	650 - 900	
	Rate (Mbps)	1.269	0.923	1.128	1.128	4.448
	Volume (Mb)	20.31	14.77	18.06	18.06	71.17
31-40 Space	Filter	1A1	1B2	2A4	2B1	
	Range (cm⁻¹)	1900 - 2250	950 - 1150	1700 - 1950	650 - 900	
	Rate (Mbps)	1.269	0.923	1.128	1.128	4.448
	Volume (Mb)	20.31	14.77	18.06	18.06	71.17
Total Interferograms:		640	640	640	640	2560

Average data rate (per scan): 4.565 Mbps

Average data volume (per scan): 73.04 Mb

Total volume per sequence (40 x 16 sec scans): 2.92 Gb

Average volume per interferogram: 1.141 Mb

Revised 3/21/99

126

Table XLVI: GLOBAL SURVEY CALIBRATION EXTENSION MISSION PLAN

(Ancillary Special Product)

ACQUISITION: Obtain sequences similar to Bracketing Calibrations in order to verify that short (4 second) calibration scans can be interpolated to calibrate long (16 second) scans. Also used to determine whether any "sharp line" features due to contamination are evident.

Runs obtained twice/year during off-days.

Scans are long (truncated to short scans for interpolation tests).

10 scans each Space & Black Body for each of two filter sets, repeated at least 10 times (i.e., sequence is 40 scans, run is 10 sequences).

If other filters are ever used at the limb, they must be added to this plan.

ORBIT DATA: Each sequence occupies $4[(10 \times (16 + 1.2)) + 2.6] = 698.4$ seconds. Run length is therefore 6984 seconds ($\sim$ 1.1 orbits)

ANNUAL ACQ. TIME: 12,800 sec

DATA VOLUME: 2560 interferograms/sequence (2.92 Gb)
25600 interferograms/run (29.22 Gb)
51200 interferograms/year (58.43 Gb)

Table XLVII: SUMMARY OF TES DATA RATE & ANNUAL VOLUME ESTIMATES

Note: 1 TES "year" = 368 days = 3.18×10^7 sec

OBSERVATION TYPE	ON-TIME (sec)	AV. RATE (Mbps)	NUMBER OF INTERFEROGRAMS	RAW SCIENCE VOLUME (Tb)
Global Survey Nadir	1.56×10^6	4.34	2.49×10^7	6.76
Global Survey Limb	9.35×10^6	4.53	3.74×10^7	42.31
Embedded Calibration	1.56×10^6	4.57	2.49×10^7	7.11
Bracketing Calibration	7.95×10^5	4.57	1.27×10^7	3.63
TOTAL STANDARD PRODUCTS	1.33×10^7	4.50	9.99×10^7	59.81
Intensive Campaigns	4.76×10^4	4.56	5.0×10^5	0.21
Special Events	9.63×10^5	4.44	1.54×10^7	4.30
Other Calibration	1.38×10^4	4.68	6.66×10^4	0.06
TOTAL SPECIAL PRODUCTS	1.02×10^6	4.47	1.16×10^8	4.57

WORST CASE DATA RATE (any observation type): 4.935 Mbps for 16 sec

AVERAGE DATA RATES computed for active time only

Revised 3/21/99

8: GROUND DATA SYSTEM CONCEPTS

8.1: Data Acquisition

8.1.1: Types. All the science data to be transmitted to the ground are of a similar type: samples of the amplitude of the interferogram as a function of FTS optical path difference.

8.1.2: Rates. The data rates vary filter-to-filter (Table XIX). The worst case combination of filters (never, in fact, used) generates 4.935 Mbps. The average during identified operations is about 4.5 Mbps.

8.1.3: Volumes. The data volumes are totally determined by the allowable duty cycle. The single-scan (actual science) volumes range from 3 to 20 Mb. For the mission scenarios discussed in §7, total volumes can reach 312 Gb per day at Level 0 (Global Survey). The expected annual volume is summarized in Table XLVII.

8.2: Data Product Level Definitions

8.2.1: Algorithm Overview.

TES data processing falls naturally into 3 groups:

1) At Level 1A the raw data from the spacecraft are decommutated and the instrument outputs (called *interferograms*) reconstructed. File headers also contain important state data such as time, date, spacecraft and target location, and instrument pointing angle.

2) At Level 1B, the interferograms are phase-corrected, Fourier transformed to spectra (Table XLVIII shows the nominal sizes of the arrays), radiometrically-calibrated and re-sampled onto a common frequency grid. Certain data quality flags are added to the header at this juncture and the results passed to Level 2 [described in the *Level 1B Algorithm Theoretical Basis Document (ATBD)*; JPL D-16479, 1999].

3) At Level 2, vertical concentration profiles of the selected species are extracted from the data through a process of *retrieval* (*Level 2 ATBD*; JPL D-16474, 1999]:

Briefly, all modern retrieval algorithms are somewhat alike: based on an initial estimate of the physical/chemical state of the atmosphere at the time and location of the observation (the so-called first guess), the appropriate version of the Equation of Radiative Transfer is solved to provide an estimate of the expected spectral radiance as seen by the instrument. This forward model is compared to the true spectral radiance and the parameters of the atmospheric state adjusted (using specified rules) to bring the forward model into closer agreement with the observation. The process is iterated until, by other specified rules, convergence is achieved.

The resulting state vector of atmospheric parameters is the desired result. Most algorithms, including the one used by TES, also provide an objective estimate of the accuracy of the retrieval.

8.3: Science Team Participation

8.3.1: Algorithm Development, Test and Verification. Responsibility for development of algorithms to produce standard data products through Level 3 will rest with the TES Science Team using the SCF. High level processing modules (e.g., retrieval codes) will be tested to the extent possible by comparing results with other codes and running simplified test cases. Once the Science Team is satisfied with the performance of these algorithms, they will be implemented to meet EOS and JPL software engineering requirements, including documentation, and installed at the DAAC or PI Processing Facility for subsequent operational usage. Simulated data will be generated at JPL and processed by the DAAC to verify that the retrieval code is operating properly at the system level.

Note that, in order not to become backlogged, TES Standard Products must be generated within 8 days or less of process initialization.

8.3.2: Data Quality Assurance. The TES Science Team will monitor and analyze selected data products from the DAAC daily, using the Science Computing Facility (SCF) at JPL. Processing of a limited subset (probably less than 0.1%) of the TES data using the original Science Team algorithms will insure agreement between expected results and products generated by the DAAC. Field validation experiments (see §4.4 & §6.3) will provide crucial data with which to evaluate the integrity of the basic retrieval algorithms and as such these data will be analyzed in a timely fashion. All anomalies, either discovered during the daily routine monitoring or after the aforementioned field validation experiments, will be immediately reported to the DAAC.

8.3.3: Special Products. All Special Products will be generated "on demand" at the JPL SCF.

8.3.4: Reporting of Results. The principal method of communicating the scientific results from the TES experiment will be publication in the open peer-reviewed literature and presentation of conference papers. An overview of the TES experiment with anticipated results will be published prior to launch. Post-launch publication of instrument performance and initial results from TES will meet the schedule established by the EOS project. Principal authorship on papers by the investigator team will be encouraged in order to disseminate TES results to the Atmospheric and Earth Sciences community.

Table XLVIII: FILTER BAND INTERFEROGRAM SIZE & TRANSFORM REQUIREMENTS

Filter ID	Filter Half-Power Points, cm⁻¹		Sampling Step	Sampling Alias	Alias Boundaries cm⁻¹		Sampling Rate kHz	Short Scans No. of Points	Short Scans FFT* K	Long Scans No. of Points	Long Scans FFT* K
Array 1A (1900 - 3050 cm⁻¹)											
1A1	1900	2250	8	4	1761	2348	4.959	19836	32	79344	128
1A2	2200	2450	9	5	2087	2609	4.408	17632	32	70528	128
1A3	2425	2650	12	7	2348	2740	3.306	13224	16	n/a	n/a
1A4	2600	2850	8	5	2348	2935	4.959	19836	32	n/a	n/a
1A5	2800	3050	9	6	2609	3131	4.408	17632	32	n/a	n/a
Array 1B (820 - 1150 cm⁻¹)											
1B1	820	1050	8	2	587	1174	4.959	19836	32	79344	128
1B2	950	1150	11	3	854	1281	3.607	14426	16	57704	64
Array 2A (1100 - 1950 cm⁻¹)											
2A1	1100	1325	10	3	939	1409	3.967	15869	16	63475	64
2A2	1300	1550	8	3	1174	1761	4.959	19836	32	79344	128
2A3	1500	1750	10	4	1409	1879	3.967	15869	16	63475	64
2A4	1700	1950	9	4	1566	2087	4.408	17632	32	70528	128
Array 2B (650 - 900 cm⁻¹)											
2B1	650	900	9	2	522	1044	4.408	17632	32	70528	128

* If used

Revised 7/15/97

131

THIS PAGE INTENTIONALLY LEFT BLANK

APPENDIX A: EQUATION DERIVATIONS

A.1: The Interferometer Equation

The interferometer equation is fundamental to much of the system analysis. It is easily derived if it is noted that the basic optical system (Fig. A1) can be reduced to Fig. A2 by the beamsplitter reflection.

Fixed Arm

Collimator

Source

Input Frequency
ν cm^{-1}

Beamsplitter

Condenser

Moving Arm
Velocity V cm/sec

Detector
Output Frequency 2.V$\bar{\nu}$ Hz
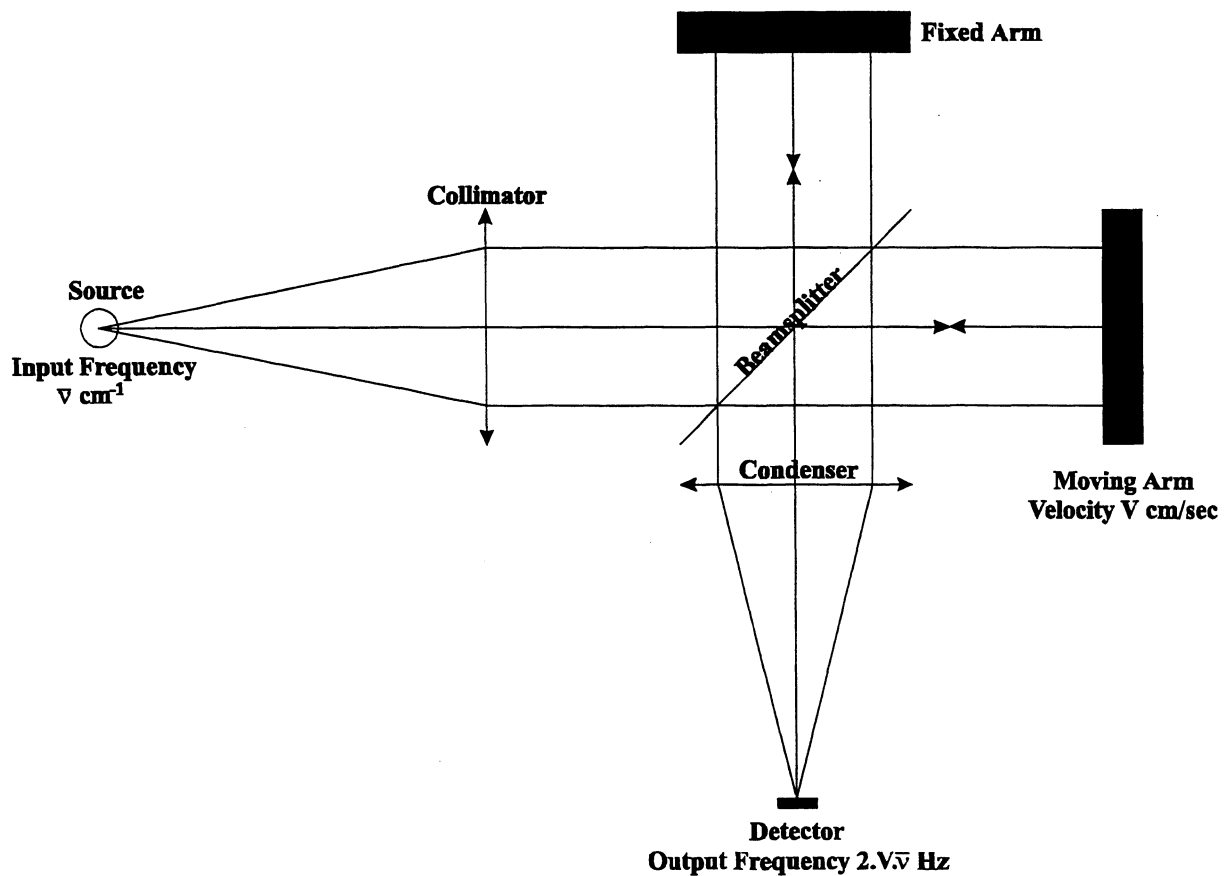
Fig. A1: Schematic of a Michelson Interferometer
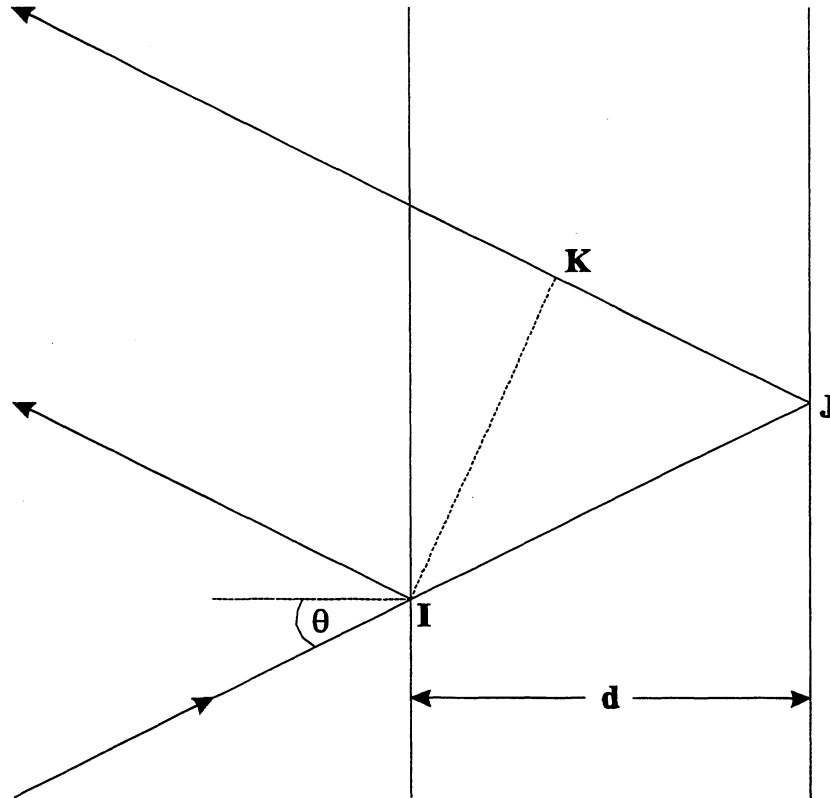
Fig. A2: Optical equivalent of Fig. A1

The *physical* path difference is obviously the distance IJ + JK. From elementary trigonometry,

$$IJ + JK = d/\cos\theta + \cos2\theta \cdot d/\cos\theta = 2 \cdot d \cdot \cos\theta \qquad (A1)$$

Interference maxima (or minima, depending on the phase change at the beamsplitter) occur when the path difference equals an integral number of wavelengths:

$$n \cdot \lambda = 2 \cdot d \cdot \cos\theta, \quad n = 1, 2, 3, \ldots \qquad (A2)$$

If the interferometer is in a medium of refractive index μ, the apparent wavelength is reduced by a factor λ/μ, so the equation becomes:

$$n \cdot \lambda = 2 \cdot \mu \cdot d \cdot \cos\theta, \quad n = 1, 2, 3, \ldots \qquad (A3)$$

134

Finally, if we choose to work with *frequency* ν (units of cm^{-1}) rather than wavelength λ:

$$n = 2 \cdot \mu \cdot \nu \cdot d \cdot \cos\theta, \quad n = 1, 2, 3, \ldots\ldots \tag{A4}$$

For a given ν and d, this expression defines a series of concentric rings, centered on the optic axis.

Note also that non-integral values of n are valid. That is, n can be treated as a continuous variable.

A.2: Intensity distribution for two interfering beams

Assume two electromagnetic waves of frequency ν and phase ϕ_1 and ϕ_2 with amplitudes a_1 and a_2. When superimposed, the resultant complex amplitude is

$$A \cdot \exp[i \cdot \Phi] = a_1 \cdot \exp[i \cdot \phi_1] + a_2 \cdot \exp[i \cdot \phi_2] \tag{A5}$$

The intensity is the square of the amplitude:

$$I = A^2 = a_1^2 + a_2^2 + a_1 \cdot a_2 \cdot \{\exp[i \cdot (\phi_1 - \phi_2)] + \exp[-i \cdot (\phi_1 - \phi_2)]\} \tag{A6a}$$

$$= a_1^2 + a_2^2 + 2 \cdot a_1 \cdot a_2 \cdot \cos(\phi_1 - \phi_2) \tag{A6b}$$

That is, it is only the *phase difference* between the beams that matters, so we may arbitrarily set $\phi_2 = 0$ and, if the linear path difference is x, we may write

$$\phi_1 = 2 \cdot \pi \cdot \nu \cdot x \tag{A7}$$

Replacing the amplitudes by intensities, we get

$$I(x) = I_1 + I_2 + 2 \cdot \sqrt{(I_1 \cdot I_2)} \cdot \cos(2 \cdot \pi \cdot \nu \cdot x) \tag{A8}$$

In the most usual case, $I_1 = I_2 = I_o$ (say), whence

$$I(x) = 2 \cdot I_o \cdot [1 + \cos(2 \cdot \pi \cdot \nu \cdot x)] \tag{A9}$$

$$= 4 \cdot I_o \cdot \cos^2(\pi \cdot \nu \cdot x) \tag{A10}$$

This represents a sinewave that alternates between 0 and $4 \cdot I_o$ with a mean value $2 \cdot I_o$. While it was calculated for a linear path difference, the path difference created by off-axis angles also generates an intensity alternation that is near-sinusoidal. The resultant ring pattern seen in monochromatic light therefore looks like Fig. A3.
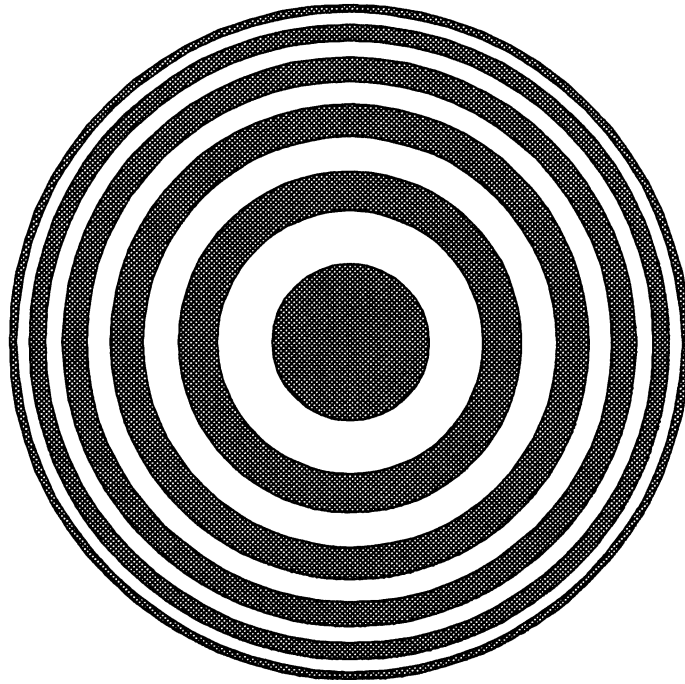
Fig. A3:   *Sketch of the ring (fringe) pattern seen when an interferometer is illuminated with diffuse monochromatic light*

A.3: Modulation Efficiency

Modulation efficiency is now easily understood. Referring to Fig. A1, the light in each arm is reflected once and transmitted once. If the intensity reflection and transmission coefficients are R and T, respectively (absorption loss = A, so that $I_{in} = R + T + A$), we see that

$$I_o = R \cdot T \tag{A11}$$

and

$$I(x) = 4 \cdot R \cdot T \cdot \cos^2(\pi \cdot v \cdot x) \tag{A12}$$

Modulation index is simply the ratio of the sinewave peak-to-peak amplitude relative to the incident (unmodulated) intensity.

A.4: The Interferogram Equation

Referring back to Eq. A9, it is easily seen that it can be generalized for a frequency interval v_1 to v_2:

$$I(x) = \int_{v_1}^{v_2} F(v).[1+\cos(2\pi vx)].dv \qquad (A13)$$

Subtracting out the constant term (the mean value of the interferogram) leaves

$$I'(x) = \int_{v_1}^{v_2} F(v).\cos(2\pi vx).dv \qquad (A14)$$

That is, I'(x) and F(v) form a Fourier Transform Pair, whence

$$F(v) = \frac{1}{L}\int_{0}^{L} I'(x).\cos(2\pi vx).dx \qquad (A15)$$

Eq. A15 is the fundamental equation for extracting a spectrum from an interferogram.

A.5: Off-axis properties of an FTS

In order to use an FTS in an imaging mode, it is essential to keep the detector elements small enough to permit the desired spectral resolution to be achieved.

From Eq. A4, in a vacuum ($\mu \equiv 1$) at a given path difference d and order n, we have

$$v(\theta) = (2 \cdot n/d) \cdot \sec\theta \qquad (A16)$$

On-axis, $\theta = 0$, whence $v(0) = 2 \cdot n/d$ and

$$v(\theta) = v(0) \cdot \sec\theta \qquad (A17)$$

The angular dispersion $\delta v/\delta\theta$ (along any radius from the optic axis) is

$$\delta v/\delta\theta_r = v(0) \cdot \sec\theta_r \cdot \tan\theta_r \qquad (A18a)$$

which, for the small angles of interest here, becomes

$$\delta v/\delta\theta_r \approx v(0) \cdot \theta_r \qquad (A18b)$$

If the desired height resolution at the limb is δL_r and the range to the tangent point is R, then the required *angular* resolution is

$$\delta\phi_r = \delta L_r/R \qquad (A19a)$$

For a unit magnification system, the internal and external angles are the same, so

$$\delta\theta_r = \delta\phi_r = \delta L_r/R \qquad (A19b)$$

Similarly, if the required height coverage is L_r and recognizing that the optic axis will be centered on this range (i.e., angles go plus and minus), we have

$$\theta_r = L_r/(2 \cdot R) \qquad (A20)$$

Thus the requirement in the radial direction becomes

$$\delta v \geq v_{max} \cdot L_r \cdot \delta L_r/(2 \cdot R^2) \qquad (A21)$$

In the other (tangential) direction, the plan is to use a single element that is as large as possible. The limiting factor, then, is the size of the central fringe for which we can write from Eq. A17)

$$\delta v = v(\theta_t) - v(0) = v(0) \cdot (\sec\theta_t - 1) \tag{A22}$$

or, for small angles,

$$\delta v \approx v(0) \cdot \theta_t^2/2 \tag{A23}$$

By similar arguments to those for the radial axis, if the tangential spatial resolution is δL_t, we have

$$\theta_t = \delta L_t/(2 \cdot R) \tag{A24}$$

or

$$\delta v \geq v_{max} \cdot \delta L_t^2/(8 \cdot R^2) \tag{A25}$$

**** Equations A21 and A25 must be satisfied simultaneously. ****

There is an additional interesting implication of Eq. A21: the possible *number* of pixels N_r is pre-defined if independent requirements are placed on the spectral and spatial resolution (δv and δL_r) and the coverage is a free variable given that the range R is defined by the spacecraft orbit:

$$L_r \leq 2 \cdot \delta v \cdot R^2/(v_{max} \cdot \delta L_r) \tag{A21b}$$

whence

$$N_r = L_r/\delta L_r \leq 2 \cdot (R/\delta L_r)^2 \tag{A26}$$

139

A.6: Frequency shifts

Off-axis pixels. Eq. A22 implies another property engendered by using an FTS off-axis (in the radial direction): an apparent frequency shift is induced. The magnitude of the shift is

$$\Delta v(\theta) = v(0) \cdot (\sec\theta - 1) \tag{A27a}$$

$$\approx v(0) \cdot \theta^2/2 \tag{A27b}$$

Finite field-of-view. The finite field-of-view for each pixel introduces an additional, almost constant, shift (≈ 0.01 cm^{-1}) to the data. Furthermore, the Instrumental Line Shape becomes asymmetric with increasing off-axis distance (Niple *et al*, S.P.I.E. $\underline{364}$, 11 [1982] and §5.4)

Eq. A9 applies only to the on-axis ray. For an off-axis ray at an angle θ, the equation becomes

$$I(x) = 2 \cdot I_o \cdot [1 + \cos(2 \cdot \pi \cdot v \cdot x \cdot \cos \theta)] \tag{A28}$$

As before, for small angles, we can replace $\cos\theta$ by $1 - \theta^2/2$

Now, as we go off-axis, the phase difference between the central ray and the off-axis ray becomes π, at which point the resultant intensity goes to zero (the first dark ring). That is

$$2 \cdot \pi \cdot v \cdot x \cdot \theta^2/2 = \pi \tag{A29a}$$

or

$$\theta^2 = 1/(v \cdot x) \tag{A29b}$$

At maximum path difference, $x = X_{max}$ and the "worst case" occurs at the highest frequency of interest v_{max}.

The solid angle associated with θ is $\Omega_{max} = \pi \cdot \theta^2$, so we get

$$\Omega_{max} = \pi/(X_{max} \cdot v_{max}) \tag{A30}$$

The general near-on-axis case is solved by integration across Ω. It can be shown that the result for a circular aperture centered on the axis is

$$F(x) = \int_0^\Omega I(x).d\Omega = 2I_0[1 + \text{sinc}\{\pi vx\frac{\Omega}{2\pi}\} \cdot \cos(2\pi vx\{1 - \frac{\Omega}{4\pi}\})] \tag{A31}$$

That is, the resolution is degraded by an amount given by the sinc function (sincϕ = sinϕ/ϕ) and frequencies are shifted by [1-Ω/(4$\cdot\pi$)].

The even-more-general solution for the effect of a finite aperture on an off-axis rectangular pixel with rays weighted to account for vignetting and non-uniform detector response (i.e., the TES case) can only be solved numerically (see §5.5).

A.7: The Optimum Filter Theorem

Assume a linear time-invariant filter whose response to a unit impulse δ(t) is the *impulse response* a(t). The *transfer function* of the filter is defined as the Fourier Transform of a(t):

$$A(f) = \int_{-\infty}^{\infty} a(t) \cdot \exp(2\pi i f t) \cdot dt \qquad (A35)$$

Since no real filter can respond to an input before it arrives, Eq. A35 can be rewritten as

$$A(f) = \int_{0}^{\infty} a(t) \cdot \exp(2\pi i f t) \cdot dt \qquad (A36)$$

The response of a filter to an arbitrary input x(t) is the convolution of the input with the filter impulse response:

$$y(t) = \int_{0}^{t} x(\tau) \cdot a(t-\tau) \cdot d\tau \qquad (A37)$$

and, if the Fourier Transform of x(t) is X(f), then by definition the output Y(f) is

$$Y(f) = X(f) \cdot A(f) \qquad (A38)$$

and

$$y(t) = \int_{-\infty}^{\infty} X(f) \cdot A(f) \cdot \exp(2\pi i f t) \cdot df \qquad (A39)$$

The *power density spectrum* is

$$|Y(f)|^2 = |X(f)|^2 \cdot |A(f)|^2 \qquad (A40)$$

Now, the Weiner Theorem states that the autocorrelation $\Phi_{11}(\tau)$ of a random function $n(t)$ is related to the power density spectrum $|N(f)|^2$ *via* a standard (cosine) Fourier Transform:

$$|N(f)|^2 = \int_{-\infty}^{\infty} \Phi_{11}(\tau) \cdot \cos(2\pi f \tau) \cdot d\tau \qquad (A41)$$

where

$$\Phi_{11}(\tau) = \int_{-\infty}^{\infty} n(t) \cdot n(t+\tau) \cdot dt \qquad (A42)$$

Thus it is legitimate to write

$$|N_y(f)|^2 = |N_x(f)|^2 \cdot |A(f)|^2 \qquad (A43)$$

where $|N_x(f)|^2$ represents the input noise power density spectrum and $|N_y(f)|^2$ the output.

The variance of the noise $<n^2(t)>$ is the autocorrelation of $N(f)$ at zero lag:

$$<n^2(t)> = \int_{-\infty}^{\infty} |N_y(f)|^2 \cdot df \qquad (A44)$$

$$= \int_{-\infty}^{\infty} |N_x(f)|^2 \cdot |A(f)|^2 \cdot df \qquad (A45)$$

Thus the expected square of the output signal-to-noise ratio given an input signal x(t) and noise n(t) is

$$\frac{|y(t)|^2}{<n^2(t)>} = \frac{|\int\limits_{-\infty}^{\infty} X(f) \cdot A(f) \cdot \exp(2\pi ift) \cdot df|^2}{\int\limits_{-\infty}^{\infty} |N_x(f)|^2 \cdot |A(f)|^2 \cdot df} \tag{A46}$$

The objective, therefore, reduces to the problem of finding a maximum value for Eq. A46.

Lemma: *The sum of the autocorrelations of any two aperiodic functions evaluated at zero lag exceeds twice the absolute value of their cross-correlation at any lead or lag.*

Consider the integral

$$\int\limits_{-\infty}^{\infty} [f_1(t) \pm f_2(t+\tau)]^2 \cdot dt$$

Provided that $f(t) \neq f(t+\tau)$ at any τ, the integral is necessarily non-zero and positive.

Thus, after expansion

$$\int\limits_{-\infty}^{\infty} f_1^2(t) \cdot dt + \int\limits_{-\infty}^{\infty} f_2^2(t+\tau) \cdot dt \pm \int\limits_{-\infty}^{\infty} f_1(t) \cdot f_2(t+\tau) \cdot dt > 0$$

But

$$\int\limits_{-\infty}^{\infty} g_1^2(x) \cdot dx = \Phi_{11}(0) \qquad \text{, the autocorrelation at zero lag,}$$

and

$$\int\limits_{-\infty}^{\infty} g_1(x) \cdot g_2(x+y) \cdot dx = \Phi_{12}(y) \qquad \text{, the cross-correlation at lag y.}$$

Hence

$$\Phi_{11}(0) + \Phi_{22}(0) > \pm 2 \cdot \Phi_{12}(\tau); \quad -\infty < \tau < \infty$$

which is equivalent to

$$\Phi_{11}(0) + \Phi_{22}(0) > 2 \cdot |\Phi_{12}(\tau)|; \quad -\infty < \tau < \infty$$

QED

Corollary: *The autocorrelation of any normalized aperiodic function evaluated at zero lag exceeds the absolute value of its cross-correlation with any other normalized function.*

Referring back to Eq. A46, the top line is recognizable as the cross-correlation of X(f) and A(F) and, from the lemma, that

$$\int_{-\infty}^{\infty} X^2(f) \cdot df + \int_{-\infty}^{\infty} A^2(f) \cdot df > 2 \cdot \int_{-\infty}^{\infty} X(f) \cdot A(f) \cdot \exp(2\pi i f t) \cdot df$$

for all t.

Thus we may immediately infer that the top line of Eq. A46 will have a maximum value when A(f) ≡ X(f). That is, the maximum signal power (and hence information) is transmitted when the filter response exactly matches the spectrum of the input signal. Provided that the noise power density spectrum is reasonably well-behaved (N(f) constant or declining with increasing frequency f), the same condition also ensures that the maximum possible signal-to-noise ratio will be preserved. Thus the Optimum Filter Theorem is proved.

APPENDIX B: RADIATIVE TRANSFER

In a clear atmosphere and near-nadir viewing, the radiance at the detector of a passive infrared spectrometer (in watts/cm^2/sr) is

$$J(\Omega,\nu) = \int_0^\infty \Phi(\nu,\nu')[\{ A(\nu')\cdot F(\Omega,-\Omega_0,\nu')\cdot E_s(\nu')\cdot\Omega_s\cdot\tau(-\Omega_0,0,P_0,\nu')$$

$$+ \epsilon(\Omega,\nu')\cdot B(\nu',T_b)$$

$$+ A(\nu')\cdot \int_{2\pi} F(\Omega,-\Omega_a,\nu')\cdot \int_{-\infty}^{\ln P_0} B(\nu',T(p))\cdot \frac{\partial\tau(-\Omega_a,P,P_0,\nu')}{\partial(\ln P)}\cdot d(\ln P)\cdot d\Omega_a\}\cdot\tau(\Omega,P_0,0,\nu')$$

$$+ \int_{\ln P_0}^{-\infty} B(\nu',T(P))\cdot \frac{\partial\tau(\Omega,P,P_0,\nu')}{\partial(\ln P)}\cdot d(\ln P) \ ]\cdot d\nu' \qquad\qquad (B1)$$

where

$J(\Omega,\nu)$	= radiance at frequency ν into upward, directed, solid angle Ω
$\Phi(\nu,\nu')$	= instrumental absolute impulse response
ν'	= frequency integration variable
$A(\nu')$	= surface albedo
$F(\Omega,-\Omega_{o/a},\nu')$	= surface biconical reflectance function for incident (downward) solid angle $-\Omega_{o/a}$ and emergent (upward) solid angle Ω
	= $(\cos\theta)/\pi$ for a Lambertian surface, where θ is the zenith angle associated with $\Omega_{o/a}$
$E_s(\nu')$	= disk-average solar radiance
Ω_s	= solar solid angle at Earth (6.8x10^{-5} sr)
$\tau(\Omega,P,P',\nu')$	= atmospheric transmittance at frequency ν' in a direction Ω between pressure levels P and P' (P$_0$ = base pressure)
$\epsilon(\Omega,\nu')$	= surface emissivity at frequency ν' in the upward direction Ω
$B(\nu',T_b)$	= Planck function for surface temperature T$_b$
$B(\nu',T(P))$	= Planck function for atmospheric temperature T(P) at pressure level P

$$\frac{\partial\tau(\Omega,P,P',\nu')}{\partial(\ln P)} = \text{atmospheric weighting function for direction } \Omega$$

The product of the weighting function and the Planck function (i.e., the integrands on the last two lines of Eq. B1) is called the *contribution function* since it expresses the contribution of a particular pressure level P to the total outgoing radiance.

145

The first term in Eq. B1 describes the influence of the sensor (TES) on the total incoming radiance. The second term describes surface reflection of sunlight, the third term is surface emission, the fourth is downwelling atmospheric radiation reflected back upwards by the surface and the last term is the outgoing atmospheric radiation. Depending on the frequency and the viewing conditions (day, night, etc), one or other of the terms will usually dominate.

The transmissions are a product over all N species present in the line of sight:

$$\tau(\theta,P,\nu) = \prod_{i=1}^{N} \exp[-\int_0^P L(\theta,P\,') \cdot m_i(P\,') \cdot \kappa_i\{\nu',P\,',T(P\,')\} \cdot dP\,'] \qquad (B2)$$

where $L(\theta,P)$ is the ray path length (=$\sec\theta$ in a plane parallel, unrefracted, geometry) and m_i is the volume mixing ratio of the ith species with absorption coefficient κ_i.

The required output parameters from these equations are:

- m_i, the mixing ratios of all N species as a function of P;
- $T(P)$, the atmospheric temperature profile;
- T_b, the surface sensible temperature;
- $\epsilon(\Omega,\nu)$, the surface emissivity function;
- $A(\nu)$, the surface albedo.

and the extraction procedure (which is obviously non-trivial) is called *inversion*.

The same equation holds for limb sounding if the first three (surface related) terms are omitted. While the equation, therefore, seems much simpler, the path geometry in the troposphere becomes much more complicated because of strong refraction effects.

APPENDIX C: RADIOMETRIC MODEL

C.1: Introduction.

System signal-to-noise ratio and detector requirements are based on the expected thermal background and source radiances added to the internally-generated noise within the detector system. Note that since TES is a direct-reading system (no multiplexed focal planes), neither readout noise nor charge-well saturation are a consideration.

Until detailed performance parameters are available that permit analysis on an element-by-element basis, radiometric modeling is based on a *block subsystem model* (Fig. C1) that divides the system into 5 blocks: source, ambient temperature pointing system, cool spectrometer, cooler detector system (cold stops, filters and focal planes), and analog electronics. Beyond this point, the system is assumed to be noise-free. An extension of this model also permits the effect of pointing jitter to be incorporated.
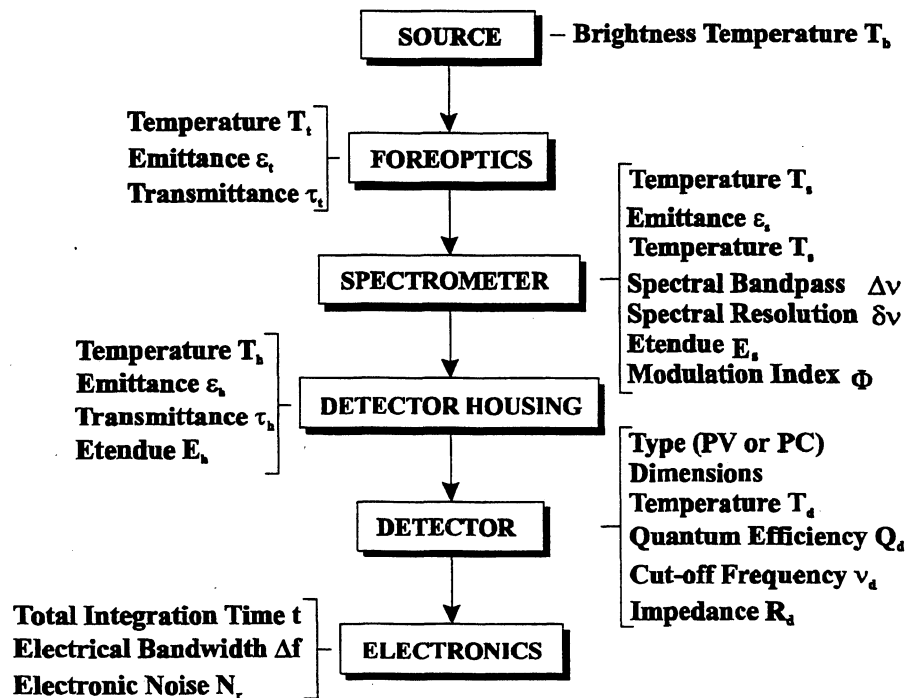
Fig. C1: TES block sub-system radiometric model

147

C.2: Analysis.

The radiometric modeling approach used for TES is somewhat unusual in that we prefer to reduce the problem to one of counting statistics, rather than the more usual "flux/radiance & D*" method. In our approach, a count of N electrons is assumed to obey Poisson statistics in which the standard deviation is $\sqrt{N}$, leading to a signal-to-noise ratio (SNR) = $\sqrt{N}$.

The model, a real-time, interactive, FORTRAN program, has 26 adjustable input parameters and provides excellent insight into the properties of each subsystem, listing the noise contributed by each in rank order, the Noise Equivalent Source Radiance (NESR), the signal-to-noise ratio and the interferogram dynamic range. Note, however, that this excludes noise due to real or apparent image motion. Although an extension of the algorithm presented below incorporates this effect, it was not used for these calculations because the exact nature (amplitude spectrum) of the disturbance must be known. For the EOS platforms, no such data are available.

A description of the input parameters follows.

Source. Three parameters are available to describe the source.

Brightness. The source intrinsic brightness can be entered as either a brightness temperature or as a radiance.

Solar Incidence Angle. Used for those spectral regions where the contribution from reflected sunlight is significant.

Geometric Albedo. Typical values range from 0.01 for certain dark surfaces up to 0.3 for very bright surfaces and even higher for clouds.

Sub-system 1: Pointing System. Three parameters define the pointing system:

Temperature. The pointing system temperature has been set to 270 K, based on estimates of the likely equilibrium temperature in near-Earth orbit.

Emittance. It was assumed that an effective emittance of 0.06 can be achieved for the pointing system.

Transmittance. The properties of modern mirror coatings are such that a reflectance of at least 0.97 or more per surface should be achievable.

Sub-system 2: Instrument Body.

Temperature. It is assumed that those parts of the instrument body that can contribute to the background either through direct emission or by scattering from other surfaces are at a uniform temperature of 180 K.

Emittance. This is the least satisfactory part of the model, since useful effective emittance data for instruments are difficult to find. Measurements of which we are aware (for the JPL Mk.IV balloon-borne FTS and AES) suggest a value of 0.32. A "default", but inaccurate, estimate is (1-transmittance).

Transmittance. Most "grass-roots" estimates of instrument transmittance seriously over-estimate its value. Typical measured values seem to range from 0.05 to 0.3, depending on complexity.

Étendue. System étendue is usually controlled by the properties of the instrument although, of course, the entire optical train must at least match this value.

Modulation Index. The signal provided by an FTS is directly proportional to the modulation index. It is rarely greater than 0.9.

Spectral Resolution. The spectral resolution is 0.1 cm^{-1} for the downlooking mode and 0.025 cm^{-1} at the limb.

Sub-system 3: Detector Enclosure. The detector enclosure (which incorporates elements such as cold-stops, band-limiting filters, condenser and field optics) is held at a lower temperature than the preceding instrumentation. Furthermore, the enclosure forms a near-perfect cavity so that the detector element "sees" the internal background through essentially 2π sr at unit effective emittance. This must be taken into account.

Temperature. Although usually held at a temperature close to that of the detector elements themselves (≥ 65 K), the temperature is often a little higher due to the input heat loads before the band-limiting filters.

Transmittance. Modern detector systems put a significant set of optics into the detector enclosure. A typical transmittance for the ensemble might be 0.56.

Filter Band Limits. The cold filter usefully limits the external background that can reach the detector. Note, however, that its effective emissivity will be close to unity in an isothermal environment.

149

Sub-system 4: Detector & Detector Electronics.

Temperature. The detector elements are usually the coldest point in the system.

Size. Rectangular elements are assumed (height and width independently variable).

Type. PV detectors are preferred whenever possible (below 12 μm currently, 17 μm in the near future); otherwise, PC detectors must be used. PC detectors exhibit generation-recombination noise. This is approximated in the program by multiplying the number of noise carriers by 2.

Cut-off Frequency. Photon detectors all exhibit a long-wavelength (low frequency) cut-off that is relatively sharp. The effect (important for computing the internally-generated background) is approximated as a discontinuity.

Quantum Efficiency. The absolute quantum efficiency of modern detectors (at least InSb and HgCdTe) lies in the range 0.5 to 0.8, with the higher values being a consequence of added anti-reflection coatings.

Resistance. The effective resistance (for PC detectors) or dynamic impedance (for PV detectors) is required to compute the contribution of "kT" noise. For InSb at low background levels, it can be the dominant source.

Algorithm.

Let

N_1 = number of electrons per sec ($e^-.s^{-1}$) generated within the detector and readout system;

N_2 = number of $e^-.s^{-1}$ generated by the detector housing internal background (π sr & unit emissivity assumed;

n_3 = number of $e^-.s^{-1}/cm^{-1}$ from instrument body emission;

n_4 = number of $e^-.s^{-1}/cm^{-1}$ from pointing system emission;

n_5 = number of $e^-.s^{-1}/cm^{-1}$ from source emission;

n_6 = number of $e^-.s^{-1}/cm^{-1}$ from solar reflection;

Δv = width of band-limiting filter (cm^{-1});

δv =   spectral resolution (cm^{-1});

Φ =   FTS modulation index;

t   =   total integration time per spectrum.

The signal count $S = \delta v \cdot \Phi \cdot (n_5 + n_6) \cdot t \quad e^{-}$

and the noise count is $C = (N_1 + N_2) \cdot t + \Delta v \cdot (n_3 + n_4 + n_5 + n_6) \cdot t \quad e^{-}$.

Thus the mean SNR (averaged across the band Δv) is

$$SNR = \frac{\delta v \cdot \Phi \cdot (N_5 + N_6) \cdot t}{\sqrt{(N_1 + N_2) \cdot t + \Delta v (n_3 + n_4 + n_5 + n_6) \cdot t}} \tag{C1}$$

where $N_1 = P \cdot \sqrt{4kT_d \cdot \Delta f / (R_d e)}$ (C1a)

and   P = 1 for a PV detector, 2 for PC
        k = Boltzmann's constant
        T_d = detector element temperature
        Δf = detector system electrical bandwidth
        R_d = detector effective resistance
        e = charge on the electron

$$N_2 = E_d Q_d \cdot \int_{v_c}^{\infty} B(v, T_h) dv \tag{C1b}$$

and E_d = detector internal étendue = $\pi \cdot$(detector area)
        Q_d = detector quantum efficiency
        v_c = detector low-frequency cutoff
        $B(v \cdot T)$ = Planck photon function for frequency v and temperature T
        T_h = temperature of the detector cavity

$$n_3 = \epsilon_s \overline{B}(\nu,T_s) E_s \tau_d Q_d \tag{C1c}$$

and ϵ_s = spectrometer effective emissivity
$B(\nu,T)$ = band-average Planck photon function for frequency ν and temperature T
T_s = spectrometer body temperature
E_s = system étendue
τ_d = transmittance of detector system optics and filters

$$n_4 = \epsilon_t \overline{B}(\nu,T_t) E_s \tau_s \tau_d Q_d \tag{C1d}$$

and ϵ_t = pointing system effective emissivity
T_t = pointing system temperature
τ_s = transmittance of spectrometer

$$n_5 = \overline{B}(\nu,T_b) \tau_o \tau_t E_s \tau_s \tau_d Q_d \tag{C1e}$$

and T_b = source emission brightness temperature
τ_o = outbound atmospheric transmittance
τ_t = transmittance of pointing system

$$n_6 = \overline{F}(\nu) G\tau_i \cos\theta \, \alpha \tau_o \tau_t E_s \tau_s \tau_d Q_d \tag{C1f}$$

and G = Sun-Earth geometric factor = 2.1645×10^{-5}
$F(\nu)$ = band-average solar radiance
τ_i = inbound atmospheric transmittance
θ = solar zenith angle at the Earth
α = directed surface reflectance

The resultant interferogram dynamic range is D, given by

$$D = (SNR) \sqrt{\frac{\Delta\nu}{\delta\nu}} \tag{C2}$$

although it is conventional to increase the value by a factor of 2 to 4 for proper noise characterization.

C.3: The impact of pointing jitter

If image motion (from any origin - jitter, smear, atmospheric turbulence, etc.) is significant, a further term

$$s'(n_5 + n_6)\Delta n \cdot t; \quad 0 \le s' \le 1 \tag{C3}$$

must be added to the denominator, where

$$s' = \frac{1}{t}\int_0^t \frac{1}{f_2 - f_1}\int_{f_1}^{f_2} S(f)\exp(-2\pi i f t)\,dt\,df \tag{C4}$$

S(f) is the *amplitude* spectrum of the scene modulation, assumed bounded by temporal frequencies f_1 and f_2, and t is the total integration time. However, with an FTS it is possible to employ a stratagem; if the amplitude spectrum is well-known (and thus f_1 and f_2), the sampling interval and scan rate can be adjusted so that the modulation frequencies are largely (or entirely) aliased into a region of zero signal. This must be done with great care but is commonly used by astronomers to put noise due to atmospheric turbulence outside the desired spectral range and is also frequently used to evade problems of electrical interference from AC lines and switching power supplies.

Assuming that S(f) is more or less random, the composite expression becomes:

$$SNR = \frac{\delta v\,\Phi\,(n_5 + n_6)t}{\sqrt{(N_1 + N_2)t + \Delta v(n_3 + n_4 + n_5 + n_6)t} + s'\Delta v(n_5 + n_6)\sqrt{(t/m)}} \tag{C5}$$

where m is the number of independent samples in the spectrum = the number of interferogram samples $\approx \Delta v/\delta v$ and s' is now to be interpreted as that portion of the signal modulation that falls within the occupied spectral interval. Of course, for uniform scenes (limb mode, oceans, snow fields etc.), S(f) is zero for all f. The worst case is a "checkerboard" scene whose boundaries exactly match the detector elements. Analysis of LANDSAT data suggests that, for typical scenes, $S(f) \propto 1/f$.

C.4: Discussion

The composite expression has interesting properties: if the first (detector) noise term dominates, then the SNR becomes independent of the spectral bandpass - this is the classic *Fellgett Advantage* of an FTS. If the second term dominates (i.e., source or background photon shot noise limited), the SNR improves if the filter bands are narrowed. This is the likely TES condition. If M' becomes large enough that the last term dominates the denominator, the SNR becomes *independent of the signal!* That is, the result is garbage and highlights the extreme importance of avoiding pointing jitter or EMI noise.

153

THIS PAGE INTENTIONALLY LEFT BLANK

APPENDIX D: INTERFEROGRAM SAMPLING

The logic of interferogram sampling is based on an extension of the Shannon Sampling Theorem. The extended theorem shows that a spectrum that is non-zero only in the interval $v_2 \geq v \geq v_1$ cm^{-1} can be *exactly* reconstructed from an interferogram undersampled at intervals δx cm given by

$$\delta x \leq 1/[2 \cdot (v_2 - v_1)]; \quad v_2 > v_1 \geq 0$$

provided that $v_2/(v_2 - v_1)$ *is integral.* This integral ratio is commonly called the *alias order.*[1]

These requirements can be reversed - given a sampling interval δx, a set of contiguous spectral intervals is defined:

Alias Order	Frequency Interval
1	$0 \rightarrow v_o$
2	$v_o \rightarrow 2 \cdot v_o$
3	$2 \cdot v_o \rightarrow 3 \cdot v_o$
.	.
.	.
.	.
J	$(J-1) \cdot v_o \rightarrow J \cdot v_o; \quad J = 1,2,3,\ldots\ldots$

Given such an interval $(J-1) \cdot v_o$ to $J \cdot v_o$, there follows the secondary requirement that the system filtering (optical and electronic) prevent optical frequencies less than $(J-1) \cdot v_o$ cm^{-1} or greater than $J \cdot v_o$ cm^{-1} from traversing the interferometer. If this is not accomplished, the phenomenon of *aliasing* occurs. Aliasing manifests itself by reflecting those parts of the spectrum that fall outside the boundaries back into the spectrum. At the very least, the effect is to distort the data; at worst, the results are useless. The effect is illustrated in Fig. D1.

---

[1] A minor issue associated with undersampling is that the frequencies computed for even-numbered aliases emerge frequency-reversed. This is easily remedied in the computation process.
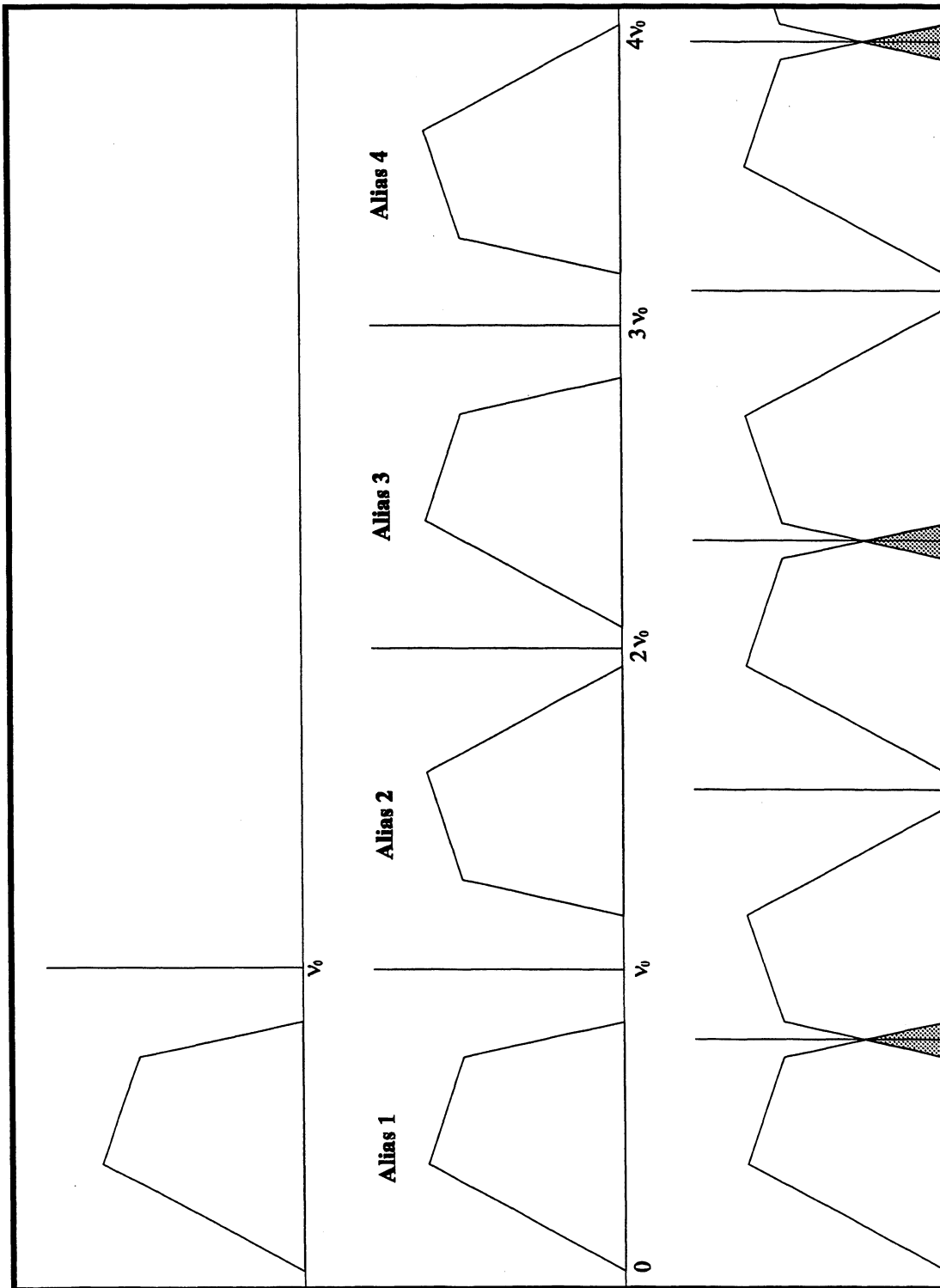
Fig D1: Top - Input; Middle - Output with proper sampling; Bottom - Effect of improper sampling (aliasing)

Now, as discussed above, the sampling interval will be defined by the zero crossings of the sinewave generated by a stabilized laser. Note that there is no intrinsic requirement that the sampling occur at *every* zero crossing. Depending on the filter characteristics, it may be possible to sample every K^{th} crossing ($K=1,2,3,.....$). The zero crossings (in any given sense) occur precisely at intervals of one wavelength of the laser. If the laser frequency is v_l, the allowable frequency intervals are therefore

$$v_{min} = (J-1) \cdot v_l / 2 \cdot K \ cm^{-1}$$

and

$$v_{max} = \quad J \cdot v_l / 2 \cdot K \ cm^{-1}$$

where $J = 1,2,3,........$ (the alias order)
and $K = 1,2,3,........$ (the sampling index).

The benefit of this type of undersampling is that, provided the rules are obeyed, it offers a form of lossless data compression. That is, the data rate and volume are both decreased without any loss of information.

THIS PAGE INTENTIONALLY LEFT BLANK

APPENDIX E: EOS & TES ORBITAL GEOMETRY

Fig. E1 shows the angles and coverage available using a simple circular-orbit model for the EOS Polar Platforms. Fig. E2 defines *range* (L_s and L_t) and *tangent height* (H).

Nadir View Angle (θ) is the angle with respect to the TES nadir provided by the pointing mirror. The calculations are for the in-track direction. However, the angular data (but not the distance and timing data) are correct for any direction in a cone centered on the spacecraft.

Earth Surface Angle (Φ) is the geocentric angle between the aimpoint and the spacecraft nadir (essentially degrees of latitude for the in-track direction).

Target Zenith Angle (α) is the angle between the line-of-sight from aimpoint to spacecraft with respect to the local vertical.

Minimum In-Track Distance (D) is the smallest distance on the Earth's surface between successive observation sequences. That is, TES stares at a point on the ground for some period of time. Meanwhile, the spacecraft has moved in its orbit, so the next possible aimpoint is some distance downrange. The results in Table X make no allowance for the fact that the mirror will require a finite time to acquire the next aimpoint (if this time exceeds the scan turnaround time of 1.2 sec).

Footprint (δD) is the in-track projection of the IFOV ($\delta\theta$) on the surface
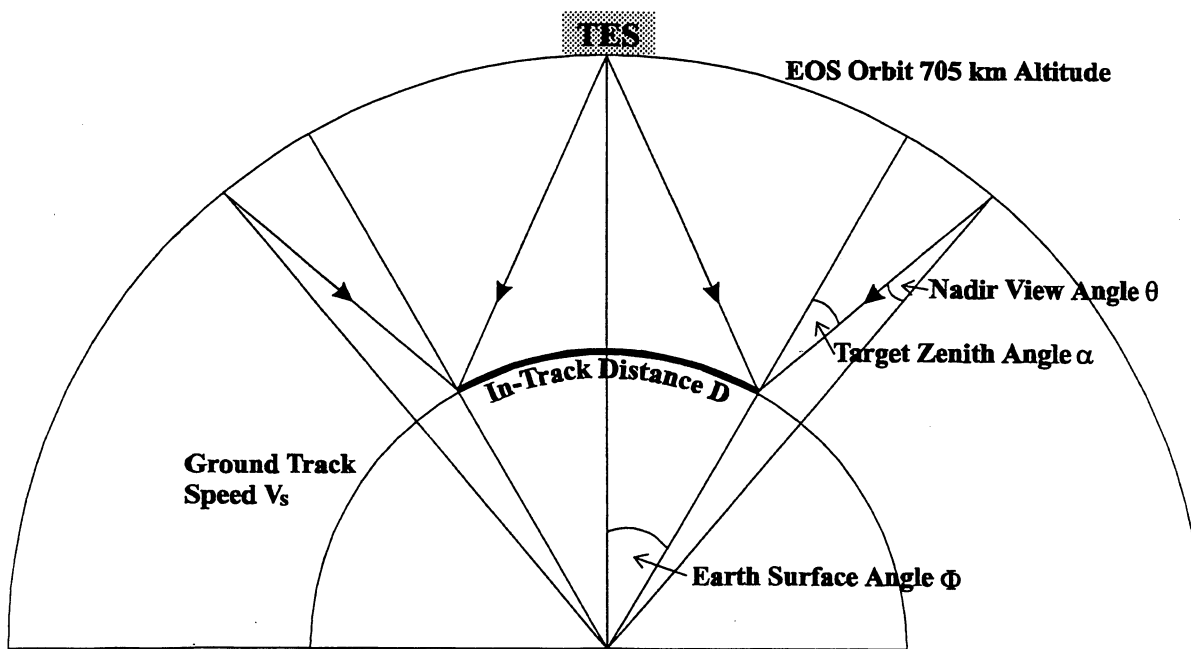
Fig. E1: Simplified model of TES viewing parameters assuming a spherical Earth and a circular orbit

159
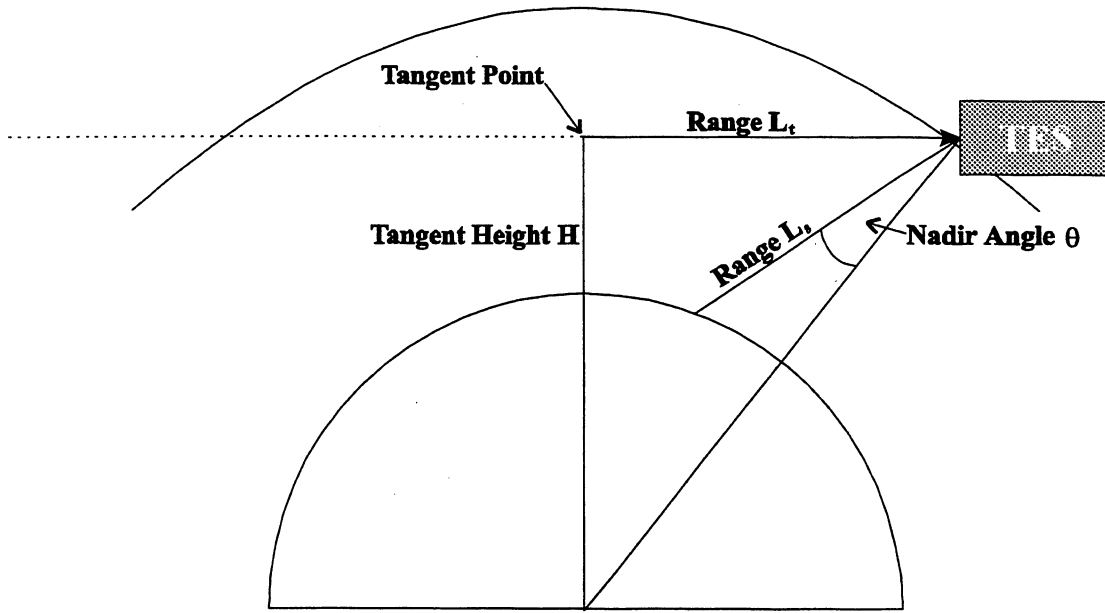
Fig. E2: Definition of Tangent Height and Slant Range
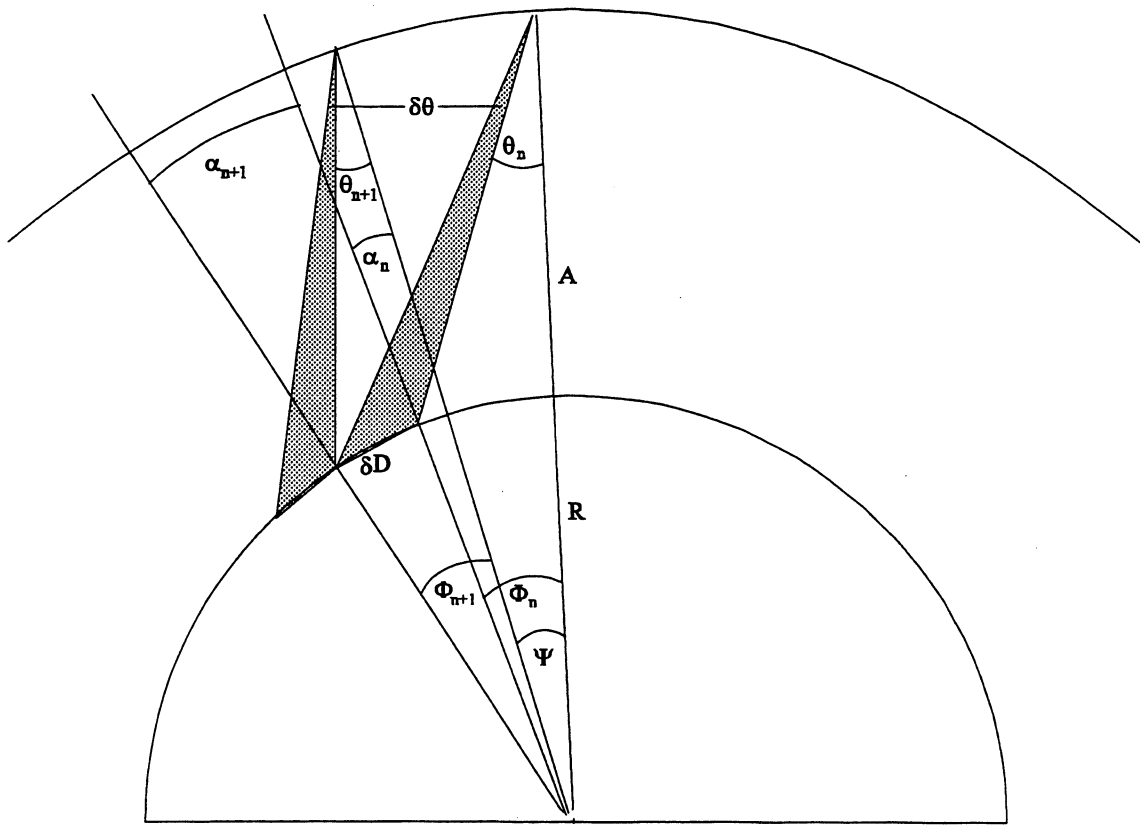
Fig. E3: Geometry of the Transect Mode

Expressions for the parameters follow from elementary trigonometry. The independent variable is θ, the nadir view angle; R is the Earth's radius; A is the spacecraft altitude, P is the nodal period, t is the (scan + turnaround) time and V_s is the average ground-track speed.

Target Zenith Angle	$\alpha = \sin^{-1}[(R+A)\cdot\sin\theta/R]$	(E1)
Earth Surface Angle	$\Phi = \alpha - \theta$	(E2)
In-Track Distance	$D = 2\cdot R\cdot\Phi$	(E3)
Total Observation Time	$T = D/V_s$	(E4)
Number of Scans	$N = \mathrm{int}(T/t)$	
Tangent Height	$H = (R+A)\cdot\sin\theta - R$ (unrefracted)	(E5)
Range to Tangent Point	$L_t = (R+A)\cdot\cos\theta$ (unrefracted)	(E6)
Range to Surface	$L_s = (R+A)\cdot\{\cos\theta - \sqrt{[(R^2/(R+A)^2 - \sin^2\theta]}\}$ (unrefracted)	(E7)
Footprint (in-track)	$\delta D = L_s\cdot\delta\theta/\cos\alpha$	(E8)

For the Transect Mode

$$\sin^{-1}[(R+A)\cdot\sin\theta_{n+1}/R] - \theta_{n+1} = \delta D_n/R - 2\cdot\pi\cdot t/P + \sin^{-1}[(R+A)\cdot\sin\theta_n/R] - \theta_n \qquad (E9)$$

This last equation is transcendental and must be solved iteratively

THIS PAGE INTENTIONALLY LEFT BLANK

APPENDIX F: TARGET LOCATION & POINTING ALGORITHMS

F1: Introduction

The lack of a field rotator in the current TES design results in a skewed footprint for off-nadir targets. This Appendix investigates both this phenomenon and the closely related problem of "blind pointing" at such targets. Finally, the corrections required for a) a rotating Earth and orbit plane; b) a non-circular orbit; c) a non-spherical Earth; d) topography and e) spacecraft attitude errors are discussed.

F2: Gimbal Terminology

Fig. F1 shows 3 views of the TES 2-axis gimbal. The "roll" axis lies parallel to the spacecraft roll axis (and also parallel to the velocity vector). The "pitch" axis similarly lies parallel to the spacecraft pitch axis, perpendicular to the velocity vector.

I have adopted a convention that zero degrees (gimbal) pitch and roll is the condition that the gimbal is collapsed to its most compact configuration so that the normal to the mirror points at nadir. Thus when actually *viewing* the nadir, the gimbal roll angle = 0° and the pitch angle is 45°.

*** Note that this convention is unlikely to be the same as that adopted by the engineering and operations teams, but the difference(s) will be simply additive constants ***

An important science parameter is the *nadir angle* of observation. This is the angle between the nadir direction (local vertical) and the line-of-sight. A science requirement has been levied that this angle shall not exceed 45° for downlooking observations (this does not apply to the limb view, where the trailing limb will be at about 68° nadir angle). Thus this condition implies that all downlooking observations will be made within a 90° circular cone centered on the nadir (and, as we shall see, in practice within a somewhat smaller elliptical cone).
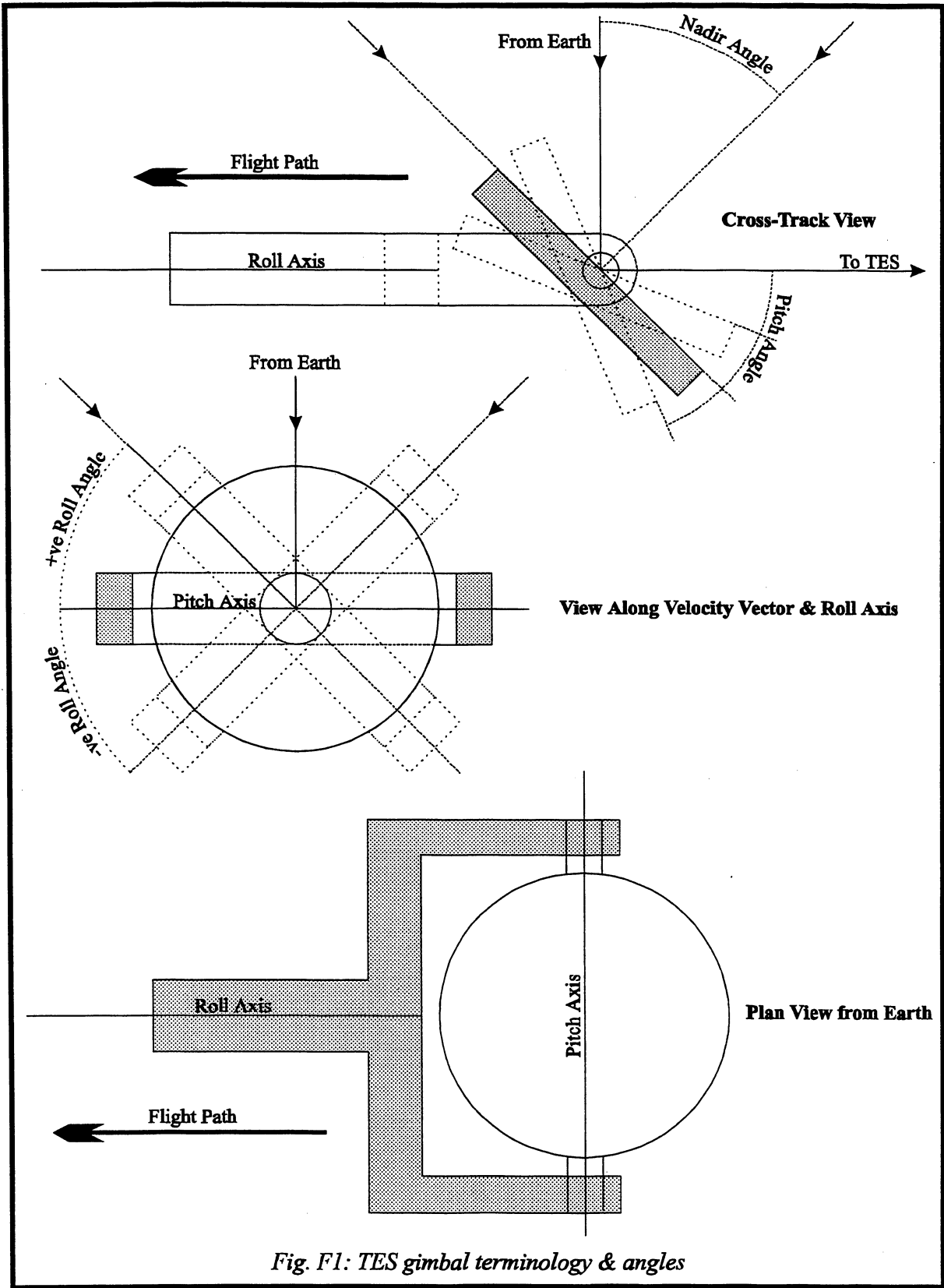
Fig. F1: TES gimbal terminology & angles

F3: Gimbal Angles

Although the light to be measured by TES actually travels from Earth to TES, for the current exercise it is simpler to imagine a beam of light *leaving* TES and being pointed at the Earth's surface. Light rays are reversible, so there is no loss in generality.

The light beam from TES is centered on the roll axis (by design). A pitch motion of the mirror through an angle κ causes the beam to rotate by an amount 2κ. Thus since we have already said that the maximum allowed deviation from nadir for downlooking views is 45°, it follows that the range of pitch angle variation will be $\pm 22.5°$ about the central 45° (i.e., in the current convention, the actual pitch angles will lie between 22.5° and 67.5°). This is illustrated in the top part of Fig. F1. Not shown are the limb and space views, which are not part of this discussion.

When pointed at nadir, the roll angle is zero. The convention I use is that when the target to be observed is to the *right* of the ground track (facing forward), the required roll angle is *positive*. Conversely, targets to the left are at negative roll angles (see middle part of Fig. F1). The bottom part of Fig. F1 serves to clarify the relationship between the two axes.

The effect of a roll angle change on the beam direction is, as we shall see, markedly different from a pitch change - a roll angle change of ρ moves the beam through ρ, *not* 2ρ! Furthermore, the skew of the footprint on the ground is a function *only of the roll angle*. The pitch angle has no effect on this phenomenon.

F4: Footprint Skew

The top part of Fig. F2 shows the motion of the footprint as the pitch angle changes. Note that, of course, the position of the footprint changes (and its size, as the range to the surface increases) but its *direction* does not. It is easily shown (and imagined) that this is true at any roll angle although the figure is drawn for zero roll angle.

Now rotate the viewpoint 90° so we are looking along the roll axis (middle part of Fig. F2). At 0° roll, the image will be pointing *in and out* of the illustration, perpendicular to the object (the input footprint). Roll the mirror 90° - the image is now *parallel* to the object. Thus in rolling the mirror through 90°, the image (and the beam direction) has also rotated through 90°. It is straightforward to convince oneself that a roll of 45° causes a beam rotation of 45° and a skew of 45°. In general, then, a roll angle of ρ rotates the beam through ρ and skews the footprint through ρ (with respect to the ground track).

Fig. F3 shows a "spacecraft's eye view" of the projection of the footprint on the ground (assuming a flat Earth) as a function of nadir angle and azimuth with respect to the ground track. As expected, the further one is off-nadir, the more skewed is the footprint. Note that the skew is always *away* from the ground track.
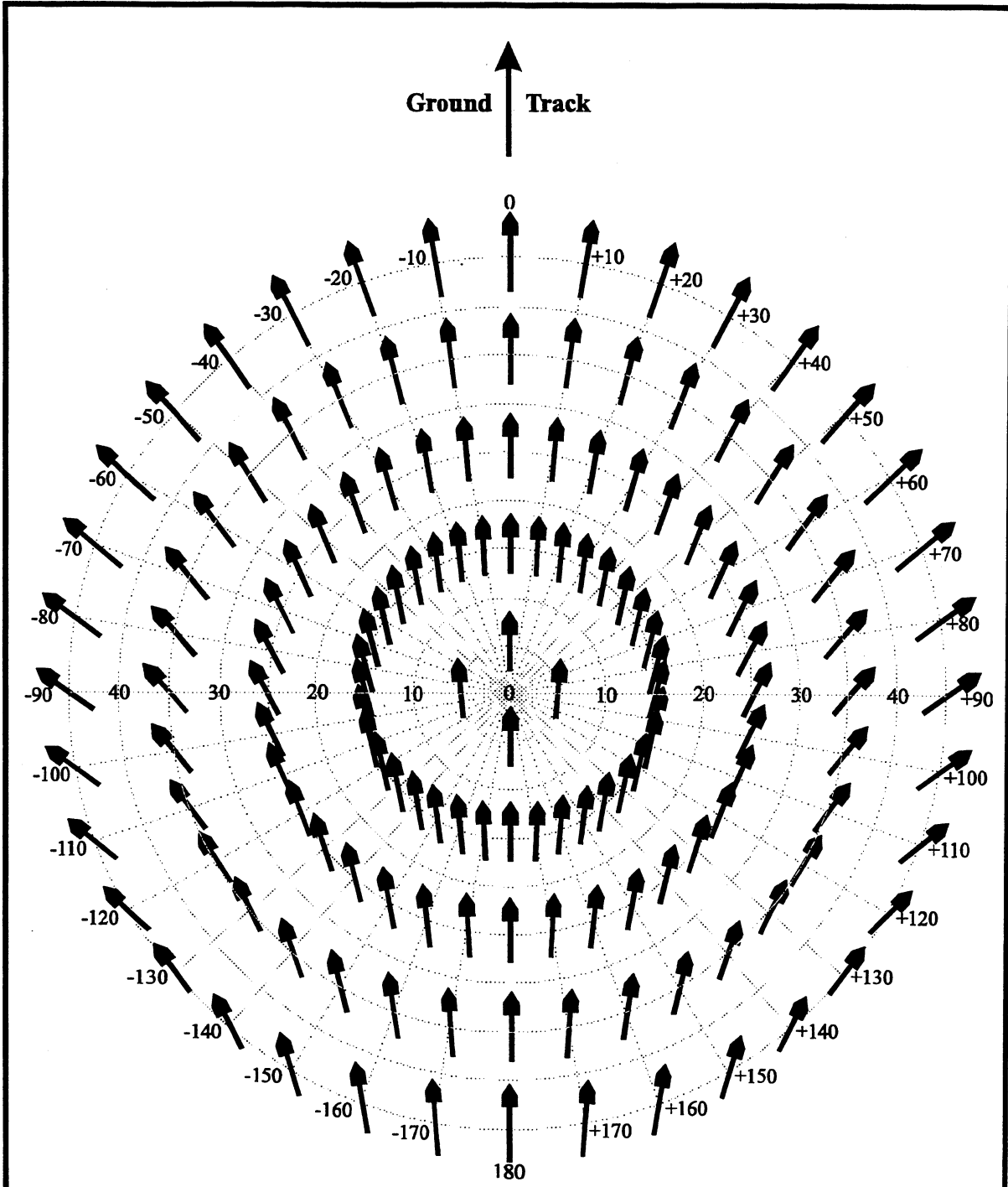
165

View along Pitch Axis

Roll Angle = 0°

Pitch Angle = 0 +/- 22.5o

Skew Angle = 0°

Image

Object

View along Roll Axis

Roll Angle = 90°

Skew Angle = 90°

Object

Image

View along Roll Axis

Roll Angle = 45°

Image

Skew Angle = 45°

Object

Fig. F2: Geometry of how the image skews with Roll Angle (but NOT with Pitch Angle)

166
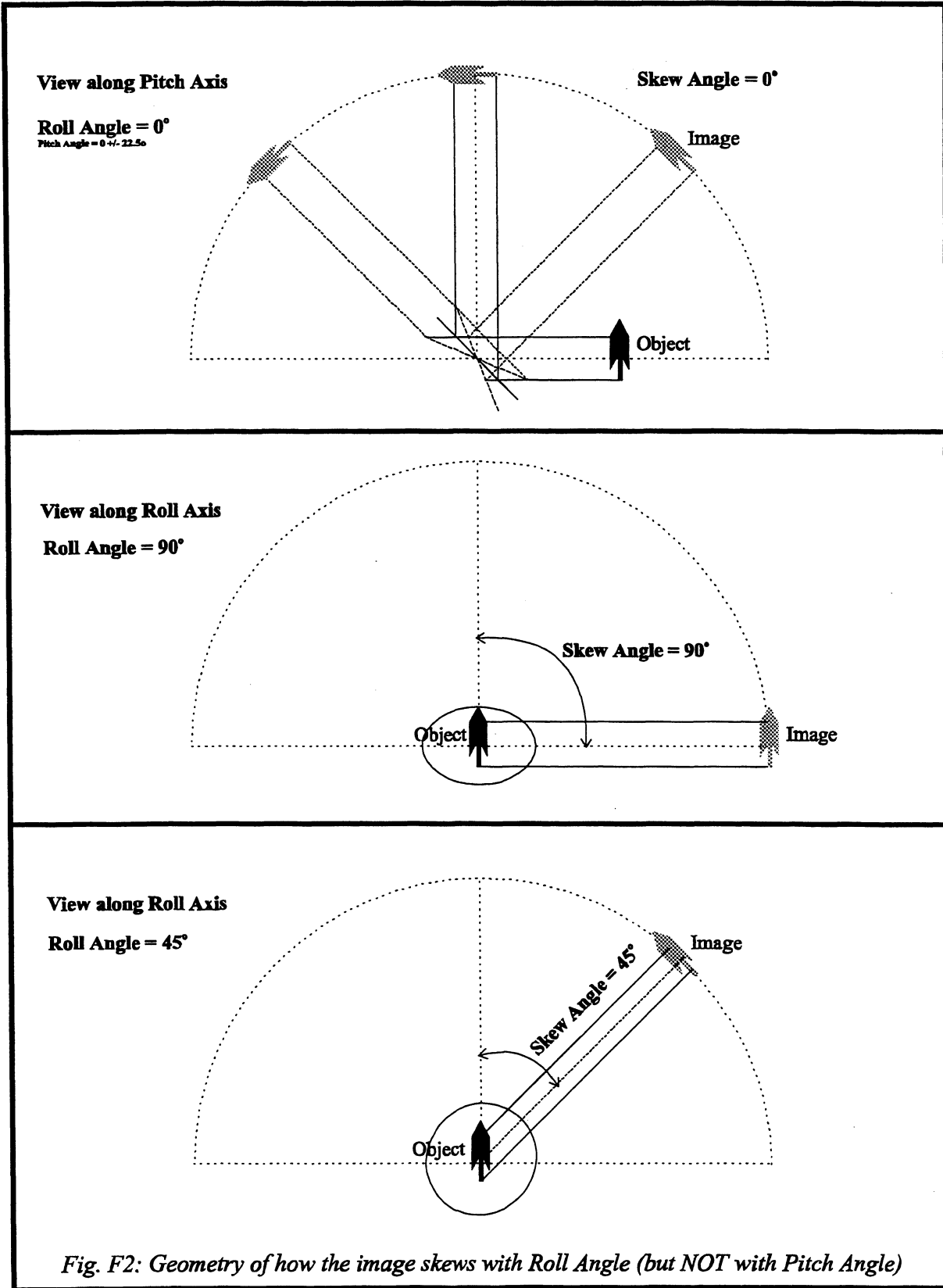
Fig. F3: Polar diagram of the skew and expansion of the TES footprint as a function of nadir angle and azimuth ("flat earth" view)

Now, imagine that we are targeting an off-nadir point on the Earth (assumed non-rotating for the moment). As the spacecraft travels along, the target *appears* to travel along a line parallel to the ground track (lay a ruler on Fig. F3 to visualize this). We have already established that the skew of the footprint is a function only of the roll angle; but the roll angle to observe this line does not change, so by the same token the skew angle will not change (the footprint size *does* change, of course, as illustrated in the figure). What is the skew angle? By inspection we see that when the spacecraft is directly abreast of the target (azimuth $= \pm 90°$), the nadir angle and the roll angle are identical. *Thus the skew angle of the footprint is numerically equal to the nadir angle at closest approach.* This is a most important result.

F5: Trigonometric Relationships and Observation Time

Let the nadir angle be θ with a minimum value θ_0. From Fig. F3 we note that the linear distance (flat Earth approximation) to a nadir angle of $45°$ is $A*\tan(45) = A$, where A is the spacecraft altitude. Similarly, the linear distance to the target at θ_0 is $A*\tan(\theta_0)$. Thus the linear distance of the target (L_{max}) from the periphery of the figure is

$$L_{max} = A \cdot \sqrt{1 - \tan^2(\theta_0)} \text{ km} \tag{F1}$$

If the spacecraft ground-track speed is V_s km/sec, the maximum observation time is

$$2 \cdot t_{max} = \frac{L_{max}}{V_s} = \frac{2 \cdot A \cdot \sqrt{1 - \tan^2(\theta_0)}}{V_s} \text{ sec} \tag{F2}$$

Fig. F4 shows the variation of maximum observation time *vs.* the minimum nadir angle θ_0 assuming an altitude of 705 km and a mean ground speed of 6.743 km/sec. It will be seen that the available time decreases rapidly as θ_0 approaches $45°$. Thus only in exceptional circumstances should values of $\theta_0 > 40°$ be used.

In general, the linear distance L from a nadir angle of θ to where $\theta = \theta_0$ is

$$L = A \cdot \sqrt{\tan^2(\theta) - \tan^2(\theta_0)} \text{ km} \tag{F3}$$

and the time to/from closest approach is

$$\Delta t = t - t_0 = \frac{L}{V_s} = \frac{A \cdot \sqrt{\tan^2(\theta) - \tan^2(\theta_0)}}{V_s} \text{ sec} \tag{F4}$$

168

Using a similar argument, we find that the azimuth angle ϕ of the target is given by

$$\phi = \sin^{-1}[\tan(\theta_0)/\tan(\theta)] \qquad \text{(F5)}$$

which takes its smallest value ϕ_{min} when $\theta = 45°$:

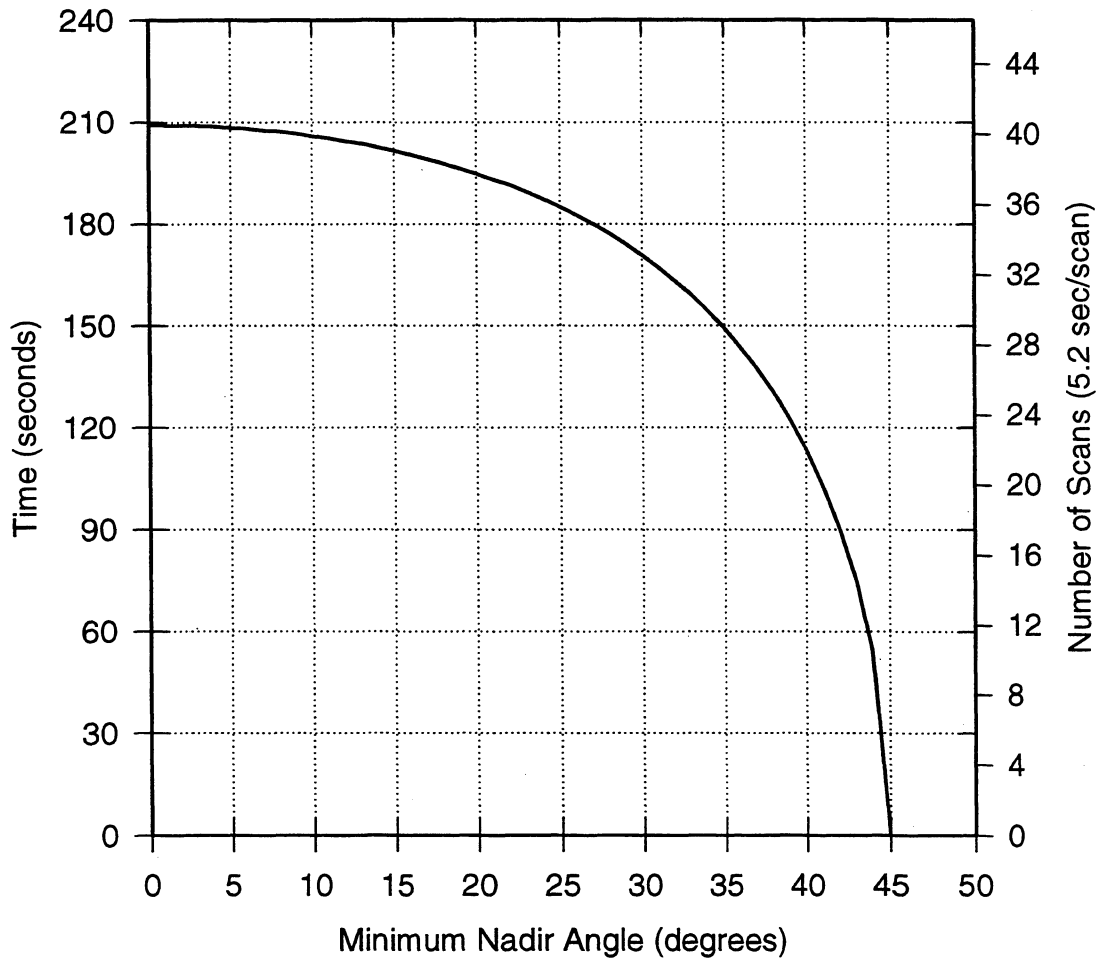$$\phi_{min} = \sin^{-1}[\tan(\theta_0)] \qquad \text{(F5a)}$$

Fig. F4: Available observation time for off-nadir targets

169

The corresponding required pitch angle κ is

$$\kappa = 45° + 0.5 \cdot \tan^{-1}[\cos(\phi) \cdot \tan(\theta)]$$

(F6)

whose starting value (i.e., when $\tan(\theta) = 1$) will therefore be κ_{min}, given by

$$\kappa_{min} = 45° + 0.5 \cdot \tan^{-1}[\cos(\phi_{min})]$$

(F6a)

The pitch angle rate is determined by differentiating the foregoing expressions (F3), (F5) & (F6) with respect to the nadir angle θ:

$$\frac{dL}{d\theta} = \frac{A \cdot \tan(\theta)}{\cos^2(\theta) \cdot \sqrt{\tan^2(\theta) - \tan^2(\theta_0)}}$$

(F7)

$$\frac{d\phi}{d\theta} = \frac{-\tan(\theta_0)}{\sin(\theta) \cdot \cos(\theta) \cdot \sqrt{\tan^2(\theta) - \tan^2(\theta_0)}}$$

(F8)

$$\frac{d\kappa}{d\theta} = \frac{\cos(\phi) - \sin(\theta) \cdot \cos(\theta) \cdot \sin(\phi) \cdot \dfrac{d\phi}{d\theta}}{2 \cdot [\cos^2(\theta) + \sin^2(\theta) \cdot \cos^2(\phi)]}$$

(F9)

and, finally, that

$$\frac{d\kappa}{dt} = \frac{V_s \cdot \dfrac{d\kappa}{d\theta}}{\dfrac{dL}{d\theta}} \ °/\text{sec}$$

(F10)

These are the general expressions and are fairly complicated. Fortunately, a dramatic simplification can be made with an appropriate parameterization:

Referring back to Eqn. F4, we can rewrite it as

$$\tan^2(\theta) = Q^2 + \tan^2(\theta_0)$$

. (F11)

170

where $Q = V_s\Delta t/A$; a dimensionless parameter. Substituting this into Eqn. F5, we get

$$\phi = \sin^{-1}\frac{\tan(\theta_0)}{\sqrt{Q^2+\tan^2(\theta_0)}} \qquad (F12)$$

and, after a little manipulation,

$$\kappa = 45° + 0.5\cdot\tan^{-1}(Q) \qquad (F13)$$

from which it follows that

$$\frac{d\kappa}{dt} = \frac{Q}{2\cdot\Delta t\cdot(1+Q^2)} \qquad (F14)$$

Parenthetically, let it be noted that when $\Delta t = 0$ (i.e., we are at closest approach), Eqn. F14 further reduces to

$$\frac{d\kappa}{dt} = \frac{V_s}{2\cdot A} \qquad (F14a)$$

The interesting thing about Eqns. F13 & F14 is that they are functions only of time Δt (the time before or after closest approach) and therefore hold for any value of θ_0 (or, equivalently, roll angle). The added advantage is that the pitch angle and rate can be set by the spacecraft clock independently of where we are looking. The variation of κ and $d\kappa/dt$ with Δt is shown in Figs. F5 & F6 (the corrections for Earth rotation are discussed later).
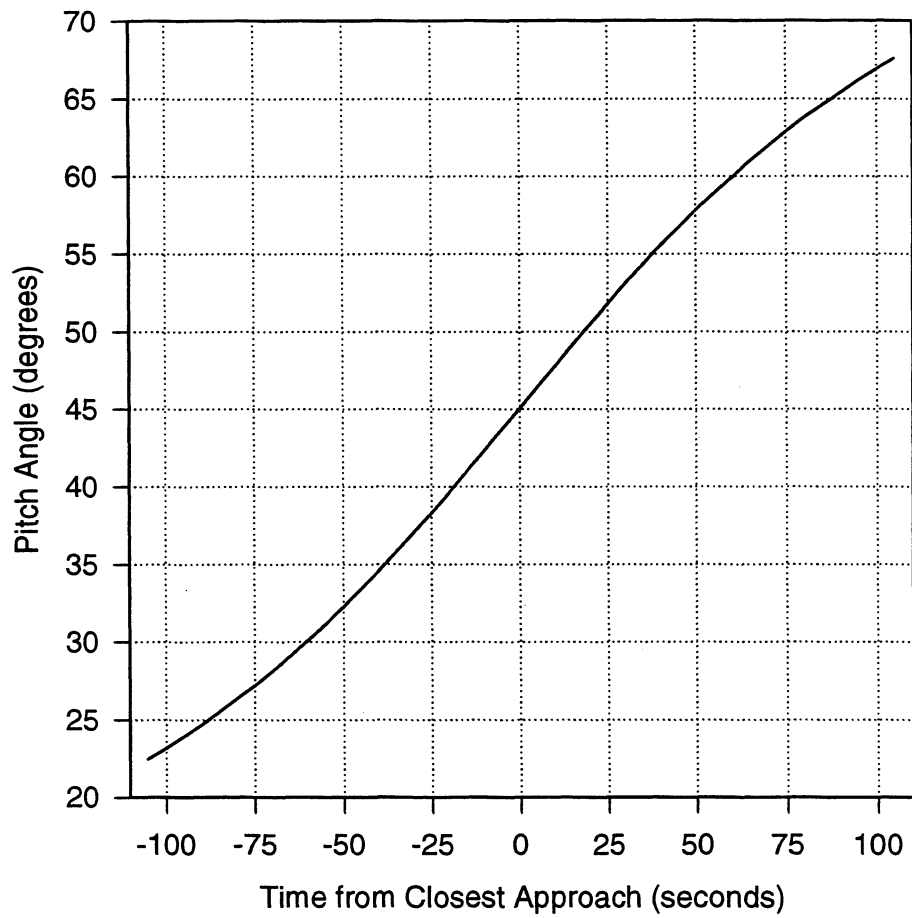
Fig. F5: Pitch Angle vs Time (non-rotating Earth)
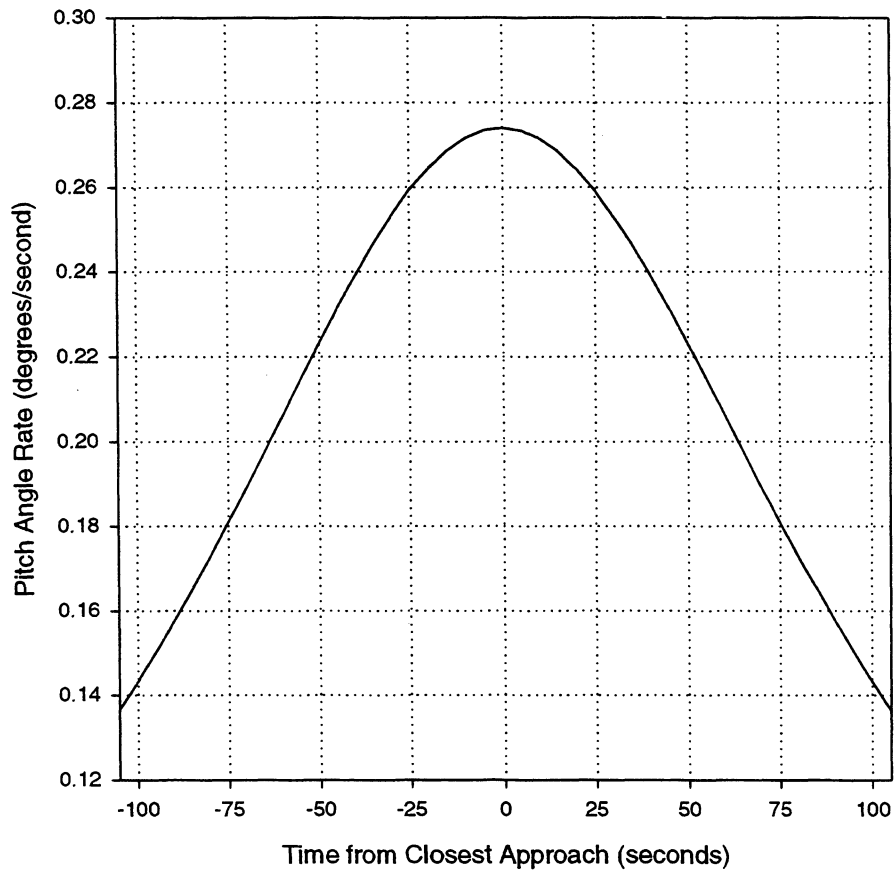
172

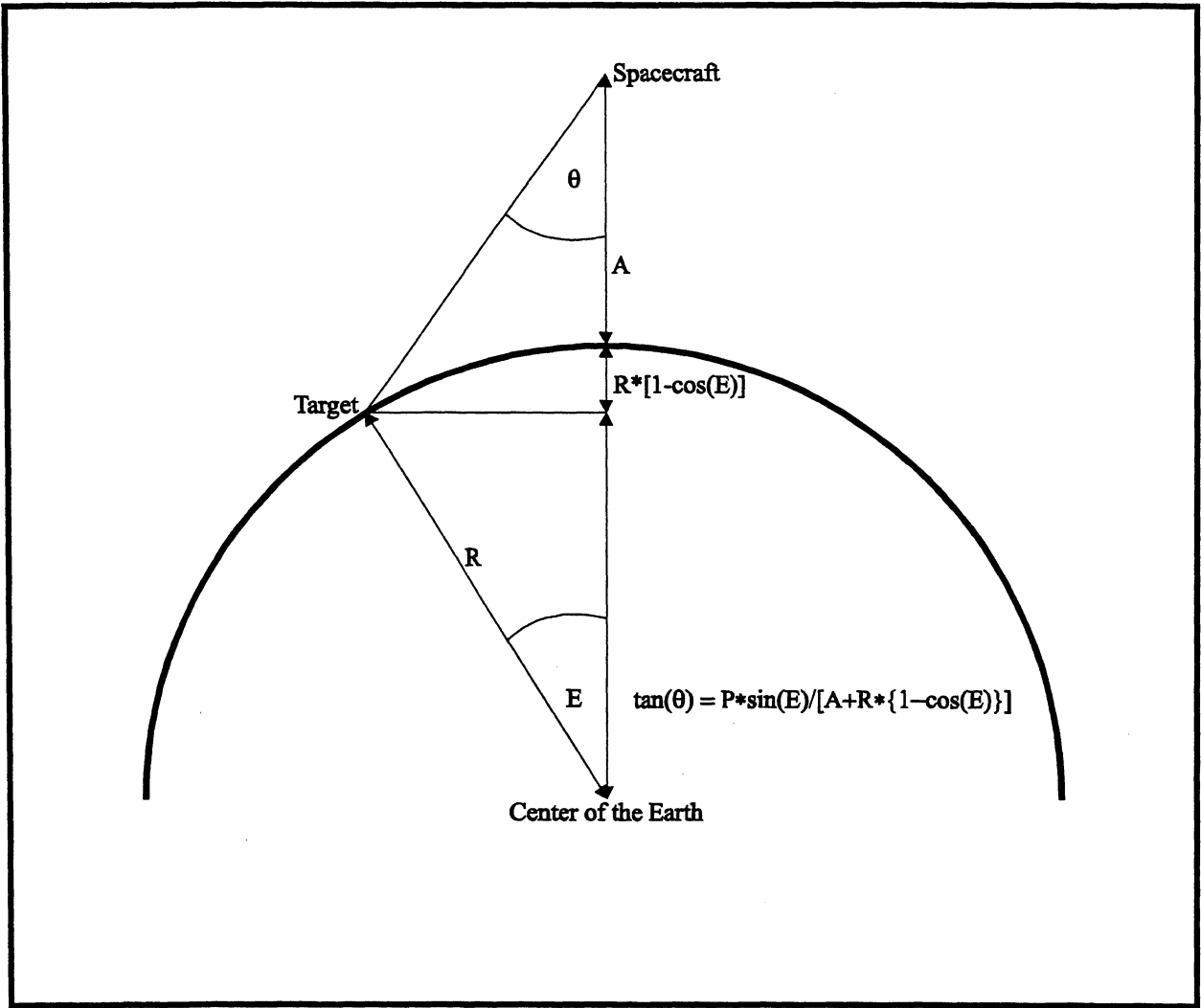*Fig. F6: Pitch Angle Rate vs Time (non-rotating Earth)*

Fig. F7: Relationship between Elongation and Nadir Angle

F6: Getting on Target

We shall now address the real issue: where must the spacecraft be in order to observe a target at a known latitude and longitude?

We begin by introducing the useful concept of *elongation* $E^\dagger$. The term originates in astronomy but for our purposes it is the angle at the center of the Earth between the target and the sub-spacecraft point. Let the target latitude and longitude be (β_1, λ_1) and the sub-spacecraft point (β_2, λ_2). Any textbook on spherical astronomy will show that

$$\cos(E) = \sin(\beta_1)\cdot\sin(\beta_2) + \cos(\beta_1)\cdot\cos(\beta_2)\cdot\cos(\lambda_1 - \lambda_2) \tag{F15}$$

The elongation and the nadir angle are directly related (see Fig. F7):

$$\tan(\theta) = \frac{R\cdot\sin(E)}{A + R[1 - \cos(E)]} \tag{F16}$$

where R is the radius of the Earth and A is the orbital altitude. For a nominal R of 6371 km and A of 705 km, a maximum θ_0 of 40° gives a maximum E_0 of 5.5545°. Remember that this is the angle on the Earth's (spherical) surface in any direction.

Referring to Fig. F8, we can easily derive some useful relationships using standard spherical trigonometry, remembering that spherical trigonometry applies *only* to triangles whose sides are great circles (e.g., meridians of longitude and the spacecraft orbit). Circles of latitude, except for the equator itself, are *small circles*, and spherical trigonometry does not apply.

The spacecraft is traveling along an orbit inclined at an angle τ (= inclination - 90°) with respect to the ascending node at longitude λ_0. All other longitudes are defined with respect to this point (i.e., we arbitrarily set $\lambda_0 = 0$). Now, it is well known that the shortest distance between two points on a sphere lies along the great circle joining them (which is why aircraft fly "over the pole" on international routes) and, obviously, this distance will be a minimum when that great circle is perpendicular to the great circle of the orbit. The question to be addressed, then, is "where must the spacecraft be in its orbit in order to minimize its elongation from a target at latitude β_1 and longitude λ_1"?

---

† In Appendix E the equivalent parameter was called the "Earth Surface Angle" but there the term was used exclusively for in-track angles. "Elongation" is more general and applicable to any direction.
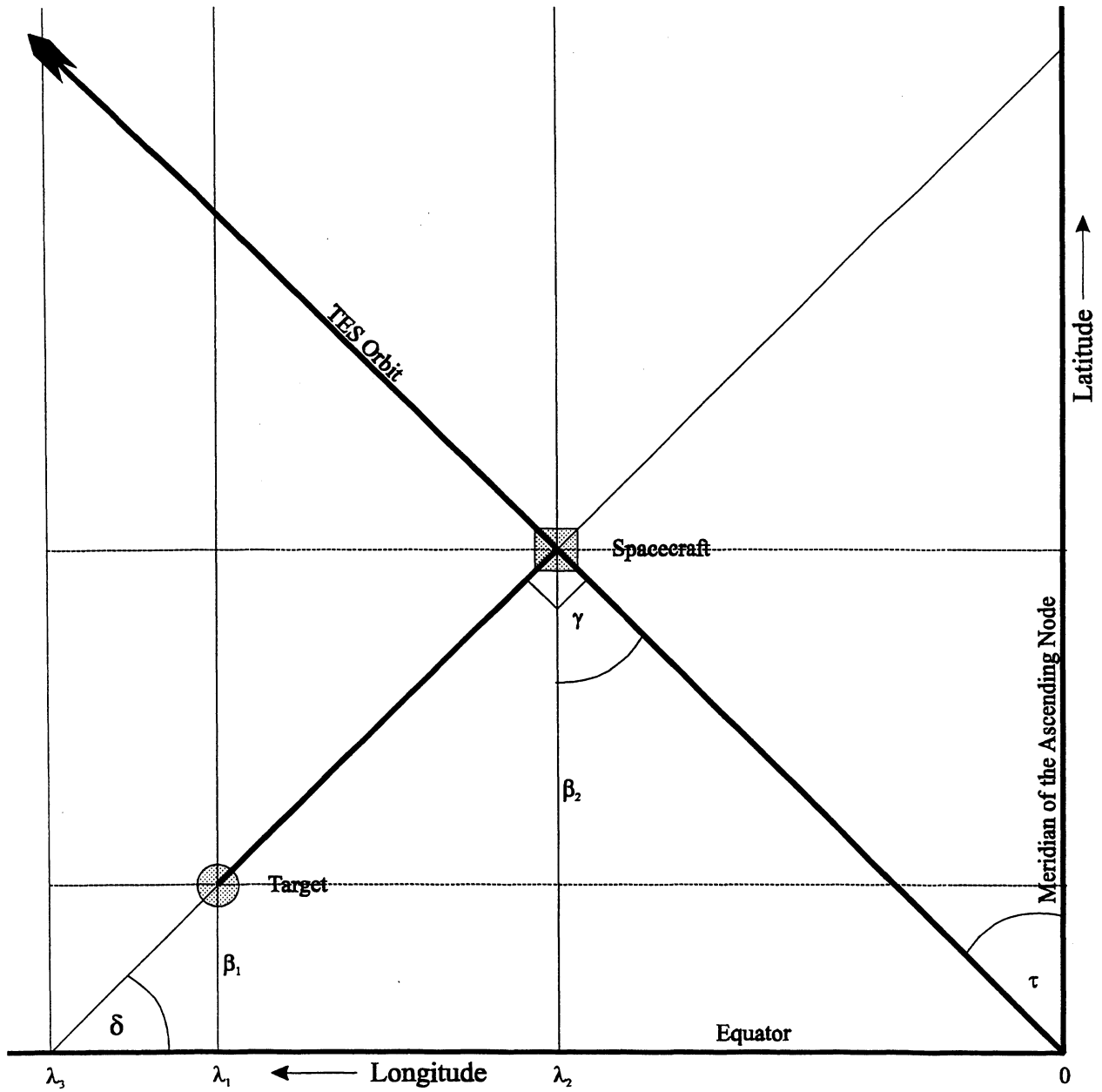
Fig. F8: Spherical trigonometry of TES target acquisition
(Note: heavy lines are Great Circles, fine lines are Small Circles)

176

Let the angle between the orbit and the meridian of the spacecraft λ_2 be γ. Then

$$\cos(\gamma) = \cos(\tau)\cdot\cos(\lambda_2) \tag{F16}$$
$$= \sin(\tau)/\cos(\beta_2)$$

and

$$\tan(\beta_2) = \sin(\lambda_2)/\tan(\tau) \tag{F17}$$

The angular length a of the orbital arc from the Southern Apex is

$$a = \tan^{-1}[\tan(\lambda_2)/\sin(\tau)] + \frac{\pi}{2} \tag{F18}$$

whence, for an orbital period P, the time t from the Southern Apex is

$$t = P\cdot\frac{a}{2\pi} + \frac{P}{4} = P(\frac{1}{4} + \frac{a}{2\pi}) \tag{F19}$$

Now, in order to define the perpendicular great circle, let this great circle intersect the equator at (relative) longitude λ_3 at an angle δ:

$$\tan(\delta) = \tan(\tau)/\cos(\lambda_3) \tag{F20}$$

But it is also true that

$$\tan(\delta) = \tan(\beta_1)/\sin(\lambda_3 - \lambda_1) \tag{F21}$$

whence, after some manipulation,

$$\tan(\lambda_3) = \frac{\tan(\beta_1)}{\tan(\tau)\cdot\cos(\lambda_1)} + \tan(\lambda_1) \tag{F22}$$

177

Thus δ and λ_3 are now defined in terms of the known parameters τ, β_1 and λ_1 and it remains only to find a relationship between them and the spacecraft longitude at closest approach $\lambda_{2,0}$. This results in another pair of simultaneous equations:

$$\tan(\delta) = \tan(\beta_{2,0})/\sin(\lambda_3 - \lambda_{2,0}) \tag{F23}$$

where $\beta_{2,0}$ is the spacecraft latitude at closest approach. Coupling this to Eqn. F17 results, after some more manipulation, in

$$\tan(\lambda_{2,0}) = \frac{\tan(\delta)\cdot\tan(\tau)\cdot\sin(\lambda_3)}{1 + \tan(\delta)\cdot\tan(\tau)\cdot\cos(\lambda_3)} \tag{F24}$$

and, since Eqn. F17 relates $\lambda_{2,0}$ and $\beta_{2,0}$, we know the location of the spacecraft at closest approach.

It is also simple to derive an expression for the minimum elongation E_0:

$$\sin(E_0) = \frac{\sin(\beta_{2,0})\cdot\sqrt{\sin^2(\delta) - \sin^2(\beta_1)} - \sin(\beta_1)\cdot\sqrt{\sin^2(\delta) - \sin^2(\beta_{2,0})}}{\sin^2(\delta)} \tag{F25}$$

The foregoing expressions can be used to make some interesting and useful plots. Fig. F9 is a Cartesian latitude-longitude plot of the TES orbit (from Eqn. F17). Since the orbit is sun-synchronous, it is trivial to change the x-axis to local solar time (assuming a 1:45 p.m. nodal crossing time). This is shown in Fig. F10. Be aware, however, that this is only part of the determination of sun angle - it may be near noon at 70° north, but if it is winter it is nevertheless pitch dark!

Fig. F11 shows a plot of the orbital angle γ vs. longitude from Eqn. F16. In "pilot-speak", (360-γ) is the heading. Fig. F12 is a plot of the length of the orbital arc from the ascending node (note that arctan has been "unwrapped" to make this plot) from Eqn. F18 and the time since the nodal crossing (using Eqn. F19 and P=5933.05 seconds) is shown in Fig, F13.
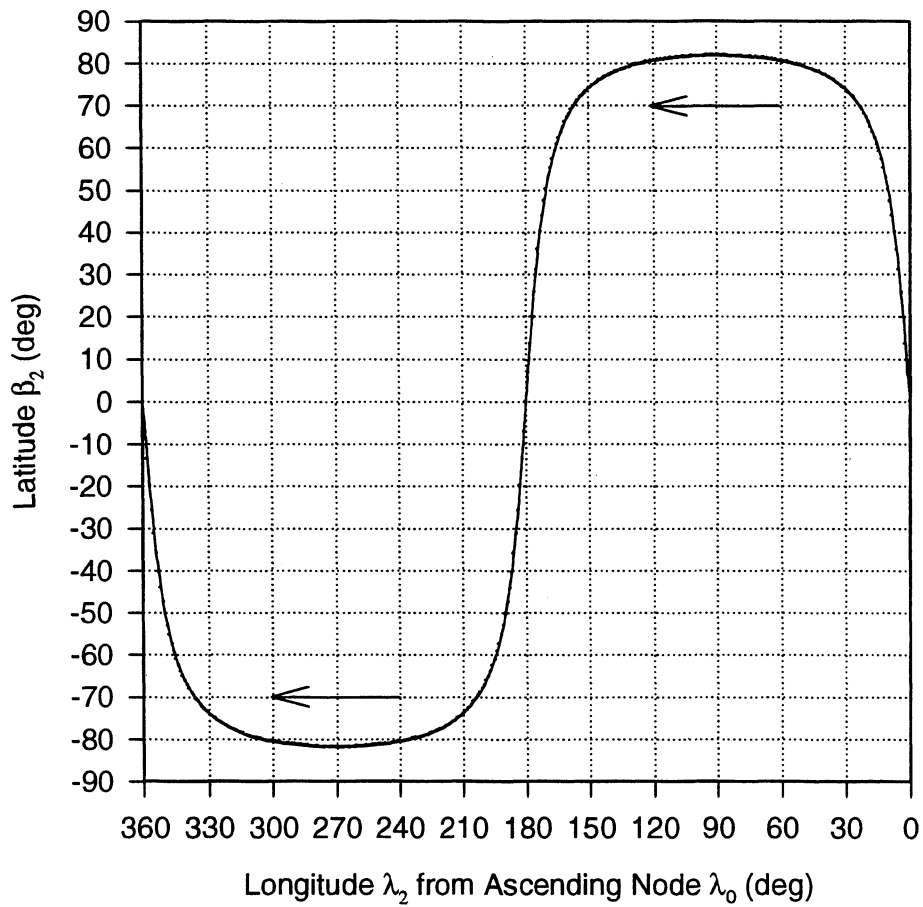
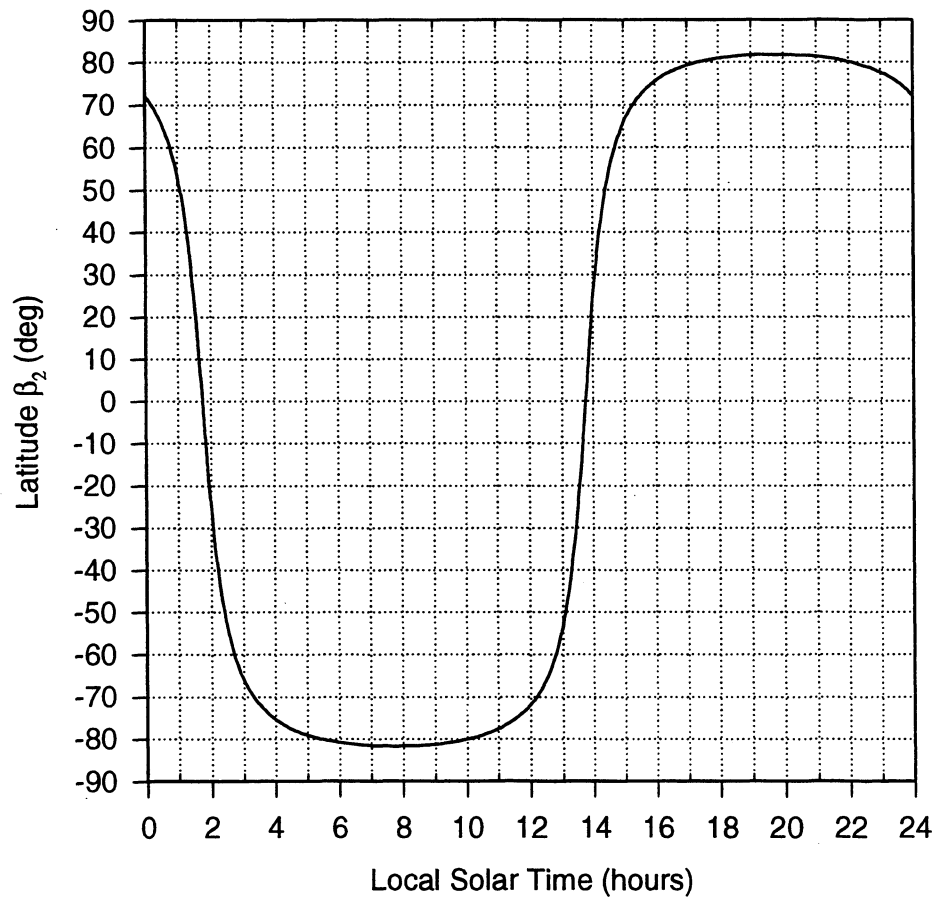*Fig. F9: TES orbit (Cartesian coordinates). Note R->L Motion (Retrograde Orbit)*

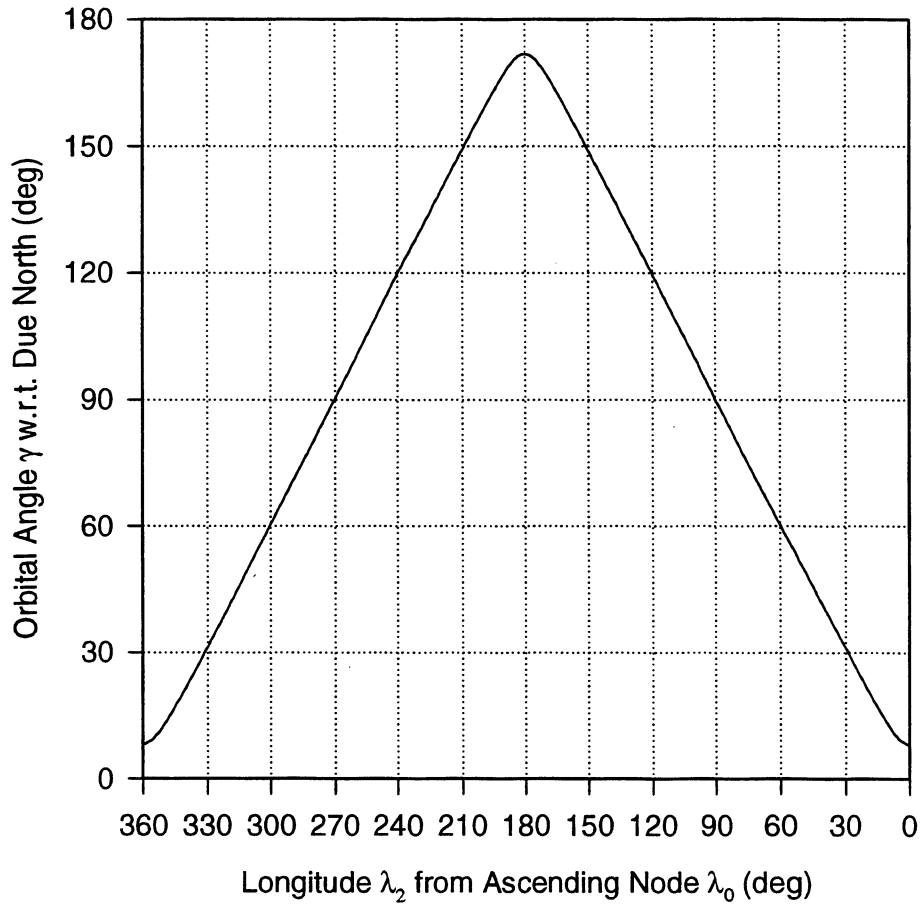*Fig. F10: Local Solar Time of the TES orbit (13:45 Nodal Crossing Time)*
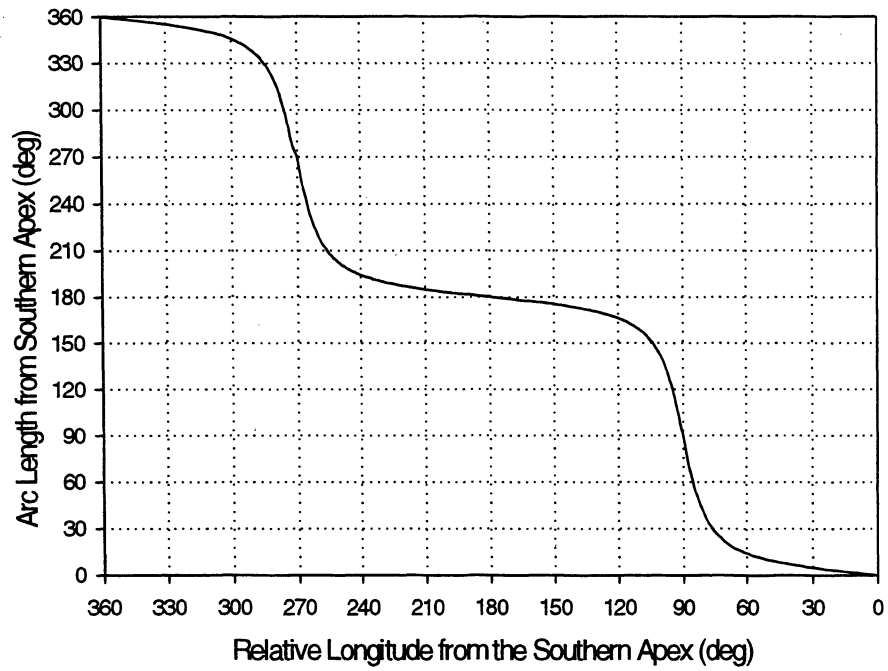
Fig. F11: TES Orbit Heading Angle

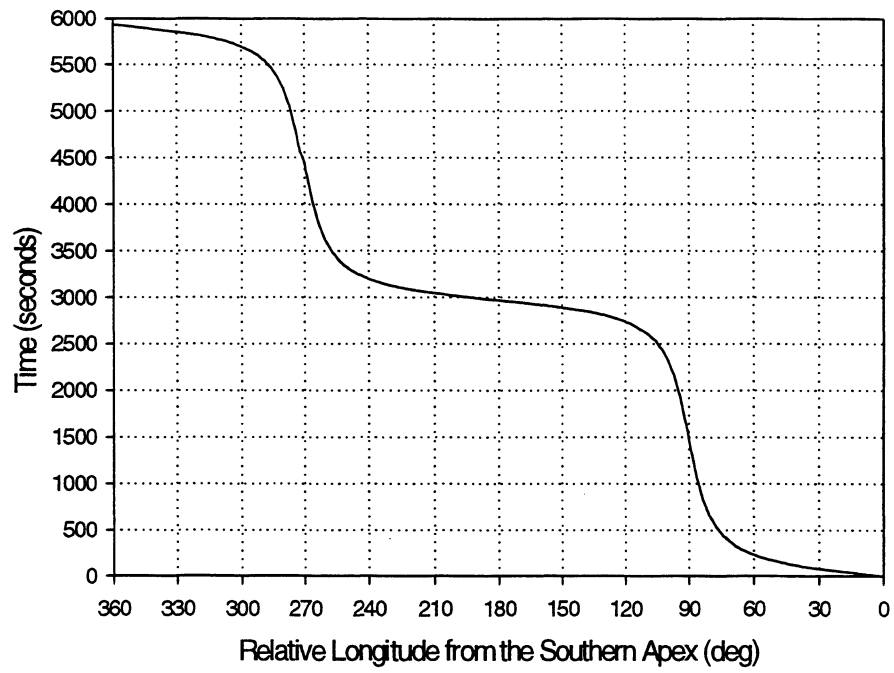*Fig. F12: Angular distance along the TES orbit from the Southern Apex*

Fig. F13: Time along the TES orbit

183

F7: The Impact of Earth Rotation

The Earth rotates fast enough that if we try to stare at a target for more than a fraction of a second, the pointing angles must be changed to compensate. For example, at the equator the target moves almost 2 km during our nominal single-scan time of 4 seconds. Over our maximum staring time of 221 seconds (Table X, §5.9), the motion can be almost 90 km - far larger than the footprint.

The impact is strongly dependent on latitude: near the equator the spacecraft is almost moving due N-S, so most of the effect will be on the roll angle. Conversely, at the orbital apices ($\pm 82°$ latitude) the spacecraft is moving E-W, so the effect will be entirely on the pitch angle rate. In between, the effect will be on both axes.

Time Base

Because we have a sun-synchronous orbit, the relevant time base is the solar day (not, as would be true for an inertially-fixed orbit plane, the sidereal day). While the mean solar day is defined as 86,400 seconds, the actual day (noon-to-noon) varies by almost ± 15 minutes during the year (local noon is "late" in February and "early" in November). Thus an exact calculation of this effect must take into account the date of observation. For now, we will assume the mean solar day.

Rates

The appropriate angular rate ω is therefore

$$\omega = 2\pi/86400 = 7.2722x10^{-5} \ \text{radians/sec} \tag{F26}$$

and the apparent eastward angular velocity ω_e of a target at latitude β_1 is

$$\omega_e = \omega\cos(\beta_1) = 7.2722x10^{-5}\cos(\beta_1) \ \text{radians/sec} \tag{F27}$$

Remembering Eqn. F16:

$$\tan(\theta) = \frac{R \cdot \sin(E)}{A + R[1 - \cos(E)]}$$

and differentiating with respect to E:

$$\sec^2(\theta)\frac{d\theta}{dE} = \frac{[A+R(1-\cos(E)]R\cos(E)-R^2\sin^2(E)}{[A+R(1-\cos(E))]^2} \tag{F28a}$$

and, further, remembering that $\sec^2(\theta) = 1 + \tan^2(\theta)$, we get

$$\frac{d\theta}{dt} = \frac{[A/R + (1 - \cos(E)]\cos(E) - \sin^2(E)}{[A/R + (1 - \cos(E))]^2 + \sin^2(E)} \cdot \frac{dE}{dt} \tag{F28b}$$

Projecting the rotation into this direction (azimuth ϕ, see Eqn. F5):

$$\frac{dE}{dt} = \omega \cdot \cos(\beta_1) \cdot \sin(\phi + \gamma) \tag{F29}$$

so the roll and pitch rates that must be added or subtracted from those previously calculated are:

$$\frac{d\rho}{dt} = \frac{[A/R + (1 - \cos(E)]\cos(E) - \sin^2(E)}{[A/R + (1 - \cos(E))]^2 + \sin^2(E)} \cdot \omega \cdot \cos(\beta_1) \cdot \sin(\phi + \gamma) \cdot \sin(\phi) \tag{F30a}$$

and

$$\frac{d\kappa}{dt} = \frac{[A/R + (1 - \cos(E)]\cos(E) - \sin^2(E)}{2\{[A/R + (1 - \cos(E))]^2 + \sin^2(E)\}} \cdot \omega \cdot \cos(\beta_1) \cdot \sin(\phi + \gamma) \cdot \cos(\phi) \tag{F30b}$$

Note that these are instantaneous value: E, ϕ and γ are all changing with time, so the corrections will entail not just additive values, but accelerations. However, their calculation is beyond the scope of this discussion.

F8: The Impact of Orbit and Attitude Errors

All of the foregoing was predicated upon a circular orbit, a spherical Earth, no terrain relief (topography) and no spacecraft attitude errors. Since none of these is strictly true, we will now investigate what corrections must be made to compensate (if possible).

Non-Circular Orbit (Altitude Errors)

In reality, the orbital altitude is not 705 km, but varies between 690 & 725 km ($\pm$ 3.5%). We can estimate the magnitude of the effect by differentiating Eqn. 16 with respect to A:

$$\sec^2\theta \, d\theta = -R\sin E \, dA/[A + R(1 - \cos E)]^2 \tag{F31}$$

Substituting for $\sec^2(\theta)$ [$= 1 + \tan^2(\theta)$] and performing some manipulation, we get

$$d\theta = -R\sin E \, dA/[A^2 + 2R(A + R)(1 - \cos E)] \tag{F32}$$

the sense being that if the true altitude is less than 705 km, θ_0 must be *increased* and *decreased* for A > 705 km.

Non-Spherical Earth (and Topography)

According to Allen's *Astrophysical Quantities* (1973), the figure of the Earth (geoid) is reasonably well represented by the expression

$$R(\beta) = 6378.164 \cdot [0.998327 + 1.677x10^{-3}\cos(2\beta) - 4x10^{-6}\cos(4\beta)] \tag{F33}$$

from which we may infer that deviations from a mean radius of 6371 km will not exceed 20 km. Note that I do not suggest that we actually use Eqn. F33 for the geoid - presumably Topex/Poseidon will give us a much better one.

For the purposes of the present exercise, topography is simply a local deviation of the Earth's radius from the geoid and the two can be treated together.

We shall use as our basis the local radius R_t at the target (because we know where it is, and how high it is) and let all the uncertainty reside in the geoid radius at the sub-spacecraft point.

From elementary trigonometry, we get

$$\frac{A+R}{\sin(E+\theta)} = \frac{R_t}{\sin(\theta)}$$

(F34a)

or

$$R = \frac{R_t \cdot \sin(E+\theta)}{\sin(\theta)} - A$$

(F34b)

Differentiating this expression with respect to θ (and then inverting it) readily leads to

$$\frac{d\theta}{dR} = \frac{\sin^2(\theta)}{R_t \cdot \sin(E)}$$

(F35)

and, substituting for θ from Eqn. F16, we arrive at

$$\frac{d\theta}{dR} = \frac{R_t \cdot \sin(E)}{2 \cdot R_t \cdot [1-\cos(E)] \cdot [A+R_t] + A^2}$$

(F36)

Pitch & Roll Errors

In the sense I use the term "spacecraft attitude errors" here, I mean *known* deviations of the attitude from the nominal, perfectly orthogonal, coordinate system of flight path and local vertical (nadir direction). Unknown errors and jitter are just that - unknown.

Since, fortunately, the gimbal roll and pitch axes are parallel to the spacecraft pitch and roll directions, the errors simply add or subtract from the gimbal angles - if the spacecraft is pitched down 1°, for example, simply add 1° to the gimbal pitch angle.

Yaw Errors

This is a little trickier, but it is obvious (see Fig. F14) that a yaw ψ of the spacecraft changes the apparent azimuth of the target. Alternatively, it can be seen that when we *ought* to have been looking at the target at closest approach, we actually are missing it. Nevertheless, the spacecraft ground track and the apparent target track are unchanged, but the linear distance to the ground *does* change from $A*\tan(\theta_0)$ to $A*\tan(\theta')$, whence it is obvious that

$$\tan(\theta') = \frac{\tan(\theta_0)}{\cos(\psi)} \tag{F37}$$

Remembering that $\theta_0 = \rho$, the original roll angle, we must set a new roll angle ρ' using the same equation:

$$\rho' = \tan^{-1}\frac{\tan(\rho)}{\cos(\psi)} \tag{F38}$$

Note that when $\psi = 0$, this expression reverts to $\rho' = \rho$, as it should.

We must also change the pitch angle to κ':

$$\begin{aligned}\kappa' &= 45° + 0.5 \cdot \tan^{-1}[\cos(\phi-\psi] \cdot \tan(\theta)] \\ &= 45° + 0.5 \cdot \tan-1[\{\cos(\phi) \cdot \cos(\psi)+\sin(\phi) \cdot \sin(\psi)\} \cdot \tan(\theta)]\end{aligned} \tag{F(39)}$$

Remembering from Eqn. F11 that $\tan^2(\theta) = Q^2+\tan^2(\theta_0)$, where $Q = V_s*\Delta t/A$, we see from Fig. F14 that

$$\sin(\phi) = \frac{\tan(\theta_0)}{\sqrt{Q^2+\tan^2(\theta_0)}} \tag{F40}$$

and

$$\cos(\phi) = \frac{Q}{\sqrt{Q^2+\tan^2(\theta_0)}} \tag{F41}$$

whence, after a little manipulation,

$$\kappa' = 45° + 0.5 \cdot \tan^{-1}[Q \cdot \cos(\psi)+\tan(\theta_0) \cdot \sin(\psi)] \tag{F42}$$

which, again, is identical to Eqn. F13 when $\psi = 0$.

Differentiating with respect to time, we get

$$\frac{d\kappa'}{dt} = \frac{Q \cdot \cos(\psi)}{2 \cdot \Delta t \cdot [1 + \{Q \cdot \cos(\psi) + \tan(\theta_0) \cdot \sin(\psi)\}^2]} \qquad (F43)$$

At $\Delta t = 0$, this reduces to

$$\frac{d\kappa'}{dt} = \frac{V_s \cdot \cos(\psi)}{2 \cdot A \cdot [1 + \{\tan(\theta_0) \cdot \sin(\psi)\}^2]} \qquad (F44)$$

Finally, we note that the target becomes perpendicular to the spacecraft (i.e., the new effective time of closest approach) after a delay $\Delta t'$:

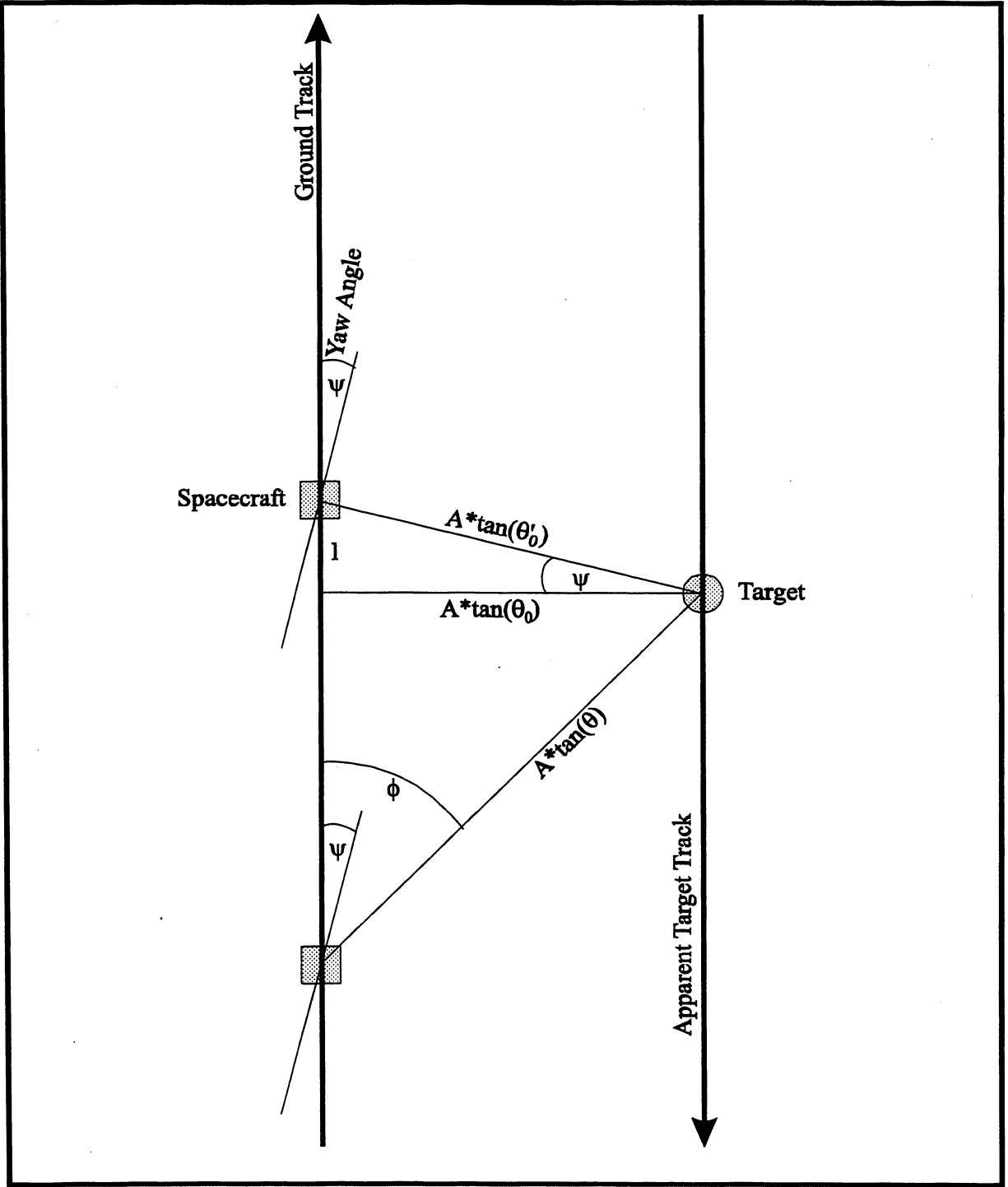$$\Delta t' = \frac{A \cdot \tan(\theta_0) \cdot \tan(\psi)}{V_s} \qquad (F45)$$

189

Fig. F14: Yaw error geometry

APPENDIX G: THE MEASUREMENT OF MODULATION INDEX

G1: Introduction

One of the most important performance parameters for a Fourier Transform Spectrometer is its *modulation index* M. For an ideal system, it is given by

$$M = 4 \cdot R \cdot T \le 1$$

where R and T are the reflectance and transmittance of the beamsplitter/recombiner. Thus if R = T = 0.5, we get M = 1.0 - a perfect system. Of course, in general, R and T are frequency (wavelength) dependent. However, even if R = 0.4 and T = 0.6, the value of M = 0.96 so, evidently, M is not a strong function of the coating reflectance/transmittance. Unfortunately, the effective value of M can be reduced by several unavoidable effects:

1) The coatings are never completely lossless. Losses can occur by absorption and scattering. If, for example, R = T = 0.45 (i.e., 10% loss), we shall have M = 0.81. That is, M is a strong function of losses in the beamsplitter.

2) Wavefront errors due to manufacturing tolerances on surfaces within the interferometer and residual misalignments means that the path difference will vary across the aperture and the effective modulation index reduced.

As a matter of practicality, one rarely finds M > 0.9.

G2: Why does it matter?

It matters because the signal recorded (the interferogram amplitude) is *directly proportional* to M. Worse yet, the background flux is independent of M - from the standpoint of photon shot noise the modulation is irrelevant. Thus it differs from a simple transmission loss through the system, which affects modulated and unmodulated photons equally.

Modulation Index is therefore an important parameter to measure during preflight calibration. Ideally, it should be measured at many wavelengths but this might be very time-consuming and expensive since it must be performed with monochromatic sources such as infrared lasers. It is therefore probably adequate to make the measurement somewhere near the mid-range of the system ($\sim$ 2000 cm^{-1}, for example) and use the known beamsplitter coating properties to propagate the value elsewhere. One should also make an allowance for the wavefront errors, which should be directly proportional to frequency.
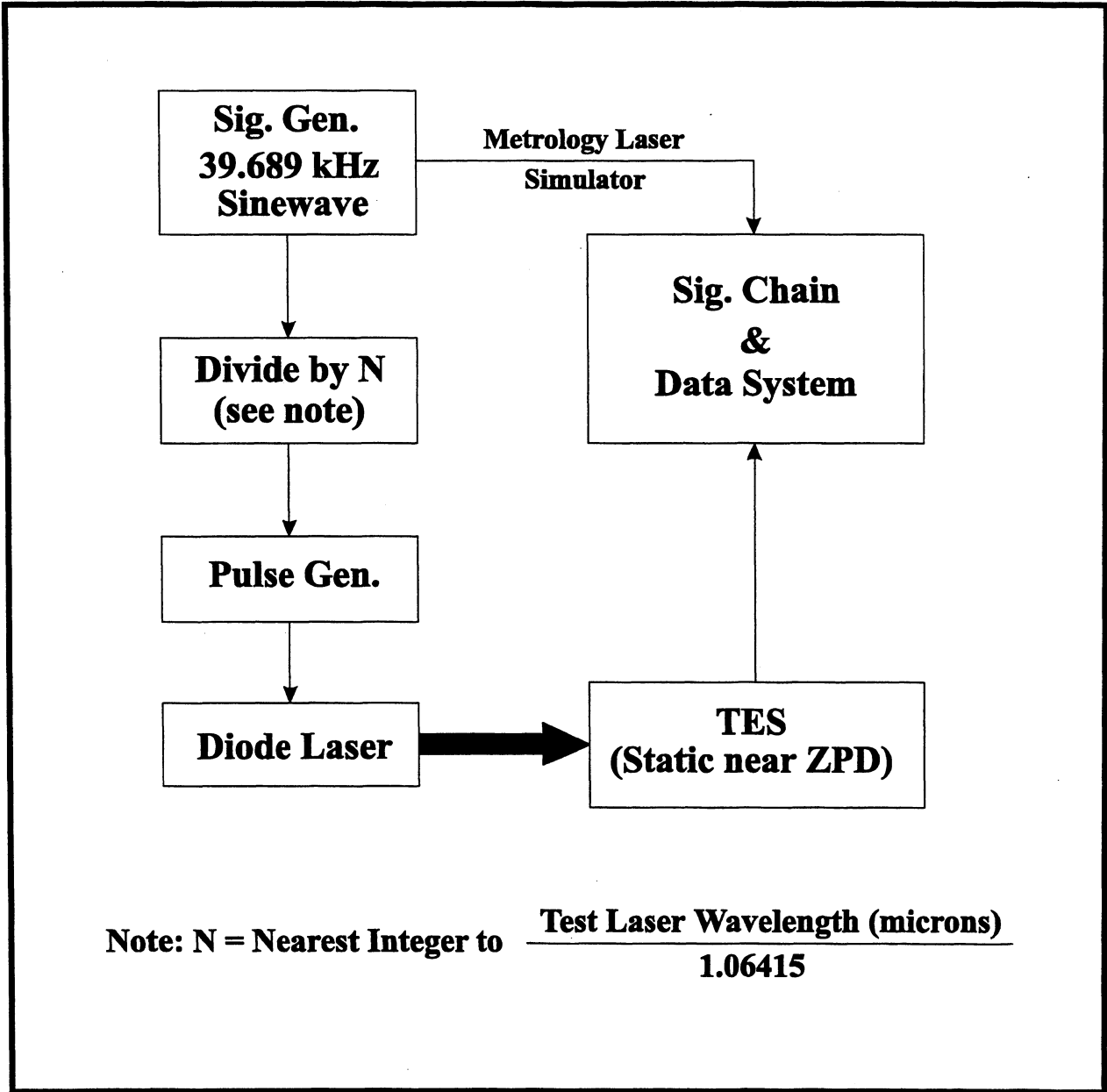
Fig. G1: Schematic of the method for measuring modulation index in an AC-coupled system

G3: Measurement method for a DC-coupled system

This is the simplest case. One simply shines the laser into the system and records the resultant fringe pattern as the system is scanned (it should be a cosine wave). The Modulation Index is simply

$$M = \frac{Maximum\ Signal\ -\ Minimum\ Signal}{Maximum\ Signal\ +\ Minimum\ Signal}$$

That is, in the ideal case, the minimum signal is zero.

G4: Measurement method for an AC-coupled system

Unfortunately, this does not work for an AC-coupled system such as TES because here it is the *mean* signal which is zero - the maximum and minimum signals are, by definition, the same (in magnitude).

The trick, then, is to modulate the source, not the interferometer - it is held static (see below). Most lasers can be pulsed on and off (100% modulation is essential). The pulse repetition rate must be as close as possible to the product of the laser frequency (in cm^{-1}) and the OPD scan rate (4.2235 cm/sec for TES). The metrology laser is replaced by a signal generator (39.689 kHz). The pulse generator must be phase-locked to the metrology laser simulator (see Fig. G1).

Procedure:

1) Move the corner reflector close to ZPD (does not have to be exact; $\pm$ 1 mm is adequate) and turn off the motor.

2) Set up the system so that at least one dewar has the appropriate filter in line.

3) Turn on the pulsed laser and the signal chains (N.B. beware of signal overloads - have an attenuator handy!)

4) Jog, nudge or otherwise *very, very slowly* change the path difference while recording the output (pushing on a reflector mount will probably suffice).

5) The *apparent* fringe amplitude will vary from some maximum value through a minimum. Compute M as before:

$$M = \frac{Maximum\ Signal\ -\ Minimum\ Signal}{Maximum\ Signal\ +\ Minimum\ Signal}$$

Once again, in the ideal case, the minimum signal is zero.

6) Using the measured properties of the beamsplitter, compute M over the entire TES range (650 - 3050 cm^{-1}). The calculated value at the test laser frequency should be at least as large as the measured value (if it isn't, you made a measurement or computation error!)

7) The difference between the ideal M and its measured value is an estimate of the loss due to absorption and wavefront errors. Make the assumption that the effect is proportional to frequency and correct the calculated values accordingly. You now have a reasonable estimate of M across the entire spectral range.

APPENDIX H: FREQUENCY DECALIBRATION

H.1: Introduction

This appendix is called "Frequency Decalibration" because it concerns the process that takes place after the *physical* calibration (observation of standard gases in the laboratory or in the real atmosphere). In other words, it addresses the question "Now what?".

H.2: Frequency Grids

The output of a Fourier Transform Spectrometer (FTS) at Level 1B is an array of discrete ordinates having a frequency spacing Δv with the frequency of the first point in the array having an absolute frequency v_0. Both Δv and v_0 are integer sub-multiples of the (apparent) metrology laser frequency v_l. Incidentally, all these numbers need to be held with at least 10 significant digits of precision.

Thus the frequency of the nth point ($n = 0,1,2,3, \ldots$) is simply

$$v_n = v_o + n \cdot \Delta v$$

which, among other things, avoids the need to carry the frequencies along with the spectral ordinates.

As was pointed out in the main text (§5.5), there are numerous phenomena that can cause the apparent laser frequency to differ from the expected value (with laser drift being one of the least significant). They all have one thing in common, though: they are indistinguishable from Doppler shifts - $\delta v / v$ is constant.

****

Frequency decalibration therefore reduces to a determination of the apparent laser frequency

****

The procedure, then, is to assume values of v_0 and Δv based on available *a priori* knowledge (which will be reasonably good, certainly better than 1%) and thereby assign apparent frequencies to the position of well-known spectral features (CO_2, CO and N_2O are good candidates). From the error in the apparent frequencies it is elementary to deduce the correct values for v_0 and Δv.

The next question is, therefore, "What is the best method for determining the apparent frequency of spectral features?". Algorithms that perform this function are known generically as *Linefinder Routines*. Note that this is not simply a matter of finding the sample point closest to the peak (although that is an inevitable starting point). The goal must be to determine the peak to 1% (or better) of Δv.

H.3: Linefinder Routines (Classical)

1) Preselect a set of isolated, relatively weak ($\tau_{nu} < 1$), spectral features within the range of interest;

then

2a) Take the finite-difference derivative of the line and fit a function (nearly a straight line). Accept the zero crossing as the best estimate of the line center position;

or

2b) Use center-of-gravity (COG) weighting[2].

Both methods have an outstanding defect: if the line is blended (even imperceptibly), the answer will be wrong. Their great advantage is that they are computationally simple.

There is a better way, but it is more computationally-intensive.

H.4: Linefinder Routines (Improved)

1) Set up a model spectrum of the standard (CO_2 and/or N_2O and/or CO) over a window of 2-5% of the local frequency. Eliminate strongly saturated lines ($\tau_{nu} > 10$; do this by editing the line list). The model spectrum need not be very accurate in intensity and can therefore be pre-computed and canned. Furthermore, there is no especial need for the selected lines to be isolated (but they should not be too heavily blended);

---

[2] See, for example, D.G. Cameron, SPIE Journal **233**, 216 (1985). The same paper suggests that the other obvious approach of polynomial fitting (or, equivalently, Voigt function fitting) is the worst choice of all.

2) Cross-correlate the model with the real data (± 256 points in correlation space suffices) There should be a pronounced single maximum near zero lag and a "noise" level markedly less than that in the original spectrum;

3) Identify the index N of the ordinate closest to the peak (note that the ordinate spacing remains exactly Δv);

4) Extract ordinates from around the peak that have an amplitude $\geq 10\%$ of the peak (25% might be safer if it leaves enough points);

5) Now use center-of-gravity weighting to find the correlation peak

or

6) Zero-pad the correlation function to the closest 2^n (if necessary) and take a real-to-complex FFT. This should be very fast because it will probably be over no more than 64 or 128 points;

7) On a point-by-point basis, compute arctan(IMAG/REAL);

8) Fit a straight line to the result. Save the SLOPE and the RMS residual (DeltaSLOPE);

9) The frequency shift is

$$\delta v = N \cdot \Delta v - SLOPE/(2 \cdot \pi) \pm DeltaSLOPE/(2 \cdot \pi)$$

The beauty of the cross-correlation approach is that it uses many lines simultaneously to determine the shift and is much more robust against inevitable frequency errors in the line list. It also provides substantial noise averaging; thus it even works when the lines in the real data are below the noise level (however, this is not a recommendation - use clearly visible features). Numerous tests with ATMOS data show that the accuracy is at the 0.1% level (in Δv) for reasonable spectra.

H.5: Decalibration

Cross-correlation assumes that the shift is frequency independent. This is the reason why the computational band must be limited - too wide a band will cause decorrelation and reduced accuracy. With ATMOS data it is found that 2-5% is as wide as one should go. Let the central frequency in the window be v_c (if you used one of the "classical" approaches, substitute the tabulated line frequency). The shift parameter $p = \delta v/v_c$.

If the assumed laser frequency was v_l, the corrected value is $v'_l = v_l \cdot (1+p)$ and the revised values for v_o and Δv are:

$$v_o = (J-1) \cdot v'_l/(2 \cdot K)$$

and

$$\Delta v = v'_l/(2 \cdot K \cdot M)$$

where J, K and M (all integers) are the alias order, the sampling interval and the FFT size respectively (see Appendix D). Values for these parameters will be found in columns 4,5, 10 & 12 of Table XLVII. At least one value changes for each filter.

APPENDIX I: GLOSSARY

Interferogram. The output of an interferometer (e.g., a Fourier Transform Spectrometer, FTS). For an FTS, the interferogram is (ideally) symmetric about the condition of Zero Path Difference (ZPD). An interferogram is a mathematically real array. *See also* Spectrum.

Spectrum. For a Fourier Transform Spectrometer (FTS), the spectrum is the result of performing a Fourier transformation on the interferogram (*q.v.*). The spectrum is a mathematically complex array in which, however, only the real part contains signal. The imaginary part (ideally) has only noise.

Scale Height. Scale height H is the altitude range over which a parameter declines by a factor 1/e. It is usually (but not necessarily) applied to pressure or partial pressure, in which case

$$H = \bar{m}g/kT$$

where $\bar{m}$ = mean molecular weight of the atmosphere (or the actual molecular weight if partial pressure is meant), g = acceleration due to gravity, k = Boltzmann's constant and T is the absolute temperature.

In the lower atmosphere, H ≈ 8 km.

Potential Temperature. The temperature Θ that a parcel of air would achieve if it were adiabatically compressed to some standard pressure P_o (e.g., sea level, 1013.25 mbar = 101.325 kpa). It is given by

$$\Theta = T(P_o/P)^\kappa$$

where κ is the ratio of the gas constant for dry air to the specific heat at constant pressure (= 0.286). Its importance is twofold: it is convenient way of subsuming the connected parameters of temperature and pressure into a single value and it is observed that air masses tend to move along surfaces of constant potential temperature.

THIS PAGE INTENTIONALLY LEFT BLANK

APPENDIX J: ACRONYMS

AES	Airborne Emission Spectrometer (JPL)
ATBD	Algorithm Theoretical Basis Document
CFC	Chlorofluorocarbon
DAAC	Distributed Active Archive Center
DAO	Data Assimilation Office (GSFC)
ECMWF	European Centre for Medium Range Weather Forecasting
ECS	EOSDIS Core System
EOS	Earth Observing System
EOSDIS	EOS Data and Information System
ESA	European Space Agency
ESE	Earth Science Enterprise (NASA Code Y)
FTS	Fourier Transform Spectrometer
GSFC	NASA Goddard Space Flight Center
HCFC	Hydrogenated Chlorofluorocarbon
HDF	Hierarchical Data Format
HFC	Hydrogenated Fluorocarbon
HiRDLS	High Resolution Dynamics Limb Sounder (NCAR/Oxford University)
HITRAN	Molecular Database (USAF/Harvard-Smithsonian)
IASI	Improved Atmospheric Sounding Interferometer (ESA)
ILS	Instrumental Line Shape (Impulse Response)
JPL	Jet Propulsion Laboratory
kb	kilobit
kbps	kilobits per second
LaRC	NASA Langley Research Center
Mb	Megabit

Mbps	Megabits per second
MIPAS	Michelson Interferometer for Passive Atmospheric Sounding (Germany)
MLS	Microwave Limb Sounder (JPL)
NASA	National Aeronautics and Space Administration
NCAR	National Center for Atmospheric Research
OMI	Ozone Measuring Instrument (Netherlands/Finland)
OPD	Optical Path Difference
PI	Principal Investigator
RCOPD	Rate of Change of Optical Path Difference
SCF	Science Computing Facility (at JPL)
TES	Tropospheric Emission Spectrometer (JPL)
VMR	Volume Mixing Ratio
ZPD	Zero Path Difference